

AN INVESTIGATION IN SURFACE

EFFECTS ON CONDUCTIVITY

by

JAMES COLLIER MITCHINSON B.Sc.

Thesis presented for the Degree of
Doctor of Philosophy of the University of Edinburgh
in the Faculty of Science.

OCTOBER 1970



ABSTRACT.

This work is concerned with the changes which occur in the electrical resistance and effective work function of thin metallic films as a result of surface effects. The surface effects considered are a result of the vacuum deposition of overlayers and gas adsorption at the film surfaces. Conductivity and work function changes which can occur are considered separately, and then an attempt is made to predict how conductivity and work function changes are related for the metals employed; viz, gold, silver and aluminium.

A suitable method of monitoring the changes in effective work function of thin metallic films is developed which can be operated during vacuum deposition of the films in ultra-high vacuum conditions. Apparatus incorporating this means of monitoring effective work function, and also the measurement of sheet resistance, was designed and built for use in conjunction with an electron-beam evaporator unit.

A simple theoretical model is presented for the growth of overlayers on metallic films which can be used to predict electrical resistance changes in reasonable agreement with the experimental results for gold deposited onto annealed gold films. The model depends upon an exponential relationship between surface coverage and mean overlayer thickness. The relationship is found to be applicable for gold, vacuum deposited onto polycrystalline silver films, and vice versa, on glass substrates.

Changes which take place in the electrical resistance of thin polycrystalline gold and silver films when aluminium overlayers are vacuum deposited onto them are explained on the basis of surface alloying and the reaction of aluminium with oxygen. Contact potential measurements made are complementary to the explanation of the resistance changes. Composite film structures with oxidised layers of aluminium were found to have very non-linear slope resistance characteristics.

ACKNOWLEDGEMENTS.

Thanks are due to Professor W.E.J. Farvis and Dr. R.D. Pringle who supervised this work, and who have been a great source of help and encouragement during the period of study.

The many useful discussions that the author had with fellow post-graduate students in the Electrical Engineering Department, where the work was carried out, is gratefully acknowledged. Also, the author recognises the valuable assistance given by the workshop staff during the construction of the apparatus.

Thanks are given to Dr. D.S. Campbell who gave permission to make reference to several Plessey Co. Ltd. (Allen Clark Research Centre, Caswell) research reports.

Finally, thanks are due to the Science Research Council for a maintenance grant which made this study possible.

CONTENTS.

Abstract.		(i)
Acknowledgements.		(iii)
CHAPTER 1.	<u>Introduction.</u>	
	Introduction.	1
1.1	Definition of surface effects.	1
1.2	Thin metal films.	2
1.2.1	Early work.	2
1.2.2	Modern ideas of conductivity.	4
1.2.3	Conductivity with overlayer structures.	8
1.2.4	Field effects.	9
1.2.5	Oxidation and adsorption.	10
1.2.6	Nucleation and growth.	11
1.2.7	Film surfaces.	13
1.3	Application of thin films.	15
1.4	Object of this investigation.	17
CHAPTER 2	<u>Theoretical Work on Thin Films.</u>	
	Introduction.	20
2.1	Conductivity.	20
2.1.1	Bulk metals.	20
2.1.2	Surface effects on continuous films.	26
2.1.3	Discontinuous films.	43
2.2	Work function.	

2.2	Work function.	46
2.2.1	Definition of work function.	46
2.2.2	Interpretation of work function values.	49
2.2.3	Surfaces to be considered.	51
2.2.4	Bare metal surfaces.	52
2.2.5	Gas adsorption on metal surfaces.	56
2.2.6	Metallic overlayers.	61
2.2.7	Oxide growth.	70
2.2.8	Work function complications.	71
2.3	Electrical conductivity and work function relationships.	74
2.3.1	Value of relating work function to conductivity.	74
2.3.2	Adsorption and oxidation.	75
2.3.3	Overlayers on low conductivity thin film metallic substrates.	79
2.3.4	Overlayers on high conductivity thin film metallic substrates.	80
CHAPTER 3	<u>Work Function Measurement.</u>	
	Introduction.	83
3.1	Methods of measuring work function.	83
3.1.1	Contact potential.	84
3.1.2	Photoelectric.	87
3.1.3	Field emission.	88
3.1.4	Thermionic emission.	89
3.1.5	Ion emission.	90
3.2	Selection of contact potential method.	

3.2	Selection of contact potential method	90
3.3	Proposed system for measuring contact potential.	93
3.3.1	Theory of operation.	93
3.3.1	Instrumentation required.	97
3.3.3	Performance of system.	98
CHAPTER 4	<u>Design and Construction of Apparatus.</u>	
	Introduction.	102
4.1	Vacuum chamber.	102
4.1.1	Vacuum chamber required.	102
4.1.2	Vacuum system employed.	104
4.2	Design of vacuum chamber contents.	106
4.2.1	Dynamic capacitor.	106
4.2.2	Evaporator.	111
4.2.3	Film thickness.	114
4.2.4	Electrical resistance.	115
4.3	Instrumentation.	117
4.3.1	Contact potential recording.	117
4.3.2	Other quantities recorded.	120
CHAPTER 5	<u>Experimental Procedures and Results.</u>	
	Introduction.	123
5.1	Preparing apparatus.	123
5.1.1	Cleaning procedures.	123
5.1.2	Assembling and testing.	126
5.2	Evacuating chamber.	

5.2	Evacuating chamber.	127
5.2.1	Pumping.	127
5.2.2	Bake-out.	129
5.3	Growth of gold films.	131
5.4	Silver and gold overlayers.	135
5.4.1	Silver overlayers on gold.	135
5.4.2	Gold overlayers on silver.	137
5.5	Aluminium overlayers.	139
5.6	Examination of the films after venting the vacuum chamber to the atmosphere.	142
5.6.1	Contact potential changes on venting chamber.	142
5.6.2	Optical microscope.	143
5.6.3	Scanning electron microscope.	144
5.6.4	Transmission electron microscope.	145
5.6.5	Other examinations.	146
CHAPTER 6	<u>Discussion and Conclusions.</u>	
	Introduction.	148
6.1	Thin gold films.	148
6.1.1	Film conductivity during initial growth.	148
6.1.2	Work function of gold.	151
6.2	Conductivity changes with gold and silver overlayers.	152
6.2.1	Silver overlayers on gold.	152
6.2.2	Gold overlayers on silver.	157
6.3	Conductivity changes with aluminium overlayers.	

6.3	Conductivity changes with aluminium overlayers	161
6.4	Conclusions.	167
6.5	Further work.	171
	Appendix.	174
	References.	178

CHAPTER 1.

INTRODUCTION

Introduction.

The work described in this thesis is concerned with the preparation and properties of thin metal films. The metals used are gold, silver and aluminium. The films are prepared by vacuum deposition and the properties of principal interest are electrical conductivity and work function. In this first chapter an outline of thin film development will be given together with the progress made in the measurement and understanding of some of their properties. From this, the reasons for this work will be given and its aims explained.

1.1. Definition of Surface Effects.

In electronic engineering it is very important that the physical properties of the materials used are well known. In modern circuit and device design work the electrical conductivity appears in the necessary calculations more often than any other. Tables of accepted values for stated conditions of temperature and crystallographic orientation are well documented for most materials. However, the technology of circuit manufacture has changed so rapidly in the last twenty years that such tables of conductivity must be used with caution. These values are perfectly valid providing "bulk" conditions are being considered i.e. that all the dimensions are very much larger than the mean free path of

the charge carriers in the material. Typically, the mean free path in a good conductor is a few hundred angstroms. Thus, for metal films having a thickness less than a few thousand angstroms the bulk conductivity can be significantly modified by the state of the surface of the material. These modifications are said to be the result of size and/or surface effects. In this work they will be referred to as surface effects.

1.2. Thin Metal Films.

1.2.1. Early Work. Thin metal films formed at low pressures were first reported over a century ago by workers in the glow discharge field. These films were inadvertently sputtered on to the glass envelope containing the glow discharges. When developing the filament lamp in the latter half of the nineteenth century experimenters reported metal films appearing on the inside of the lamp envelope. During this period no serious attempts were made to investigate the properties of such films. This is not a reflection on the ability of experimenters of the time, but shows the inadequacy of their instrumentation and apparatus for a systematic investigation of the preparation and properties of these deposits. Not until the turn of the century did the experimental and theoretical work on thin films make real progress.

Drude ⁽¹⁾ in 1900 proposed his electron gas theory on electrical conduction in metals. He postulated that a metal contained mobile negatively charged particles analogous to a volume

of gas molecules. The charged particles were to be in random thermal motion like gas molecules and would undergo collisions with each other which would result in a "mean free path" for these particles. From this theory Thomson ⁽²⁾ deduced that if a metal conductor was of such a size that the thickness (t) was of the same order as the bulk mean free path (Λ_0) of the charge carriers, then the charge carriers, (electrons), would undergo further collisions at the conductor surfaces. This resulted in an expression for a reduced mean free path, (Λ_1), given by

$$\Lambda_1 = t \left(\frac{3}{4} + \frac{1}{2} \log \frac{\Lambda_0}{t} \right) \quad (1.2.1)$$

This relationship resolved the apparently anomalous results obtained by workers at about the same time for the resistivity of thin films. For thick conductors the relationship between resistivity (ρ) and thickness (t) is

$$\rho \propto \frac{1}{t} \quad (1.2.2)$$

It had been found for thin metal films that the resistivity (ρ) increased much faster than the normal relationship of equation (1.2.2) would predict.

Since, from equation (1.2.1), Λ_1 will decrease with decreasing t the resistivity trend for decreasing film thickness was in qualitative agreement with the experimental results. Swann ⁽³⁾ in

1914 could not theoretically account for the measured resistivity and temperature coefficient of his thin metal films. The temperature coefficient was of the wrong polarity and the resistivity value too high to be accounted for by the Thomson (2) theory. This led him to deduce that thin film structures were in fact aggregated, and were not thin smooth plates as had been assumed. His reasoning for the cause of aggregation has been shown to be wrong, but the basic idea of island structure during initial film growth has been verified (4). Swann (3) further added that since there was an open structure with gaps between clusters of condensed atoms, only electrons with sufficient velocity could travel from cluster to cluster. As the film grew the clusters became closer and thus it became easier for the electrons to move under the influence of an applied electric field. As Swanson (5) has pointed out "Effectively Swann suggested that conduction in an aggregated film is activated and that the activation energy decreased as the film thickness increased." Thus, Swann (3) was able to account for the positive temperature coefficient and for the high resistivity values.

1.2.2. Modern Ideas of Conductivity. Even with Swann's (3) substantially correct picture for the stages of metal film growth, it was several decades before the theory of conduction in discontinuous structures yielded results in agreement with experiments. Thermionic emission (6), field emission (7), quantum mechanical tunneling (8), substrate conduction (9) and semi-

conductor - like band conduction ⁽¹⁰⁾ have all been employed in building up the modern theory for conduction in aggregated metallic structures.

For continuous films several equations similar in form to equation (1.2.1) appeared in the literature ^{(11) (12)}, but all of them suffered from the inability to always agree with experimental results. Fuchs ⁽¹³⁾, in 1938 solved the Boltzmann transport equation with the appropriate boundary conditions for the case of inelastic scattering at the surface of a film. Sondheimer ⁽¹⁴⁾ (1952) derived an equation based on Fuchs' ⁽¹³⁾ analysis for the change in conductivity which results if only a fraction of the electrons were inelastically scattered at the surface. Thus, a fraction (P) of the electrons are scattered specularly, and a fraction (1-P) diffusely. It was further assumed that this fraction (P) was not a function of the angle of incidence of the electrons. The equation can be written as

$$\frac{\sigma}{\sigma_0} = 1 - \frac{3}{2k} (1-P) \int_0^{\infty} \left(\frac{1}{T^3} - \frac{1}{T_0^3} \right) \frac{1-e^{-kT}}{1-Pe^{-kT}} \cdot dT \quad (1.2.3)$$

where:-

σ is the thin film conductivity

σ_0 is the equivalent bulk conductivity

t is the film thickness

Λ is the electron mean free path

and $k = t/\Lambda$

Thus, the change in conductivity is a function of the

fraction P , film thickness and bulk mean free path. The only other variable present in equation (1.2.3) which was not present in much earlier equations is P . A simplification which can be made to equation (1.2.3) with, as before

$$k = \frac{t}{\lambda} \quad (1.2.4)$$

is to rewrite it in the form given by Juretschke (15) as

$$\frac{\sigma}{\sigma_0} = \phi(k, P) \quad (1.2.5)$$

where ϕ is a tabulated function. This theory has been used to explain the observation that gold films deposited on freshly prepared bismuth oxide underlayers have an initial P value of close to zero which increases to approximately 0.9 when the films are annealed in air at 350°C . (16) (17).

An extension of the above theory was made by Lucas (18) (19) to allow for different fractions of electrons being scattered specularly at the upper and lower surfaces of a thin film. If P and Q are the fractions scattered specularly at the surfaces then the change in conductivity can be expressed as

$$\frac{\sigma}{\sigma_0} = 1 - \frac{3}{4k} \int_0^k \frac{(T - T^3) \left\{ 1 - e^{-k/T} \right\}}{1 - PQ e^{-(2k/T)}} \times \left[2 - P - Q + \{ P + Q - 2PQ \} e^{-k/T} \right] dT \quad (1.2.6)$$

or, using the Juretschke functional form

$$\frac{\sigma}{\sigma_0} = \frac{(1-P)(1-Q)}{(1-(PQ)^{1/2})^2} \phi(k, (PQ)^{1/2}) + \left\{ 1 - \frac{(1-P)(1-Q)}{(1-(PQ)^{1/2})^2} \right\} \phi(2k, PQ) \quad (1.2.7)$$

If the electron reflection coefficient at the film surface is dependent on the angle of incidence of the conduction electrons, then the mathematical analysis for the derivation of the above relationships must be considered. Parrot (20) assumed that for all angles (θ) to the surface normal up to some angle, (θ_0), all the incident electrons would be diffusely scattered and that they would be specularly scattered for all larger angles. Based on this assumption the conductivity equation obtained, as shown by Juretschke (21), can be written as

$$\frac{\sigma}{\sigma_0} = 1 - \frac{3}{2k} \int_0^{\sec \theta_0} \left(\frac{1}{T^3} - \frac{1}{T^5} \right) (1 - e^{-kT}) dT \quad (1.2.8)$$

As for equation (1.2.3), equation (1.2.8) can be written in the form

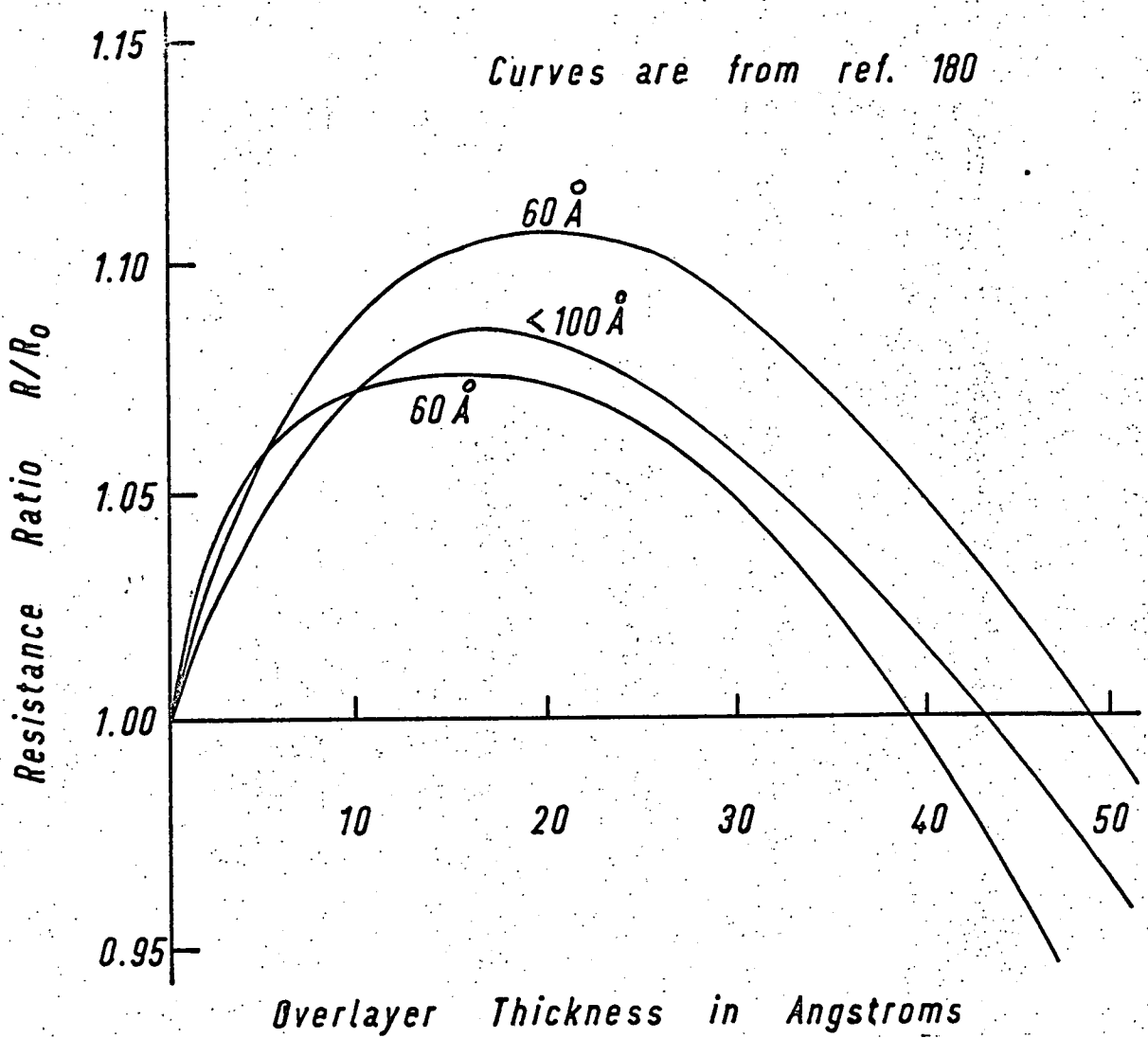
$$\frac{\sigma}{\sigma_0} = \phi(k, \theta_0) \quad (1.2.9)$$

An extension of this theory is to make allowance for the cut-off angles being different at the upper and lower surfaces. If θ_1 and θ_2 are the cut off angles for the upper and lower surfaces, then equation (1.2.9) is modified to

$$\frac{\sigma}{\sigma_0}(k; \theta_1, \theta_2) = \phi(k, \theta_1) + \phi(2k, \theta_2) - \phi(2k, \theta_1) \quad (1.2.10)$$

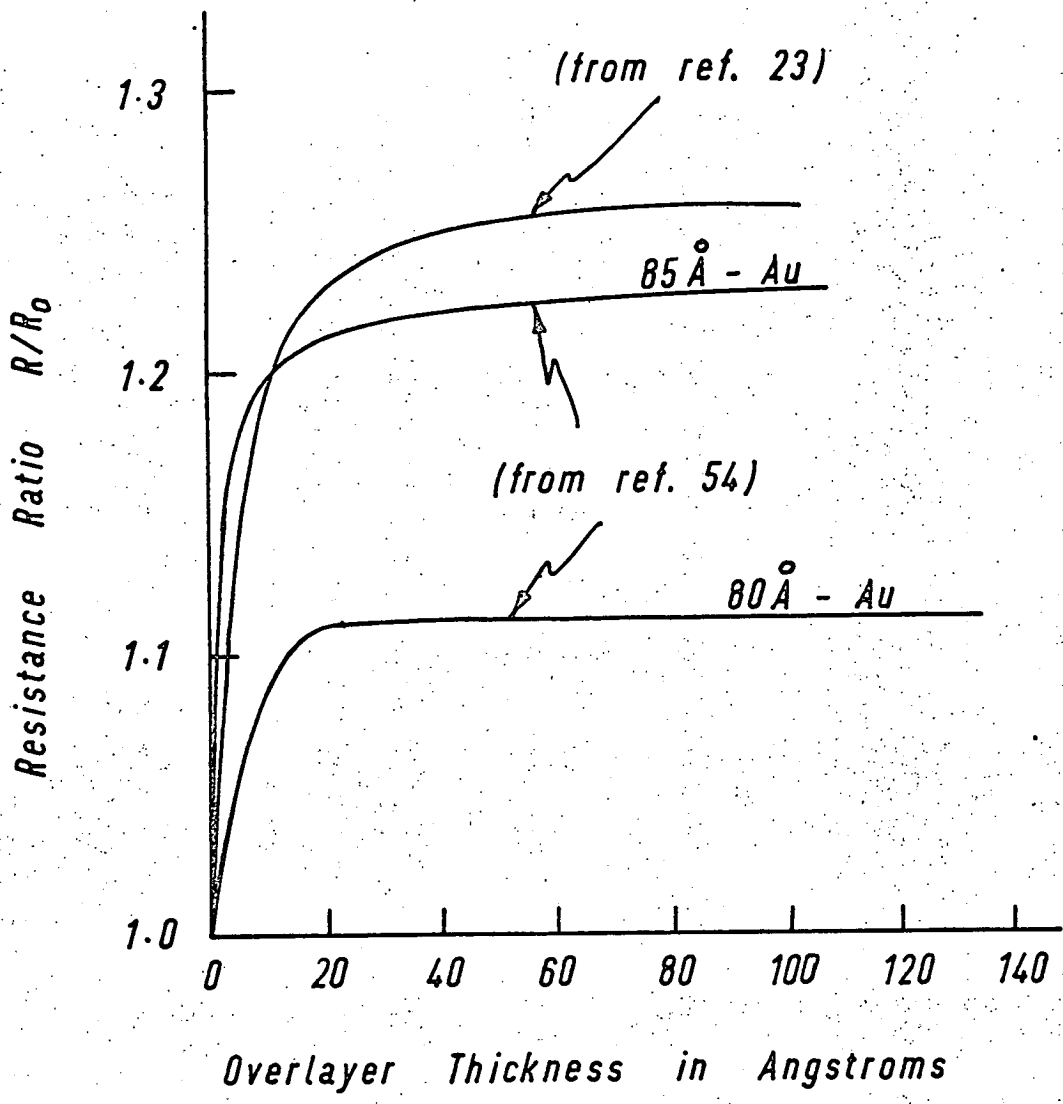
Parrot's theory ⁽²⁰⁾ and that of Fuchs-Sondheimer-Lucas ⁽¹⁸⁾ both predict approximately the same variations from bulk for conductivity values of thin films at temperatures close to ambient. However, the theories predict different behaviour at low temperatures when the mean free paths of the charge carriers become extended. The experimental evidence available ⁽²²⁾ suggests that neither of the theories satisfactorily predicts low temperature behaviour. This is perhaps the result of insufficient consideration being given to the structure of real thin films.

1.2.3. Conductivity with Overlayer Structures. Realising that an annealed gold film on bismuth oxide could have a scattering coefficient (P) of approximately 0.9, Lucas ⁽²³⁾ ⁽¹⁸⁾ argued that depositing a further layer of gold could make P decrease again to zero. This was provided that the gold overlay was left unannealed, and that the annealed gold to unannealed gold boundary was completely transparent to the passage of electrons. By this method he hoped to increase the resistivity of a thin annealed gold film by the addition of further gold until the shunting effect of the added gold caused the resistivity to decrease. Experimental work carried out demonstrated that this was possible,



— Figure 1.2.1 —

— Effect of Gold Overlayers on Annealed Gold Films —



— Effect of SiO₂ Overlayers on Thin Gold Films —

— Figure 1.2.2 —

and the results of some of this work are shown in figure 1.2.1. Lucas (18) applied the analysis developed by Fuchs and Sondheimer to solve the Boltzmann transport equation for electrons in a two layer structure. In the analysis it was assumed that the layers were formed of thin platelets and that the boundary of the two layers did not interfere with the passage of conduction electrons. The resulting equation for the ratio of the composite film conductivity, $(\bar{\sigma})$, to the bulk conductivity of the first layer, (σ_{bulk}) , is expressed as a function of the ratios of thickness to corresponding bulk mean free path for the layers (k_1, k_2) , the fraction of specular scattering at the top and bottom faces of the composite structure (P, Q) and the actual thickness (a, b) of the layers

i.e.

$$\frac{\bar{\sigma}}{\sigma_{\text{bulk}}} = F(k_1, k_2, P, Q, a, b) \quad (1.2.11)$$

The shunting effect of the overlayer can be eliminated by using an insulator instead of a good conducting overlayer material. Several workers have demonstrated that if a dielectric overlayer is deposited on an annealed gold film, then the resistance of this composite structure increases to a constant value (23) (24) (25) (26). Figure 1.2.2. shows this effect.

1.2.4. Field Effects. On theoretical grounds it appears possible to modulate the conductivity in a thick metallic film by the

<i>Gas</i>	<i>Fraction of Surface Covered</i>	
	<i>at 760 torr</i>	<i>at 10⁻⁸ torr</i>
<i>Hydrogen</i>	$1.16 \cdot 10^{-3}$	$1.5 \cdot 10^{-14}$
<i>Oxygen</i>	$2.9 \cdot 10^{-2}$	$3.8 \cdot 10^{-13}$
<i>Nitrogen</i>	$2.7 \cdot 10^{-2}$	$3.5 \cdot 10^{-13}$
<i>Carbon monoxide</i>	$2.7 \cdot 10^{-2}$	$3.5 \cdot 10^{-13}$

— Table 1.2.1 —

— Surface Coverage with Physical Adsorption —

application of a transverse electric field. Juretschke (21) (27) derived the theoretical relations defining this effect for the Fuchs-Sondheimer-Lucas (18) and the Parrot (20) theories of conduction in thin films. Recently experiments have been carried out (28) which suggest that the effect, if present, is not so pronounced as the theory of Juretschke predicts. This is particularly true at low temperatures, where an enhancement of the effect should take place.

1.2.5. Oxidation and Adsorption. Oxidation and gas adsorption can cause the resistivity of thin metal films to change appreciably. For a given metal these effects are very much dependent on the ability of the metal to form oxides and the reaction kinetics at the film surface with the particular gases involved. Two types of adsorption may take place at the solid-gas interface, namely physical and chemical adsorption. If the temperature and pressure are favourable then physical adsorption will take place irrespective of the type of solid presenting the surface for adsorption. Chemisorption has the nature of a chemical reaction between the surface atoms and the adsorbed gas molecules. The latter type of adsorption is very much dependent on the particular combination of gas molecule and surface atom system being considered. Table 1.2.1. shows the fraction of a surface covered for pressures of 760 torr and 10^{-8} torr for equilibrium physical adsorption at room temperature. From the table it is seen that physical adsorption does not take place to any great

extent at low pressures for the commonly occurring gases. However, oxygen, hydrogen, nitrogen and carbon monoxide can be slowly chemisorbed on metallic surfaces and can be rapidly adsorbed to monolayer coverage even at low pressures. This rapid uptake of gas molecules on a metallic surface can be demonstrated with oxygen and aluminium. A monolayer of oxygen forms on a fresh aluminium surface in a few minutes at a pressure of 10^{-6} torr (29). There is a corresponding increase in the resistivity of a thin aluminium film during oxygen adsorption, which is considered to be the result of the electrons in the metal becoming part of the electron shells of oxygen atoms (30). On further exposure to oxygen the resistance of an aluminium film increases further as a result of oxide growth at the surface. This is a chemical reaction which slowly turns the conducting aluminium into the insulating aluminium oxide to a depth of many monolayers. The aluminium valence electrons are then prevented from taking part in a conduction process, thus increasing the resistance of the film.

1.2.6. Nucleation and Growth. Wood (31) in 1915 showed that the probability of an impinging vapour atom or molecule condensing on a substrate was not unity, but depended on the substrate temperature. He showed that for cadmium on glass it was necessary to lower the temperature to approximately -90°C . before condensation or sticking of the cadmium atoms occurred. This was

the start of the idea of a critical substrate temperature for condensation to take place. Langmuir ⁽³²⁾ put forward in 1916 his theory of condensation and re-evaporation. Unlike Wood, who had thought that the impinging atoms were either reflected or condensed, Langmuir postulated that all atoms were condensed, but only remained on the surface for a time determined by

- a) Intensity of substrate binding forces
- b) Substrate temperature.

If an atom remained on the surface long enough for another atom to collide with it then a pair might be formed, either atom of which would require more energy than before for re-evaporation. Thus, the rate of arrival of atoms at a constant substrate temperature would be closely related to the rate of nucleation. Frankel ⁽³³⁾ in 1924 extended Langmuir's theory of nucleation by suggesting that there existed a critical nucleus size at which the nucleus free energy reached a maximum. Below this critical size, growth is not probable because the free energy of the nucleus would increase with the addition of a further atom, and this is not favoured thermodynamically. Above the critical size growth is probable because the free energy will decrease with the addition of a further atom. From his theory Frankel reasoned that the probability of nucleation would depend on substrate temperatures and incidence rates, which would themselves be mutually dependent. This theory is still considered basically valid, but more modern

ideas of nucleation theory will be considered in chapter 2.

1.2.7. Film Surfaces. The properties of the surface of a thin metallic film may depend on

- a) The type and purity of the metal used.
- b) The preparation, layout and environmental conditions during film formation.
- c) The history of the surface after film formation.

For surfaces prepared by condensation from the vapour phase of the metal, an example can be given for each of these possible dependencies. Since the work function value of a metal tends to be peculiar to that metal (can be from 2 to 6 eV), the type and purity of a metal can greatly influence the electron emission properties of a surface. One atomic percent of titanium in rhenium gives a surface work function approximately 2 eV lower than that of pure rhenium ⁽³⁴⁾. As shown in section 1.2.6., the type and state of the surface onto which the condensation takes place, together with the metal vapour density, largely determines the crystallographic structure of thin films, and hence the crystal orientation at the surface. It has been amply shown for tungsten that the work function is dependent on surface crystal structure. The work function can be over 5 eV if the surface is predominantly of the (110) plane ⁽³⁵⁾, but is approximately 4.55 eV if polycrystalline ⁽³⁶⁾. It was shown in section 1.2.5. that gas adsorption by metal films can rapidly take place even at low

pressures which can modify the electron clouds of surface atoms. This modification results in a surface potential which can increase or decrease the effective work function of the surface depending on how the adsorbed atoms or molecules are integrated with the film surface (30). Huber and Kirk (29) have shown that for water vapour on aluminium, the surface work function is reduced by approximately 1 eV. This reduction with water vapour is a relatively fast process, but much slower processes frequently take place. At atmospheric conditions of pressure and temperature an oxide on aluminium takes approximately one week to grow to a thickness of 20 angstroms (37). During this period the surface potential changes by approximately 350 mV, causing an increase in the effective surface work function by this amount (37).

The crystalline structure and composition of metal surfaces have been investigated by employing various experimental techniques. These techniques can be classified as follows

- (i) The monitoring of surface work function and the study of gas adsorption. This leads to deductions concerning chemical bonding (38) at the surface, and gas molecule interactions with film surface atoms. Eley and Wilkinson (39) and Huber and Kirk (29) have used this technique in the study of aluminium surfaces.
- (ii) Optical microscope. The best resolution possible

of the optical microscope is approximately 5000 angstroms which is inadequate for studies on an atomic scale. However, optical microscopy can show up surface blemishes such as scratches, smears and dust particles.

- (iii) Electron diffraction.
- (iv) Electron microscope.
- (v) X-ray diffraction.
- (vi) Field emission and field ion microscope.

The last four techniques have been discussed by Pashley ⁽⁴⁾ and others ⁽⁴⁰⁾ ⁽¹¹²⁾ and allow surfaces to be examined on an atomic scale. The resolution possible with electron microscopes varies from ~ 100 angstroms with the scanning electron microscope ⁽⁴¹⁾, to less than the spacing of neighbouring atoms (~ 3 angstroms) with the field ion microscope ⁽⁴²⁾. Using electron diffraction it has been possible to determine crystallographic surface structure, and to detect and examine foreign atoms incorporated into metal surfaces. Many workers have been able to examine the growth and adsorption behaviour of metal films using microscopy and diffraction. This has led to an understanding of nucleation, growth and surface phenomena of thin films.

1.3. Application of Thin Films.

Thin films prepared by vacuum deposition have been used for several decades in the optical industry. It is however more recent

that their magnetic and electrical properties have been commercially exploited. The electronics industry in its quest for smaller, cheaper and more reliable electrical circuits has found many uses for thin films. Thin films prepared by vacuum deposition may be active or passive circuit elements, or interconnecting patterns for circuit elements. The function of these films depends on the materials deposited, the sequence of depositions, and the geometrics of the deposits.

Thin film resistors and capacitors having useful values of resistance and capacitance with quite predictable characteristics can easily be manufactured, unlike inductors which can only be made with very small values of inductance. Several review articles (43) (44) have considered such passive elements in detail, with particular reference to chromium alloy resistors and capacitors with silicon oxide as the dielectric material. Active devices directly prepared by vacuum deposition have not yet proved themselves to be serious competitors to the conventional type of device. Great effort has been expended by many workers towards this end. Providing the momentum is maintained, it seems likely that a reliable thin film transistor will eventually be developed. At present the most probable type to become successful appears to be the field effect transistor (45). However, as vacuum techniques become more sophisticated it may become possible to make the necessary thin dielectric layers and single crystal structures

necessary for good hot electron ⁽⁴⁶⁾ and bipolar ⁽⁴⁷⁾ types of device respectively. Making thin-film interconnection "wiring" patterns is relatively straightforward using pure metal films having a thickness of typically a few thousand angstroms. The desired pattern is either vacuum deposited directly, or alternatively, it is etched from a suitable low resistance layer over the entire circuit area.

1.4. Object of this Investigation.

Entire electrical circuits made by vacuum evaporation and deposition provide a very attractive method for circuit manufacture. The only reason for this not being completely realised successfully is the lack of a reliable active device. Thus, it is very important that all of the possible ideas which may lead to its development be examined. In order to be in a position to do this it is essential that the properties of materials which may be used for making devices are well understood. Since vacuum deposition almost certainly results in thin films, (say less than a few thousand angstroms) it is the properties of thin films and not of bulk materials which must be considered. This is an important point because the properties of bulk material are not necessarily the same as these when the material is in a thin film form. A good example of this is the electrical conductivity of metals as discussed in section 1.2.

The state of the surface of a thin film is very closely

related to its electrical properties, and hence it seems only reasonable that any apparatus used for an investigation of electrical conductivity of thin films should have incorporated into it some means of surface examination. Not all of the methods outlined in section 1.2.7. for examining surfaces were available for this work. Only two of these methods were initially available. These were firstly work function monitoring and the study of gas adsorption, and secondly the scanning electron microscope. Optical microscopy was not considered to be a useful possibility because of its resolution limitation.

The materials considered for evaporation were gold, silver and aluminium. Gold and aluminium are frequently used in thin film electronics, and silver not only has several properties similar to gold, but also, like aluminium, is known to form an oxide. Since freshly prepared metal surfaces even under high vacuum can be very quickly covered with oxides, water vapour layers etc., it is essential that a good vacuum be maintained during the investigation period. This appears to make the scanning electron microscope helpful only if either the films are prepared in the microscope itself, or if no significant change occurs to the film surfaces during the transfer period of the film from the vacuum chamber where it is prepared to the microscope chamber. Preparation in the microscope is not considered a possibility for two reasons: firstly the space limitation in the microscope chamber and secondly

the relatively poor vacuum conditions present. Transfer to the microscope for examination is certainly useful because any surface contamination on the film does not usually show up unless it has led to electrostatic charging of the surface. Unfortunately, this use of the microscope would only allow examination of the surface of the film some time after its formation, and not during or immediately after formation while it is still in a high vacuum chamber. Hence the method of monitoring the work function and studying gas adsorption would appear to be best suited for this investigation. Accordingly, much effort has been directed towards developing a suitable method for monitoring the surface work function of thin films. The work function measurements can then yield information on the state of the surface of the metal films, which can be used to explain changes in conductivity of thin metal films during and after their formation by vacuum deposition. It is hoped that this investigation will contribute towards a better understanding of thin metallic films which may someday provide the active devices necessary for a totally vacuum deposited circuit technology.

CHAPTER 2.

THEORETICAL WORK ON THIN FILMS.

Introduction.

It is proposed to monitor the surface work function of thin metallic films to explain electrical conductivity changes which can occur as a result of surface effects. Both the work function and the conductivity of a thin film are very much dependent on its structure and composition. Consequently, this chapter is devoted to outlining theoretical work which can relate work function and conductivity to the structure and composition of thin metallic films. This work is used to establish relationships, suitable for this study, between surface work function values of thin metallic films and their corresponding values of electrical conductivity or resistance. Thus, there are three sections in this chapter. There is firstly the electrical conductivity of thin films with various different types of surface effect present, secondly, work function of different thin film structures, and thirdly the expected variations of conductivity or electrical resistance with surface work function for these films.

2.1. Conductivity.

2.1.1. Bulk Metals. The analysis of electron conduction in metals is made more complex than for bulk conditions if surface effects have to be considered. Thus before examining thin films with these complications it is useful to consider the conduction of electrons in bulk material. It can then be shown how ideas

of conduction for bulk conditions can be suitably modified to take account of, at least qualitatively, the special case of thin films.

Electron waves can propagate through structures having periodic potential fields with no loss of energy provided the structures are exactly regular. Bloch (48) showed that as a result of the wave structure of an electron, it can pass through the periodic potential of a perfect crystal lattice with no loss of energy. If an electric field is applied across a conductor having such a structure, then conduction electrons will constantly increase their energy by an energy exchange process with the applied field until their associated wavelength is such that they interfere with the lattice structure. This will result in the electrons being elastically scattered. However in real crystal lattice structures, scattering caused by deviations from the periodicity of the potential field will result in the electrons losing their ~~energy~~ ^{momentum} by ~~inelastic~~ collisions much more probable ~~than by suffering elastic collisions.~~ Hence these lattice deviations will largely determine the conductivity of metals.

In 1928 Sommerfeld (49) modified the electron gas theory of metals of Drude (1) and Lorentz (50) by replacing the Maxwellian-Boltzmann distribution then used with Fermi Dirac statistics. This led to the following expressions for the carrier density and conductivity of a pure metal

$$n = \frac{8\pi}{3} \left(\frac{m \cdot V_f}{h} \right)^3 \quad (2.1.1)$$

and

$$\sigma = \frac{n \cdot e^2 \cdot \Lambda}{m \cdot v_f} \quad (2.1.2)$$

where σ = Conductivity

n = Number of electrons per unit volume

$-e$ = Electronic charge

Λ = Mean free path of charge carriers

m = Mass of electron

v_f = Fermi velocity

h = Planck's constant

In the above equations the velocity used is the Fermi velocity, (v_f), which is the electron velocity corresponding to the Fermi energy. The mean free path (Λ) is the average distance an electron travels between collisions, and is related to the Fermi velocity through a relaxation time constant (τ).

i.e. $\Lambda = v_f \cdot \tau \quad (2.1.3)$

This relaxation time is classically described as the time an electron would take to come to equilibrium by collisions alone if an applied electric field was suddenly removed. More simply it can be regarded as the mean time between collisions at lattice points where deviations from periodicity exist. The probability of collisions taking place at different types of deviations are statistically mutually exclusive and hence additive. Furthermore,

these probabilities are inversely proportional to the relaxation times associated with each type of deviation, and hence the overall relaxation time $\bar{\tau}$ can be expressed in terms of a sum involving the individual times of each type of lattice imperfection.

$$\text{i.e.} \quad \frac{1}{\bar{\tau}} = \sum_{k=1}^j \frac{1}{\tau_k} \quad (2.1.4)$$

Where τ_k is the relaxation time of the k^{th} type of a total of j distinct types of deviation. From equations (2.1.3) and (2.1.1) the total resistivity, (ρ_0), of a metal is proportional to the inverse of the relaxation time, and hence using equation (2.1.4) the following result is obtained

$$\rho_0 \propto \sum_{k=1}^j \frac{1}{\tau_k} \quad (2.1.5)$$

This is Matheissen's Rule (51) and can be stated as:- the total resistivity of a metal is equal to the sum of individual resistivity values all of which can be accounted for by ascribing to each one a different type of lattice potential imperfection. Matheissen's Rule is valid provided the number of free electrons is not changed by the scattering mechanisms present, and that the vibrational spectrum of the lattice is undisturbed. Sondheimer (52) has shown that provided the free electron theory is applicable, then the error involved in using this rule is usually less than 1%. In practical terms, provided the number of lattice imperfections is less than, say, 10% of the total number of atoms, then Matheissen's

Rule can be used.

The various types of imperfection which occur can be conveniently classified for bulk metals into:-

- (i) Lattice vibrations
- (ii) Lattice defects
- (iii) Lattice impurities

Lattice vibrations are caused by thermal energy in the lattice and are characterised for each metal by a Debye temperature, (Θ_D). The temperature corresponds to the maximum frequency, ν_D , (the Debye frequency) in the frequency spectrum of lattice vibrations, and related to ν_D by

$$h \cdot \nu_D = k \cdot \Theta_D \quad (2.1.6)$$

where h = Planck's constant

k = Boltzmann's constant

The contribution to the total resistivity (ρ_T) as a result of lattice vibrations is temperature, (T), dependent but provided that $T \gg 0.2 \cdot \Theta_D$, then the relationship is

$$\rho_T \propto T \quad (2.1.7)$$

which is normally applicable, since Θ_D for most metals is a few hundred degrees Kelvin.

Lattice defects can occur as point defects, dislocation or grain boundaries. The contribution to the total resistivity as a

result of structural defects, (ρ_s), is virtually independent of temperature for reasonably small temperature excursions of say less than 100°C ., and, also provided that the lattice vibration spectrum is not altered.

~~Lattice~~ **I**mpurity scattering occurs when foreign atoms are present in a metal. Their effect on resistivity can be very pronounced. One atomic per cent impurity may double the total resistivity. The contribution to the total resistivity as a result of impurities, (ρ_i), is virtually independent of temperature for most materials and impurities.

Hence by Matheissen's Rule the total resistivity of a bulk metal is given by

$$\rho_o = \rho_i + \rho_T + \rho_s \quad (2.1.8)$$

When very thin samples of a metal are considered then two other terms must be added to the right hand side of the equation (2.1.8). They are firstly, a term to allow for the influence of the boundary on the resistivity, (ρ_b), and secondly a term representing the contribution to the total resistivity caused by the method of preparation, (ρ_p) ⁽²⁵⁾. Thus the complete resistivity expression for thin metal films, provided Matheissen's Rule can be applied, is

$$\rho_o = \rho_T + \rho_s + \rho_i + \rho_b + \rho_F \quad (2.1.9)$$

2.1.2. Surface Effects on Continuous Films. Thin continuous metallic films prepared by evaporation and deposition of the metal in vacuum can have their resistivities changed by one or more of the following processes:-

- a) Heat treatment
- b) Overlayers formed by vacuum evaporation and deposition of the overlayer material.
- c) Gas adsorption and oxide growth
- d) Alloy formation on the surface, and foreign atoms diffused into the film.

Other processes exist which could cause changes in resistivity, but only the above are considered in this study.

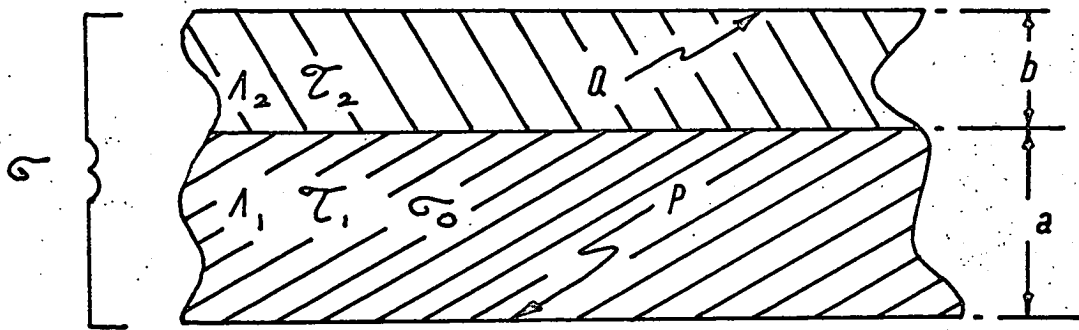
a) Heat Treatment has been shown by Meyer (53), Lucas (19) and others (54) to have an effect on the conductivity of thin gold films grown on an amorphous substrate with a nucleating layer of bismuth oxide. The change in conductivity as a result of the heat treatment can be explained in terms of the scattering parameter, (P), in the Fuchs-Sondheimer (13) (14) theory changing from a value of close to zero to approximately 0.8. Structurally the gold film grain size increases on annealing, thus tending to go from polycrystalline to single crystal, although the latter is never actually achieved in practice. Meyer (53) made a detailed study of this annealing process and concluded that oxygen, and possibly other gases, interact with a hexagonal surface phase on the gold film which acts as a wetting agent in the reduction of

surface tension forces. By using bismuth oxide as the nucleating layer, films which have conductivity values of close to bulk can be obtained even at thicknesses of only 60 angstroms (19). It is probable that a reaction with the oxygen in the nucleating layer is responsible for these thin gold films being continuous. The conductivity values of a series of thicker films prepared by Chopra, Bobb and Francombe (55) by sputtering gold on/to mica substrates confirm that the scattering parameter, (P), is close to unity for single crystal films. For polycrystalline gold films deposited on cold substrates the conductivity values measured by these authors suggested a low value of scattering parameter, and many structural defects which also contributed to the high resistivity

For more crystalline deposits on hot substrates the film structure is still considered to be largely responsible for the resistivity-thickness variation. Hence these authors do not attribute all of the change in resistivity to only one cause when thin gold films are annealed. It is reasonable to assume that the resistivity attributable to lattice defects, especially grain boundaries, in a thin polycrystalline metallic film will also change when the grain size is substantially increased. No experiments have been reported which attempt to differentiate between the effects of surface scattering changes and those of grain boundary changes when thin gold films are annealed in air.

(56)

Feldman, however, reported that the effective mean free path



— Figure 2.1.1 —

— Continuous Metallic Overlayer Structure —

- a Thickness of underlayer
- b Thickness of overlayer
- λ_1 Mean free path in underlayer
- λ_2 Mean free path in overlayer
- Q Scattering parameter at upper surface
- P Scattering parameter at lower surface
- σ Composite film conductivity
- σ_0 Bulk conductivity of underlayer
- τ_1 Relaxation time constant in underlayer
- τ_2 Relaxation time constant in overlayer

should be essentially that of the grain size when the grain size is small in all dimensions. This is largely confirmed for bismuth, which has a very long mean free path at room temperature, where an approximately linear relationship between crystallite size and conductivity was obtained.

b) Overlayers deposited on thin films may be of conducting or dielectric material, and may be continuous or discontinuous. For a continuous overlayer on a continuous metallic film the theory of Lucas (19) for the conductivity of a two layer structure can be employed by making the following assumptions:-

- i) Electron-phonon collisions are diffuse.
- ii) Parameters (P) and (Q) give the fractions of conduction electrons specularly scattered at the film surface.
- iii) No scattering of conduction electrons occurs at the interface of the two layers.
- iv) The composite films are infinite in the x and y directions, and of uniform thickness in the z direction.

A complete derivation of the equation for conductivity changes with continuous metallic overlayers in a film structure as shown in figure 2.1.1. has been given by Lucas (23)

$$\frac{\sigma}{\sigma_0} = f(\tau_1, \tau_2, \Lambda_1, \Lambda_2, a, b, P, Q) \quad (2.1.10)$$

The significance of the symbols in equation (2.1.10) is explained

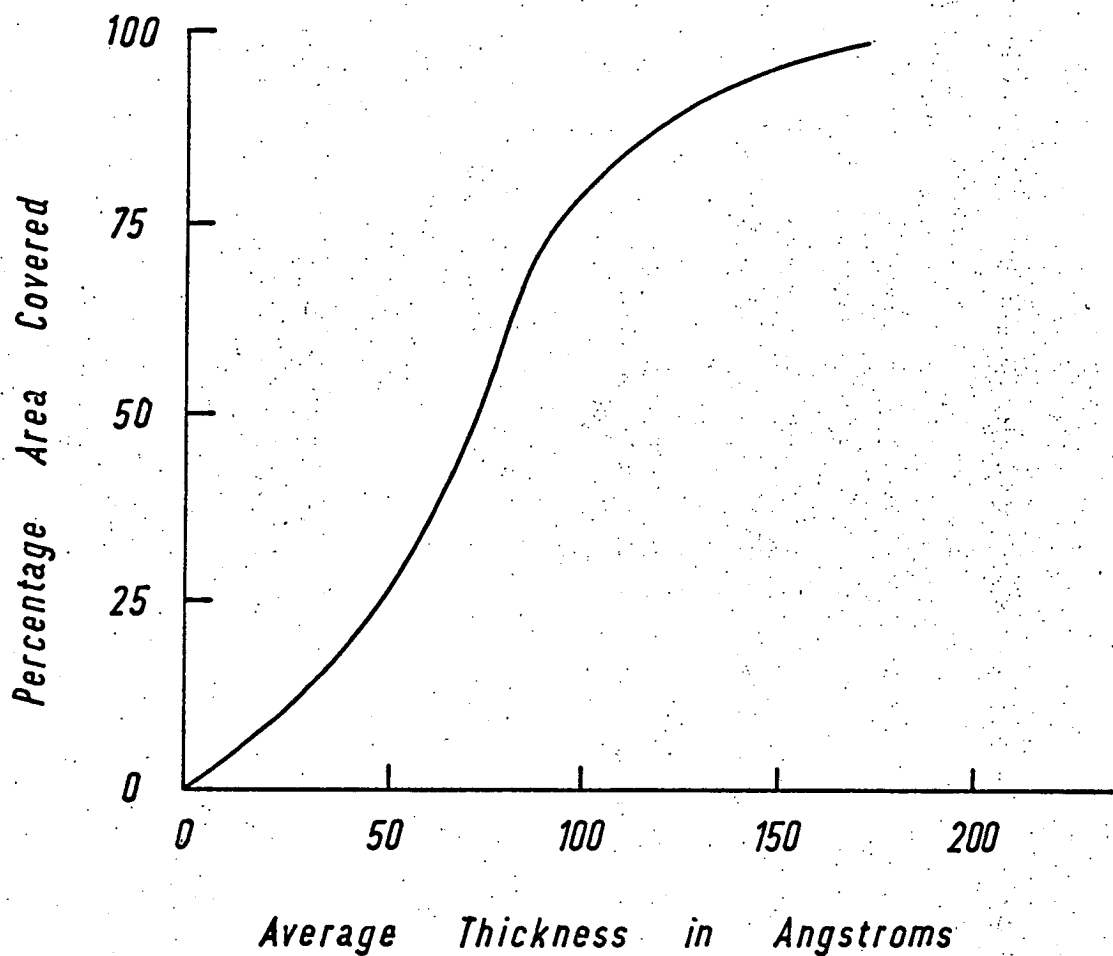
in figure 2.1.1.

If the overlayer is of a dielectric material, then the thickness, (b), is effectively equal to zero for all x and y, and equation (2.1.10) reduces to

$$\frac{\sigma}{\sigma_0} = f(\Lambda, a, P, Q) \quad (2.1.11)$$

Thus provided the overlayer is continuous, the above theory can yield calculated values of conductivity which agree with experimental results. However, if the overlayer is discontinuous then the assumption that the layer thicknesses are uniform for all values of x and y may not be reasonable. Nucleation and growth of an overlayer of gold on a continuous film of annealed gold has been shown (58) to go through stages of nucleation, island formation, island coalescence, and after a mean overlayer thickness of about 100 angstroms, an overlayer structure is obtained which is almost continuous. A very good demonstration of the fact that a quite separate gold layer grows on an annealed gold film surface is that the gold overlayer can be stripped off with Scotch Tape (58). Thus for overlayers of low mean thickness, say less than 100 angstroms, care must be taken in applying equations (2.1.10) and (2.1.11) since the overlayer thickness, (b), may vary from zero to over 100 angstroms over the surface. For dielectric overlayers it will be more important how much of the underlayer surface is covered with dielectric, rather than the mean thickness of the overlayer.

Curve from Campbell - ref. 24



— Figure 2.1.2 —

— Deduced Variation of Thickness with Coverage —

Referring to figure 1.2.2. the shape of the curves will be dependent on the growth process of the dielectric on the surface of an annealed gold film. On a qualitative basis, it is reasonable that for conducting overlayers the actual growth process will largely determine the change in conductivity of a composite structure, at least up to the point where the overlayer approaches continuity. Present theory however, because of its formulation, usually results in conductivity or resistance changes being shown graphically as a function of the mean overlayer thickness. Ascribing a scattering parameter (P) to a film surface and postulating that it changes with the addition of an overlayer, at least for the case of thin annealed gold films on bismuth oxide, as a function of the mean overlayer thickness, may be better described as follows. The original annealed gold film is almost a single crystal with a surface scattering parameter (P) of approaching unity, which results in the conductivity value being close to that of bulk. When an overlayer is grown on the surface it will cover an increasing area of it as the mean thickness increases. Figure 2.1.2. gives an indication of how this might take place (24). If the overlayer is polycrystalline, conducting and discontinuous, then diffuse scattering will occur in the overlayer islands, but specular scattering will still occur at the areas of the surface where no overlayer has yet grown. The result is an average scattering parameter having a value starting at approximately unity and decreasing as the overlayer grows, but is the result of the two distinct values for different areas of the film structure. Depending on how polycrystalline the overlayer is,

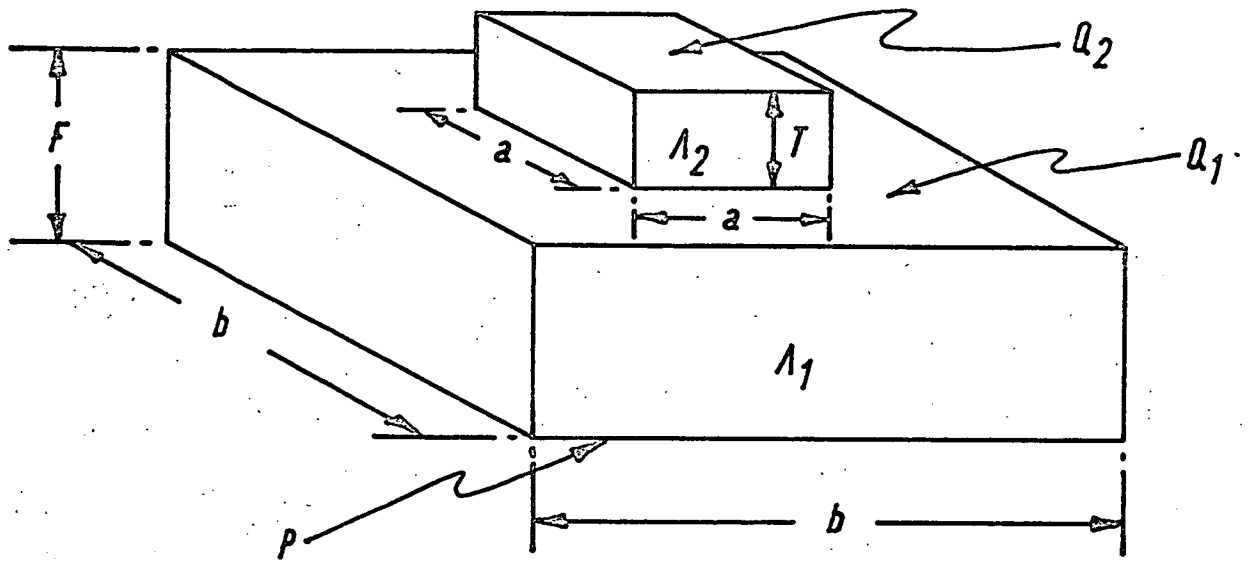
the average scattering parameter may be any value between unity and zero as the mean thickness increases. For a dielectric overlayer the almost single crystal (gold) film will be disrupted at the areas on the surface where deposition and overlayer growth has taken place. This will result in the scattering parameter being something less than unity for these areas. A consequence of this is that the average scattering parameter will be reduced, and hence the resistivity of the (gold) film will increase. Experimental results for silicon monoxide overlayers on annealed gold films can be explained by assuming that the scattering parameter is unity for the original film, but is approximately 0.8 at areas covered with dielectric. Figure 1.2.2. shows experimental curves for resistivity changes with dielectric overlayers on gold films. The resistivity in each case, as expected, reaches a constant value corresponding to complete coverage of dielectric.

The mean overlayer thickness at which the resistivity first becomes constant varies for these films from 20 to 50 angstroms. This is the order of thickness at which it is expected that a vacuum evaporated material such as silicon oxide would form a practically continuous layer on a crystalline substrate. Experimental results for gold overlayers on annealed gold films are complicated by the fact that the overlayer has a shunting effect on the film resistance since conduction electrons are considered free to cross the interface without hindrance and enter the conduction band of the overlayer material, and vice versa.

However, the results can still be explained by having two distinct scattering parameter values for different areas of the films. The explanation is consistent with the expected thickness of an overlayer before continuity is obtained. Figure 1.2.1. shows that at an overlayer thickness of approximately 20 angstroms, on an 80 angstrom thick annealed gold film, the rate of change of resistance as a result of changes in the electron scattering is equal to that as a result of the shunting effect of the overlayer. Meyer (58) found that for such structures the overlayer only became continuous for a mean overlayer thickness greater than 120 angstroms. The derivation of a mathematical relationship between the growth process of a conducting overlayer on a metallic film and the resulting change in conductivity involves a great many assumptions. These assumptions concern the following points:-

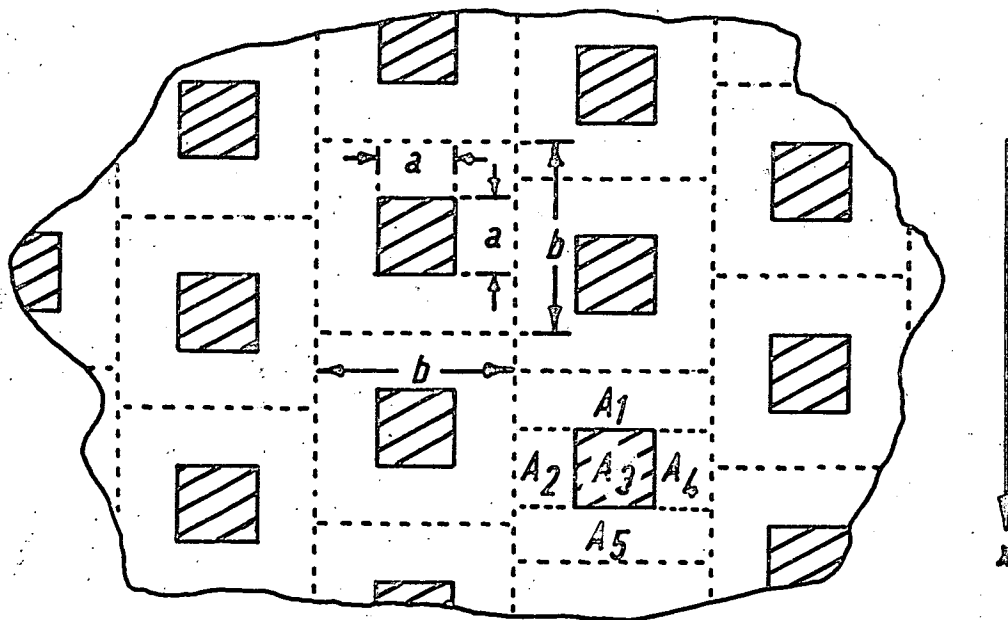
- i) The size, shape and density of the overlayer islands, and how they change up to the formation of a continuous overlayer.
- ii) Conductions in islands which may have dimensions all less than the bulk mean free path of conduction electrons in the bulk material.
- iii) Contact potentials at the layer interface, and the possibility of islands being charged.

In principal it is possible to derive a conductivity equation to take account of the overlayer growth process. In order to show that such an equation can yield conductivity changes in agreement



— Figure 2.1.4 —

— Basic Unit of Island Model —



— Figure 2.1.3 —

— Typical Plan View of Island Model —

with experimental results, an equation for a particular assumed type of overlayer growth is now derived.

Consider a section of a thin metallic film as shown in figure 2.1.3. with a discontinuous overlayer (shaded areas) having a unit structure as shown in figure 2.1.4. The electrical resistance in the x direction is made up of two terms, one for the parts of area A_1 , A_2 , A_4 and A_5 with no overlayer, and another for the part of area A_3 with an overlayer of thickness T . In the parts with no overlayer the electron mean free path is Λ_1 , and the scattering parameter at the upper and lower faces is Q_1 , and P respectively. The resistivity of these parts, (ρ_u), is given by

$$\rho_u = f_1(Q_1, P, F, \Lambda_1) \quad (2.1.12)$$

Where (f_1) is a function which can be easily derived from equation (1.2.7)

For the parts with an overlayer of thickness T the electron mean free path in the overlayer is Λ_2 , Q_2 is the scattering parameter at the upper face, and the overlayer/underlayer interface is considered completely transparent to the passage of electrons. The resistivity for these parts, (ρ_T), assuming completely spectral electron scattering on the vertical sides of the square islands, is given by

$$\rho_T = f_2(F, T, \Lambda_1, \Lambda_2, P, Q_2) \quad (2.1.13)$$

Where (f_2) is a function which can be easily derived from equation (1,2,11).

Combining equations (2.1.12) and (2.1.13) the resistance (R_T) of one unit, as shown in figure 2.1.3. of the section considered is

$$R_T = R_1 + \frac{R_2 R_3 R_4}{R_2 R_3 + R_3 R_4 + R_2 R_4} + R_5 \quad (2.1.14)$$

R_1 is the resistance of area A_1 in x direction.

R_2 is the resistance of area A_2 in x direction.

R_3 is the resistance of area A_3 in x direction.

R_4 is the resistance of area A_4 in x direction.

R_5 is the resistance of area A_5 in x direction.

Substituting for R_1 to R_5 in equation (2.1.14) yields

$$R_T = 2 \frac{\rho_u \left(\frac{b}{2} - \frac{a}{2}\right)}{b.F} + \frac{\rho_u \rho_T / F(F+T) \left(\frac{b}{2} - \frac{a}{2}\right)}{\frac{2\rho_T}{F+T} + \frac{\rho_u \cdot a}{F \left(\frac{b}{2} - \frac{a}{2}\right)}} \quad (2.1.15)$$

Thus, the ratio of the resistance with an overlayer thickness (T), to the resistance with no overlayer, (R_0), is after simplification

$$\frac{R_T}{R_0} = \left(1 - \frac{a}{b}\right) + \left\{ \frac{1}{\left(\frac{b}{a} - 1\right) + \frac{\rho_u \cdot (F+T)}{\rho_T \cdot F}} \right\} \quad (2.1.16)$$

But recognising from figure 2.1.4. that the fractional area (θ) of the underlayer covered by the overlayer is

$$\theta = \frac{a^2}{b^2} \quad (2.1.17)$$

and

$$(1 - \theta^{1/2}) = \left(1 - \frac{a}{b}\right) \quad (2.1.18)$$

equation (2.1.16) can be written as

$$\frac{R_T}{R_0} = (1 - \theta^{1/2}) + \left\{ \frac{\theta^{1/2}}{(1 - \theta^{1/2}) + \theta^{1/2} \frac{P_1}{P_T} \left(\frac{F+T}{F}\right)} \right\} \quad (2.1.19)$$

In order to relate the actual overlayer thickness (T) to the mean overlayer thickness (t), it is necessary to express the fractional area, (θ), in terms of the thickness (T). A reasonable approximation to the shape of the growth curve shown in figure 2.1.2 is

$$\theta = (1 - e^{-t/\tau}) \quad (2.1.20)$$

Where τ is a constant dependent on the materials and growth conditions considered. Several published works show that equation (2.1.20) can be in good agreement with experimental results (59) (60) (58).

Using equation (2.1.20) the thicknesses (T) and (t) are related by

$$T = \frac{t}{1 - e^{-(t/\tau)}} \quad (2.1.21)$$

Substituting for (θ) and (T) from equations (2.1.20) and (2.1.21) respectively in equation (2.1.19) yields

$$\frac{R_T}{R_0} = \left\{ 1 - (1 - e^{-t/\tau}) \right\} + \left\{ \frac{1 - e^{-t/\tau}}{(1 - e^{-t/\tau}) - 1 + e^{-t/\tau} + \frac{P_0}{P_T} (F(1 - e^{-t/\tau}) + t)} \right\} \quad (2.1.22)$$

The plan view of an area of a film made up of a great number of the sections shown in figure 2.1.4. is sketched in figure 2.1.3. The fractional change in resistance with overlayer growth of such a composite film is described by equation (2.1.22), just as for an individual section, provided the film area considered is made up of many individual sections.

Assuming $\tau, F, \Lambda_1, \Lambda_2, P, Q_1$ and Q_2 to be constants it follows from equation (2.1.22) that the fractional change in resistance is a function of only the mean overlayer thickness, (t) . In order to compare values calculated from equation (2.1.22) with experimental results, the particular case of a gold overlayer on an annealed gold film is considered with the following values ascribed to the required parameters used in figure 2.1.4.

$$\begin{aligned} F &= 60 \text{ \AA} \\ \Lambda_1 &= 400 \text{ \AA} \\ \Lambda_2 &= 250 \text{ \AA} \\ P &= 0.9 \\ Q_1 &= 0.9 \\ Q_2 &= 0.0 \end{aligned}$$

Figure 2.1.5. shows how the ratio R_T/R_0 varies as the mean

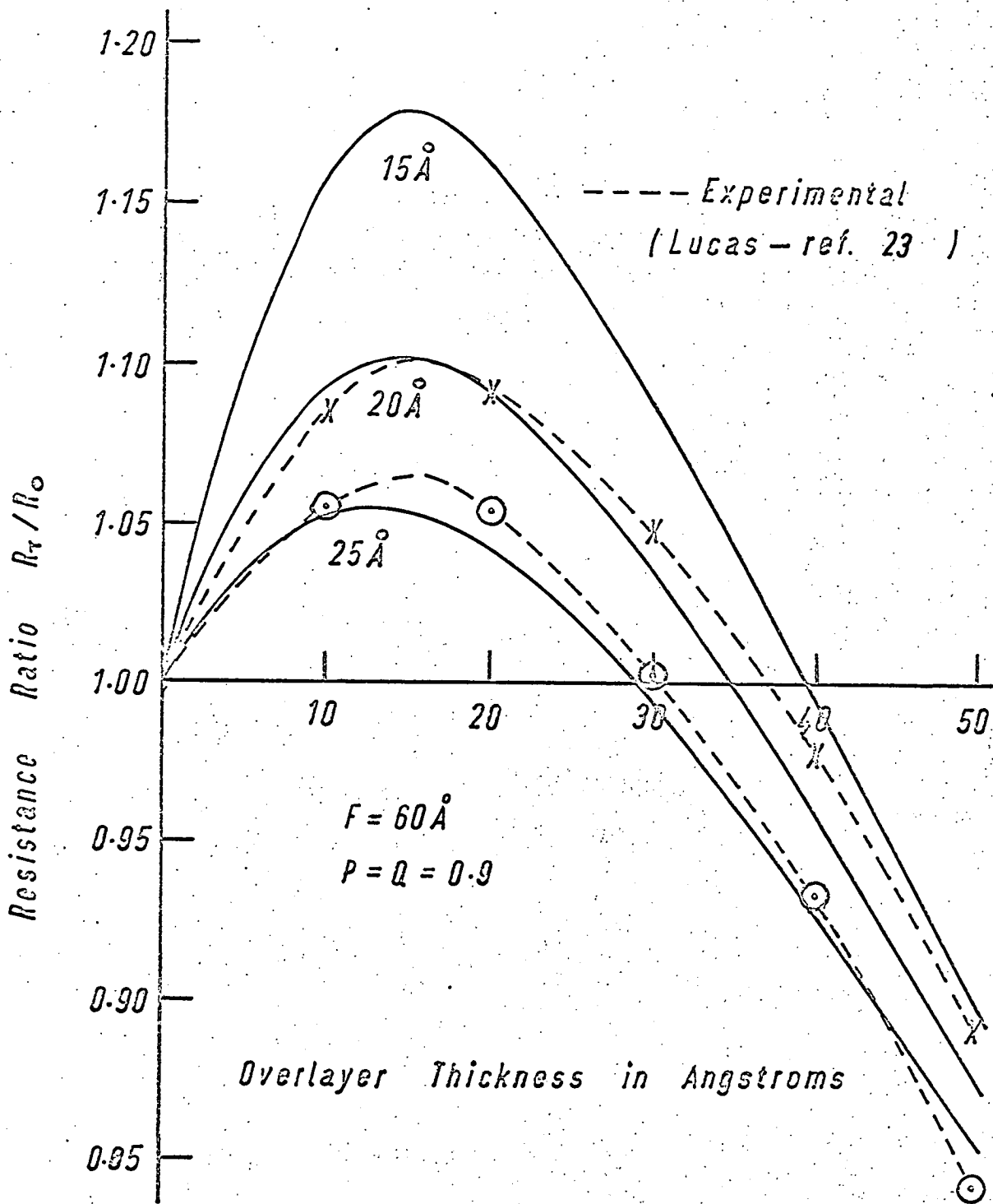
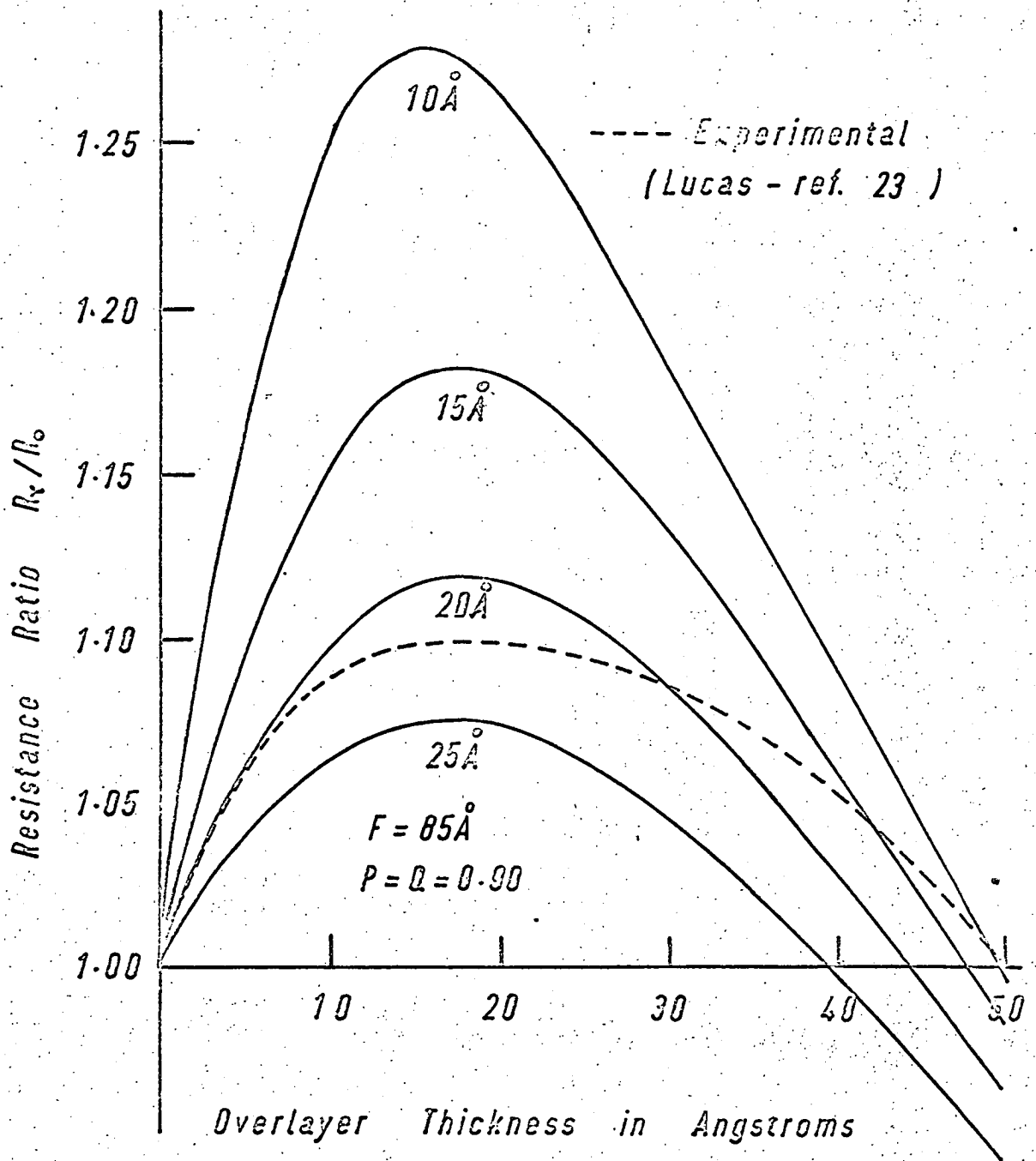


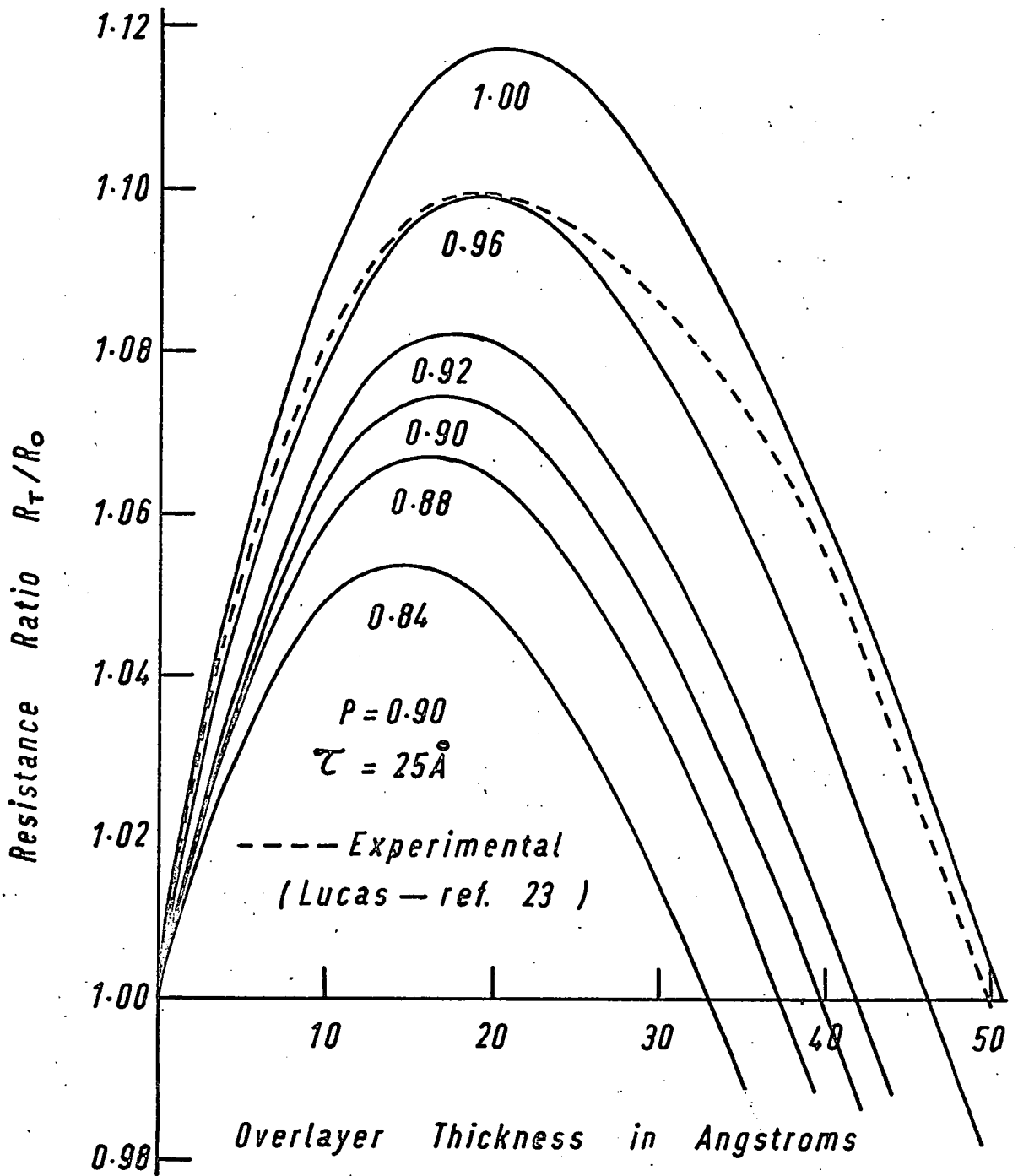
Figure 2.1.5

Effect of τ on Resistance Changes



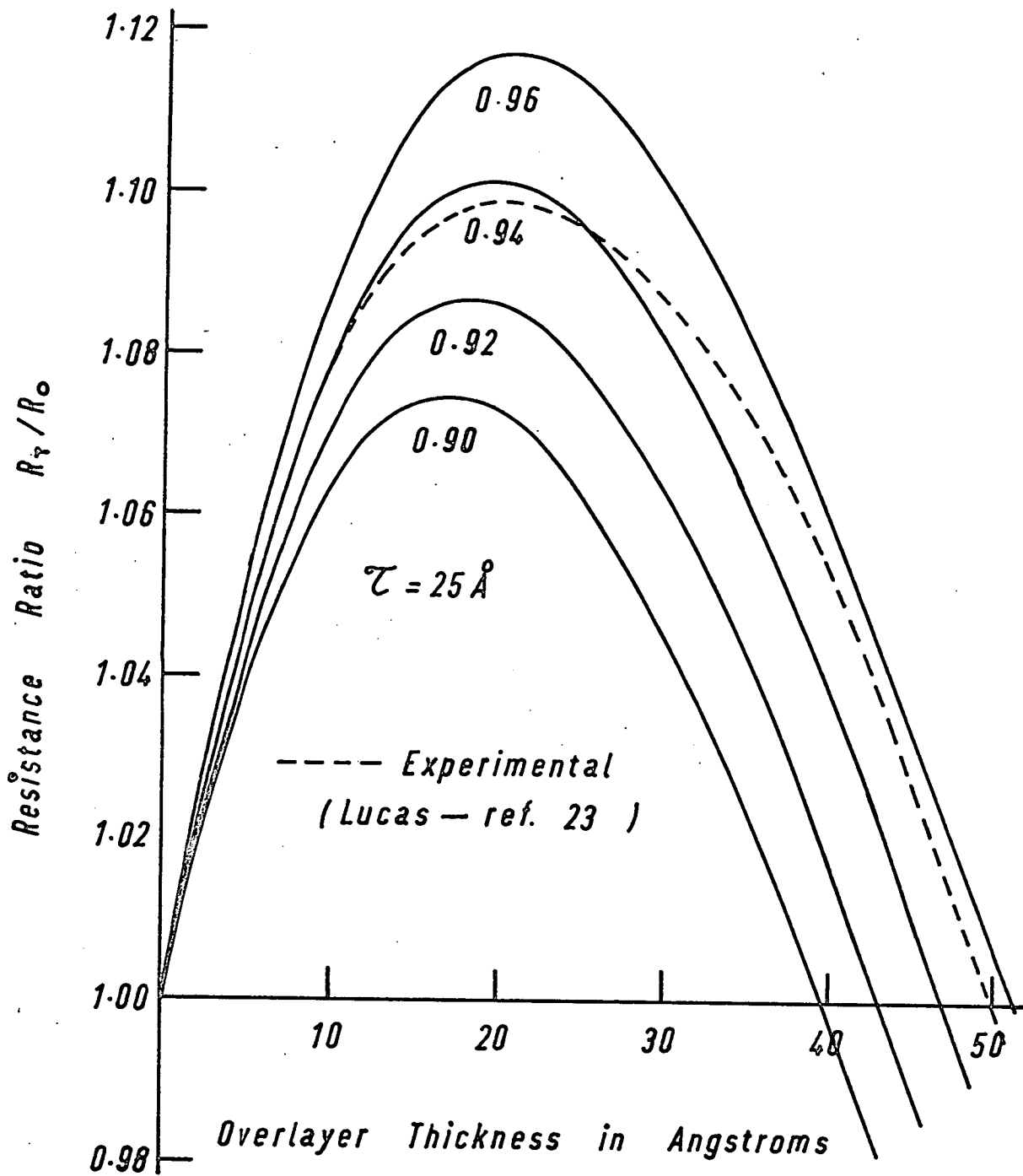
— Figure 2.1.6 —

— Effect of τ on Resistance Changes —



— Figure 2.1.7 —

— Effect of Q ($P=0.9$) on Resistance Changes —



— Figure 2.1.8 —

— Effect of $P (=Q)$ on Resistance Changes —

overlayer thickness increases from zero to 50 angstroms for three different values of τ . Experimental points obtained from reference (23) are also drawn on this graph. The best-fit lines through these points lie close to the theoretical curves, which make the assumption of the form of equation (2.1.20) for the overlayer growth appear reasonable.

Agreement between the predicted resistance changes for a thicker film, (85\AA), and experimental results, is not quite so good as the agreement for 60\AA films, the results for which are shown in figure 2.1.5. Figure 2.1.6. shows the resistance ratio drawn as a function of overlayer thickness, (t), for four values of τ . The experimentally found curve (23) (61) approximately follows the shape of the theoretical curve for $\tau = 25\text{\AA}$, but is not very close to it, and hence figure 2.1.7. was drawn up for various values of (P) with $\tau = 25\text{\AA}$. It can be seen that a value of $P = 0.96$ gives a better fit to the experimentally found curve than for $P = 0.9$ on figure 2.1.6. For figures 2.1.5., 2.1.6. and 2.1.7. it was assumed that $Q_1 = 0.9$ in agreement with others (23) (58) (16) (17). If however, (Q_1), is made equal to (P), then for $\tau = 25\text{\AA}$ figure 2.1.8. shows that the curve generated for a value of $P = 0.94$ is a reasonable fit to the experimental curve. Hence the simple overlayer model based on equation (2.1.20) can be made to fit experimental results by selecting suitable values for the scattering parameters (P) and (Q_1) with $Q_2 = 0$.

c) Gas Adsorption can have a marked effect on the conductivity of thin metallic films. Of the commonly occurring gases, oxygen is perhaps the most important since it is known to chemisorb readily on many metal surfaces and can cause substantial resistance changes (29) (39). With sufficient time exposure to oxygen, or gases containing oxygen, some metals oxidise to a depth of many monolayers in a surface layer, with a resulting increase of electrical resistance. When gas molecules are chemisorbed on a metallic surface then the conduction electrons of surface metal atoms are influenced by the presence of chemisorption bonds. This influence can be quantified by defining an electron requirement for the metal. It is defined as the number of conduction electrons removed from the metal per chemisorption bond. (30). An equation for the number of molecules or atoms adsorbed can be derived as follows. For gas molecules having an average velocity (V_a) and a density of n per unit volume, then the number of collisions, (N), that the gas particles have with a planar surface within the volume is

$$N = \frac{1}{4} \cdot nV_a \text{ collisions/unit area/unit time} \quad (2.1.23)$$

As given by classical kinetic theory.

If the collisions occur at a surface which is not planar on an atomic scale, then equation (2.1.23) is modified to

$$N^1 = \Gamma \frac{1}{4} \cdot nV_a \text{ collisions/unit area/unit time} \quad (2.1.24)$$

Where Γ is the roughness factor, which is defined as

ratio of actual surface area to apparent surface area.

After a time (t) a fraction (θ) of the surface is covered with adsorbate, and in a further time (Δt) the surface density of adsorbed gas particles, (d), increases by an amount (Δd) given by

$$\Delta d = \Delta t \cdot N' \cdot S(\theta) \quad (2.1.25)$$

Where $S(\theta)$ is the sticking coefficient which is defined as, the probability of an impinging gas particle being adsorbed when the fractional surface coverage is θ . Taking Δt to the limit, equation (2.1.25) becomes

$$d = \int N' \cdot S(\theta) \cdot dt \quad (2.1.26)$$

For most cases the sticking coefficient, $S(\theta)$, decreases as the fractional coverage, θ , increases, until it becomes equal to approximately zero at $\theta = 1$. According to equation (2.1.25) this represents a stable arrangement of the adsorbate and adsorbant gas particles since no further adsorption will take place. At equilibrium, providing the adsorbing particles do not diffuse into the bulk, the number of molecules or atoms adsorbed is dependent on the number adsorbed per active site, and the number of adsorption sites available.

The electron requirement (E_r), has been shown to be a function of fractional coverage, (θ) (29). Thus the increase in electrical resistance, ΔR , which occurs when a surface with, (d),

adsorbed gas particles constituting a fractional coverage (θ) adsorbes a further Δd , is given by

$$\Delta R \propto \Delta n \cdot E_r \quad (2.1.27)$$

Using equation (2.1.25) and assuming that the collision frequency N^1 is a constant (this is true for a constant temperature, pressure and volume of gas) the expression for the change in resistance becomes

$$\Delta R \propto S(\theta) \cdot E_r \cdot \Delta t \quad (2.1.28)$$

Assuming that the adsorption is taking place on a thin metallic film having a resistance R_0 before adsorption started, then on taking Δt to the limit the equation for the total resistance R of the film after a time t is

$$R = R_0 + C \int_0^t S(\theta) \cdot E_r \cdot dt \quad (2.1.29)$$

Where C is a proportionality constant. Equation (2.1.29) is applicable for all $\theta \leq 1$, i.e. up to monolayer coverage. When the quantity of gas adsorbed corresponds to more than one monolayer then one of two different processes is taking place. The adsorbing particles may be forming an overlayer on the adsorbing surface, or the adsorbed particles are being incorporated into the bulk of the adsorbate. An example of the first process is the adsorption of water vapour onto an aluminium surface already pre-exposed to

oxygen to monolayer coverage (29). For the second process a good example is the oxidation of a metal surface, where an oxide may form to the thickness of many monolayers with sufficient oxygen exposure. The electron requirement is proportional to the number of oxygen molecules or atoms adsorbed during an oxidation process, when each will remove the same number of conduction electrons. Hence the increase in electrical resistance of a thin metallic film as a result of oxidation is proportional to the number of oxygen atoms incorporated into the oxide layer.

d) Alloy Formation and Foreign Atom Diffusion occur when metal atoms are deposited on metal substrates. A metal atom can do one of the following when it condenses on a metal substrate:-

- i) Form, with other condensing atoms, an overlayer on the substrate.
- ii) Re-evaporate from the surface.
- iii) Form an intermetallic compound with the surface atoms of the substrate.
- iv) Diffuse into the bulk of the substrate.

Case (i) has already been considered in this section, and case (ii) is negligible for metal vapour condensing on cold substrates. The effects of cases (iii) and (iv) on the electrical conductivity of thin metallic substrates are now examined.

Pashley (4) has described the results of experiments which show that alloying can take place even when the substrate

temperature is such that bulk diffusion of the metals is negligible. For very low mutual solubility of the two metals then the condensing metal atoms form nuclei on the substrate surface. An example of this is gold on silver surfaces. However, if the two metals are reasonably soluble then alloying occurs. Experimental evidence obtained by Newman and Pashley (62), and others (63), for the deposition of metal layers on metal substrates suggests that condensing metal atoms can penetrate a substrate metal surface slightly, resulting in a region of mixed components being formed at the interface. Shirai et alia (63) have shown that, for example, aluminium deposited on silver, the surface region is in the form of intermetallic compounds of the substrate and condensing atoms. Thus with the metals used in this work it is expected that appreciable alloying will take place when aluminium is deposited on silver film surfaces, but not for gold on silver or vice versa. The effect of surface alloying on the electrical resistivity of a thin film can be attributed to two processes. One of these is the reduction of the mean free path of the electrons as a result of impurity scattering in the surface region where alloying has taken place. Assuming the Fuchs-Sondheimer-Lucas (18) theory, the other is a change in the scattering parameter, (P) , at the film surface. Provided (P) is not zero, (completely diffuse surface scattering), before alloying takes place, it is expected that (P) will be decreased. Both processes cause an increase in resistivity for thin films, which may be appreciable if either the change in (P) is large or the depth of alloying represents a significant

proportion of the film thickness.

The diffusion of deposited metal atoms into a metallic substrate is dependent on the particular combination of metals used, and the temperature of the substrate. Deposited atoms, when diffused into the crystal lattice of a metal, cause an increase in the electrical resistivity as already discussed in section 2.1.1. In this work, changes in resistivity of metallic films which are attributable to the diffusion of deposited atoms into the bulk of metallic substrates are not desired. Hence, in order to minimise this effect, it is preferable to have substrates at as low a temperature as possible and to use only very pure metals.

2.1.3. Discontinuous Films. Conduction in an aggregated film structure has been shown to be a thermally activated process (6). However, the values of activation energy found by experiment were too small to be explained on the basis of the work function of the metal constituting the islands. Neugebauer and Webb (64) in 1962 explained the activation energy as that energy required to charge an island by making available one electron for conduction. It was proposed that direct quantum mechanical tunneling of the electron then took place to an adjacent island. This theory was modified by Swanson (5) who made allowance for possible tunneling between all four combinations of charged and neutral islands. Both theories give approximately the same results for conductivity values, but differ significantly in the relationships between aggregate dimensions and temperature coefficient of resistance. Hartman (8)

in 1963 accounted for the activation energy in a different way. He postulated that because of their dimensions, there existed in the islands quantised electronic states with significant level spacing. Since tunneling can only take place between equal energy levels, the electrons would firstly be raised to the energy level corresponding to an adjacent island, and then tunneling would take place between the neutral particles. Also in 1963 Wei ⁽¹⁰⁾ compared conduction in an aggregated structure to that in a semiconductor. He suggested that the metallic microparticles act as donor impurities and the substrate contributes acceptor impurities. The density of these impurities then determines the activation energy. Following on from this work Hill ⁽⁶⁵⁾ and Herman and Rhodin ⁽⁶⁶⁾ investigated the possibility of the substrate playing a significant part in the conduction process. Both conclude that conduction takes place through the substrate, and not, as had been earlier thought, through the free space between the particles.

Although all the above theories have different explanations for the conduction process, they result in a common expression for the conductivity σ which can be written as

$$\sigma = K.P.\exp\left(-\frac{E}{kT}\right) \quad (2.1.30)$$

Where K is a constant

P is the electron tunneling probability

E is an activation energy.

k is Boltzmann's constant

T is the absolute temperature

Hill (9) (67) has recently developed a theory to account for the conductivity of aggregated metal films using quantum electronic tunneling and thermionic emission theories. He considers all combinations of islands and gap sizes, and the results can be summarized as:-

- i) Small particles and small gaps. The activation energy is high and a tunneling process is dominant because of a short tunneling path length.
- ii) Small particles and large gaps. Activation energy is high and thermionic emission takes place into the conduction band of the substrate. If the gap is larger than the mean free path of charge carriers in the substrate then the conduction is limited by bulk conduction in the substrate.
- iii) Large particles and large gaps. Activation energy is required for either thermionic emission or bulk conduction in the substrate. Conductivity is limited by the gap independence.
- iv) Large particles and small gaps. Activation energy is small and the conductivity is approaching that of the bulk material.

In order to see how the conductivity of an aggregated structure varies with temperature equation (2.1.30) is

differentiated with respect to temperature T . Assuming that K , P and E are independent of temperature the result is

$$\frac{d\sigma}{dT} = + \frac{E}{kT^2} K.P. \exp\left(-\frac{E}{kT}\right) \quad (2.1.31)$$

i.e. the temperature coefficient of resistance is negative for an aggregated structure, unlike a bulk metal which has a positive coefficient. Thus a structure of type (iv) above can have a temperature coefficient of resistance which may be positive, negative or even zero.

2.2. Work Function.

2.2.1. Definition of Work Function. The term work function first appeared in scientific literature approximately fifty years ago (68), although the concept was implied in many earlier works. Work function has been defined in a variety of ways and has several physical interpretations. However, these definitions and interpretations are, with only a few exceptions, complementary to each other. The true work function, ϕ , of a uniform surface of an electronic conductor is defined by Herrings and Nichols (69) as the difference between the electrochemical potential, $\bar{\mu}$, of the electron just inside the conductor and the electrostatic potential energy, $-e\bar{\phi}_a$, of an electron in the vacuum just outside it.

$$\text{i.e.} \quad \phi = -\bar{\phi}_a - (\bar{\mu}/e) \quad (2.2.1)$$

The quantity $\bar{\mu}$ is dependent not only on volume properties of a body, but also on the surface and external conditions. A chemical potential, μ , can be defined however, which is independent of surface and external conditions by

$$\mu = \bar{\mu} + e\bar{\phi}_c \quad (2.2.2)$$

Where $\bar{\phi}_c$ is the electrostatic potential inside the conductor.

Substituting for $\bar{\mu}$ from equation (2.2.2) in equation (2.2.1) yields

$$\phi = \left(\bar{\phi}_c - \bar{\phi}_a \right) - (\mu/e) \quad (2.2.3)$$

Thus the work function can be expressed as the sum of two terms, one of which is dependent upon surface state and volume properties, the other dependent on the structure of the interior only. Alternatively work function can be defined as an ionisation energy ⁽¹⁰⁾. For example Gyftopoulos and Levine ⁽⁷¹⁾ define the true work function of a metallic surface as the minimum quantity of energy required to remove an electron from the surface of the metal at 0°K. This definition will apply at temperatures greater than 0°K provided the electron removed has an energy corresponding to the Fermi energy level of the metal. The latter definition is very similar to that used by several others ^{(72) (73)}, especially if it is understood that the emitted electron is removed beyond the potential image barrier created by its own removal i.e.

an infinite distance, so that the potential energy of the electron is reduced to zero. Dobretsov and Matskevich (74) have given a rather compelling argument for work function being a predominantly surface rather than bulk property in contradiction to Samsonov et al (75), who believe work function to be definable in terms of bulk properties. Considering the physical interpretation of work function, it becomes apparent that it is the surface state and composition which is all important.

Although work function has been explicitly defined by equation (2.2.3) it does not readily permit of theoretical calculation. The chemical potential can be calculated by making a few reasonable assumptions (69), but the first term in equation (2.2.3) is dependent in an extremely complex way on surface structure, state and composition such that calculations of it can not be reliably made except in a few hypothetical cases. Thus at present the work function of a surface is better defined in physical terms rather than in mathematical terms i.e. by accurately stating the structure, state and composition, or exact method of preparation of a surface, its work function is then known, not by calculation but by virtue of previous reliable measurements of work function having been made on an identical surface. In the past, work function measurements have been reported without this detailed information which has rendered them much less useful than more recent reviews of work function values which have included many relevant details (69) (76) (77). The most recent and certainly the most comprehensive of these reviews is by Rivière

(76) which contains approximately 500 well documented experimental values of work function for 150 different materials.

2.2.2. Physical Interpretation of Work Function. Work function from the definitions above can then be thought of as an escape energy for electrons located at or near the surface of a conductor. The electrons can be emitted from the surface as a result of thermal, high electric field or photoelectric effects. Itskovich (78) has considered the work function of different types of electron emission. He concludes that for the same single crystal face of a metallic conductor

$$\phi_{ph} \geq \phi_t \geq \phi \quad (2.2.4)$$

and

$$\phi_{ph} \geq \phi_{fe} \geq \phi \quad (2.2.5)$$

where ϕ_{ph} is the photoelectric work function reduced to zero field

ϕ_t is the thermionic work function reduced to zero temperature

ϕ_{fe} is the field emission work function reduced to zero field

and ϕ is the true work function as defined in the previous section.

Thermionic, high field and photoelectric work functions are

normally referred to as effective work functions since they determine the level of the particular type of electron emission from a surface, unlike the true work function which is a theoretical quantity. The true work function may vary significantly from these individual values, the difference being attributed to the tangential momentum which the emitted electrons may have (78). Thus the term 'work function' must not be used indiscriminately, but instead it must always be made clear what quantity is being referred to when the term is used. Even different crystallographic planes of the same single crystal have different magnitudes of dipole layers of charge at the surface, resulting in different values of effective work function for each plane present. Thus, when polycrystalline surfaces are considered the problem of interpretation is further complicated. The effective work function of a clean polycrystalline conductor surface is principally dependent upon which crystal planes are present, in what proportion, how large these areas are, the conductor temperature, the effect of any electric fields present at the surface and the method of measuring the work function. Also, Lewis (79) has shown that the effect of irregularities on the surface can considerably influence the effective work function value. The degree of dependence is a consequence of which material is under consideration since any two samples of different materials, even with the same crystal structure and environmental conditions, will in general have different values of effective work function. If the conductor surface is not 'clean' but has adsorbed on it atoms

or molecules of some foreign species, these changes will almost inevitably take place in the electron energies at the surface. The result is a dipole layer formed at the surface which may increase or decrease its effective work function depending on just how the foreign atoms or molecules are bonded to the surface. This change in work function from that of the uncontaminated surface is called the surface potential, and is the quantity frequently monitored during investigations in work function changes.

For a further physical interpretation of work function which does not involve the actual emission of electrons into space, consider two metals in intimate contact at the same temperature. By free energy considerations, if the metals are connected electrically externally, with no voltage source present, the electrochemical potentials must be the same value in both metals. From equation (2.2.1) it is seen that this means that electrons will flow from one metal to the other until a difference in the electrostatic potentials just outside each metal equals the difference in the work function values of the two metals. As will be seen later this potential, usually called 'contact potential difference', does exist and can be used to good effect for investigating work function changes.

2.2.3. Surfaces to be Considered. The different types of surface which are to have their work functions investigated are:-

- i) Single crystal and polycrystalline metal surfaces



with no overlayers or surface contamination.

- ii) Metal surfaces with gas adsorption taking place at the surface.
- iii) Single crystal and polycrystalline surfaces with overlayer structures.
- iv) Metal surfaces where oxygen incorporation or oxidation is taking place to a depth of perhaps many monolayers.

Each of the above structures will now be considered in turn.

2.2.4. Bare Metal Surfaces. If an electrically neutral "body" consisting of only one atom is considered, then the energy required to remove one electron from the "body" is dependent on the electronic configuration of the atom. Elements which are good conductors have loosely bound valence electrons which are removed much more easily than say the electrons of the inert gases which have very stable electronic configurations. Thus there is a large spread of energies required to remove electrons from atoms of different elements. If not one atom, but a large group of atoms (or molecules) is considered which together make up some form of crystal structure, then obviously to remove one electron will still vary depending on the element(s) present. However, one must now consider how these atoms or molecules arrange themselves at the boundary of the "body", and what effect they have on the electron clouds associated with each other at the crystal lattice terminations. The crystal structures of good conducting elements are mostly either body centered cubic (b.c.c.), face centered cubic

(f.c.c.) or hexagonal close packed (h.c.p.). The metals considered in this work, namely gold, silver and aluminium, are of the f.c.c. type, and the three simplest surface arrangements that are possible for f.c.c. crystals are the (111), (100) and (110) faces. Other faces are of course possible. The values of work function for these planes of tungsten crystals (normally a b.c.c. structure) have been reported to be different by as much as 0.89 eV (80). By the same measurement technique others have reported somewhat less variation (81), especially between the values for the (100) and (110) planes (82). The actual values reported by the latter are $\phi_{(100)} = 4.65 \pm 0.01$ eV and $\phi_{(110)} = 5.14 \pm 0.01$ eV. Although these results are not in very close agreement, they still demonstrate that different crystal planes can have work function values which differ considerably. Insufficient data is available to make a similar comparison for gold, silver, or aluminium faces since most of the work in individual planes has been done on the refractory metals tungsten and molybdenum. In practice, imperfections always exist in metal crystals which tend to reduce the work function of any face. (83).

When metal crystals are prepared by vacuum evaporation and deposition onto a 'cold' glass substrate the resulting thin film does not have a single crystal structure. Instead it is composed of many small crystallites with grain boundaries existing between them. The surface is now polycrystalline which means that it is most probable that all possible crystal planes are present at the metal surface in proportions which are dependent upon the

experimental conditions. The true work function of ^{such} a surface is a rather meaningless quantity, and its effective work function is dependent on the method of measurement used. A useful quantity for a polycrystalline surface is the average work function, $\bar{\phi}$, which is defined as follows (69) "If ϕ_i is the true work function of the i^{th} patch having a fractional area f_i ; then the average work function is $\bar{\phi} = \sum f_i \cdot \phi_i$ ". Patch in the definition means an area at the metal surface all of the same crystallite.

The work function of polycrystalline surfaces of gold, silver aluminium has been reported using a variety of measurement techniques. For gold films deposited on glass, values of 5.45 eV (84), 5.22 eV (85) and 5.30 eV (86) have been recently found experimentally. The mean value of these results is approximately 5.35 eV. This is considerably higher than the generally accepted value of ~ 4.70 eV which was used until 1966. The difference between the old value of ~ 4.70 eV and the more recent value of approximately 5.35 eV has been accounted for by Huber (85). He discovered that the difference was the result of a strongly adsorbed layer of mercury on films prepared in mercury diffusion pump systems as used for the vacuum systems employed to prepare these earlier films. For silver films few recent measurements are available, however in 1964 a value of 4.30 eV was reported for a silver film prepared by vacuum deposition onto a glass substrate (77), Huber and Kirk (29) during a study of chemisorption on aluminium concluded that the work function of a freshly prepared

<i>Material</i>	<i>Reference</i>	<i>Work Function</i>	<i>Measurement Technique</i>	<i>Substrate</i>
<i>Au</i>	<i>84</i>	<i>5.45 eV</i>	<i>Retarding potential</i>	<i>Gold on glass</i>
<i>"</i>	<i>85</i>	<i>5.22 eV</i>	<i>Contact potential</i>	<i>glass</i>
<i>"</i>	<i>84</i>	<i>5.45 eV</i>	<i>Photoelectric</i>	<i>glass</i>
<i>"</i>	<i>86</i>	<i>5.30 eV</i>	<i>Retarding potential</i>	<i>Gold on glass</i>
<i>"</i>	<i>76</i>	<i>4.7 eV</i>	<i>Average value of several experiments</i>	
<i>Ag</i>	<i>77</i>	<i>4.30 eV</i>	<i>Contact potential</i>	<i>glass</i>
<i>Al</i>	<i>29</i>	<i>4.2 eV</i>	<i>" "</i>	<i>"</i>
<i>"</i>	<i>87</i>	<i>4.19 eV</i>	<i>" "</i>	<i>"</i>

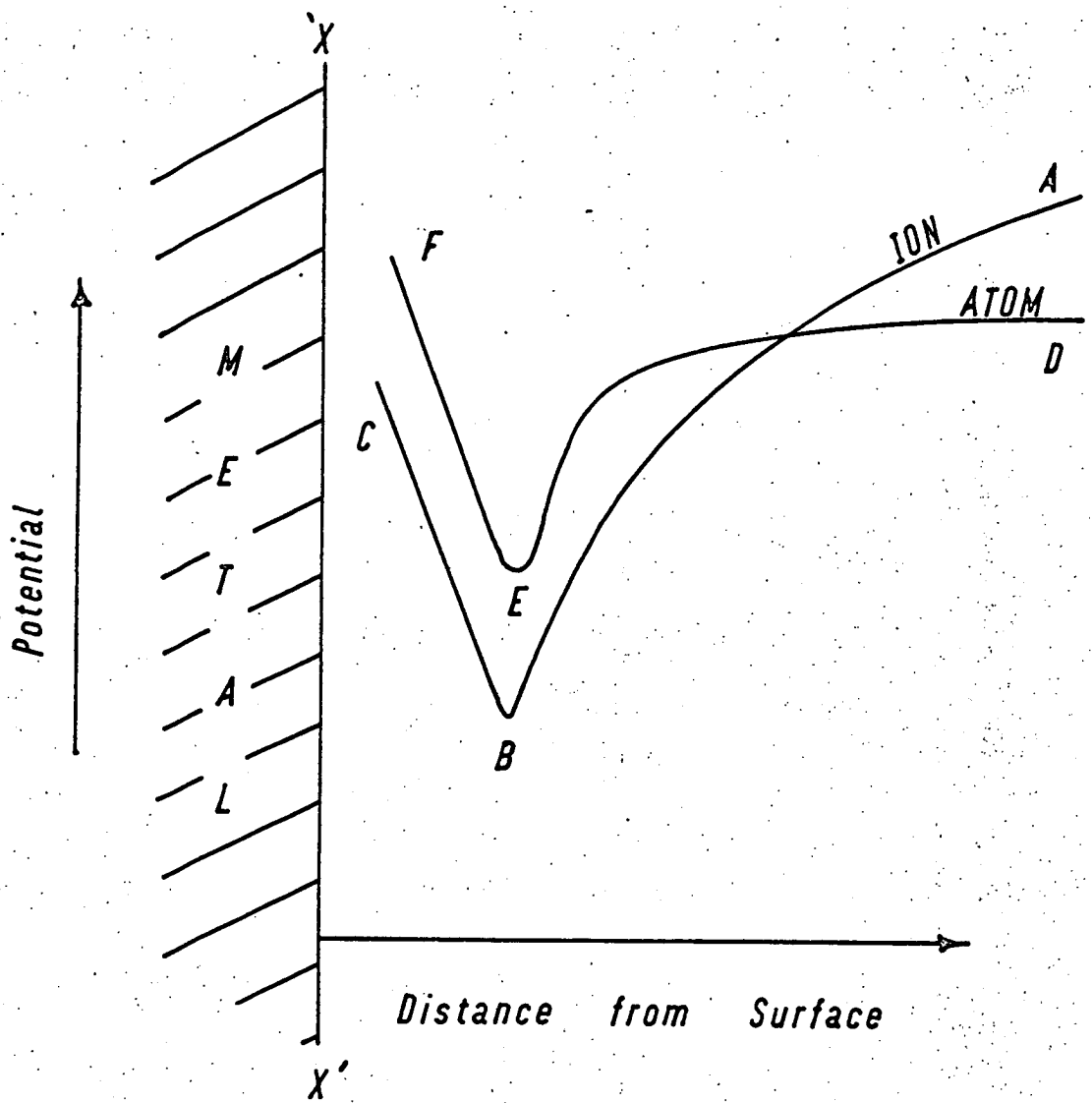
— Table 2.2.1 —

— Work Function Measurements for Gold, Silver and Aluminium —

polycrystalline thin film of aluminium was approximately 4.30 eV, in agreement with earlier measurements ⁽³⁶⁾. These values of work function are shown on table 2.2.1.

The work function of a gold film surface prepared at room temperature by evaporation in high vacuum is lower than that of a clean polycrystalline bulk gold surface ⁽⁸⁷⁾. Similar results were previously reported for silver, where a decrease in the work function of 0.18 eV took place when a bulk silver surface was coated with a thin film of silver ⁽⁸⁸⁾. The difference is presumed to be the result of the bulk metal samples having been formed for a considerable time, hence a slow self-annealing process could have taken place which would cause larger crystallites with fewer faults to be formed which have higher work function values. This is substantiated for gold ⁽⁸⁷⁾ and silver ⁽⁸³⁾ by heating newly prepared film samples so that the annealing process is accelerated, with a corresponding increase in work function values to that of bulk samples. Similar results have been obtained for iron ⁽⁸⁹⁾. That the work function increases are dependent upon the amount of overlayer deposited, or residual gas pressure during deposition, has been discounted for the experiments of Clark and Farnsworth ⁽⁸³⁾. Such a self-annealing process was invoked by Lucas ⁽²³⁾ to explain decreases which took place in the electrical resistivity of thin gold films prepared by vacuum deposition.

How the value of work function for a polycrystalline surface varies with the measurement technique employed will be considered



— Figure 2.2.1 —

Potential Diagram for an Ion or Atom near a Metal Surface

in chapter 3.

2.2.5. Adsorption on Metal Surfaces. Adsorbed atoms or molecules can have one of three possible methods of bonding to a metal surface.

- i) Covalent bonding
- ii) Ionic bonding
- iii) Attraction by Van der Waals forces

The first two are known as chemisorption processes and the latter as physical adsorption. Chemisorption processes are characterised by an electron transfer between the substrate and the adsorbate, unlike a pure physical adsorption process where polarization takes place but no electron transfer occurs. A comprehensive review of bonding processes has been written by Dowden (90).

Consider in figure 2.2.1. a metal surface 'XX' with the potential energy DEF of an atom drawn as a function of the distance from the surface. Since both the atom and the metal are polarizable, Van der Waals forces will attract and hold the atom onto the surface. These forces vary as the inverse of the sixth (and higher) power of the distance from the surface, and hence are short range forces. If, however, the atom has an electron transferred to the metal surface, then the potential energy curve ABC is obtained which varies as the inverse of the distance from the metal since the attraction potential is now a Coulomb attraction.

From the observation that ϕ is lower than ϕ_0 on the potential diagram it follows that adsorption of an ion, and not an atom, will take place. This ionic bonding is typical for many adsorbates, especially some commonly occurring gases. Ionic bonding will cause an increase, or decrease, in the work function of the surface depending on whether the resulting double layer of charge at the surface has a negative, or positive, charge outwards. If the electronegativity of the adsorbed species is less than the work function of the substrate surface, then a net positively charged layer is present on the surface. Conversely if the electronegativity is larger, then a net negatively charged layer exists. This increase or decrease in work function caused by the double layer is the result of a change in the difference between the potential energy just outside and just inside the metal surface, and hence in the surface potential. Whereas ionic bonding depends upon electrostatic forces, covalent bonding depends on an electron exchange for reaching an equilibrium state. However, such bonds still result in a dipole layer at the metal surface with the attendant change in the surface potential. Physical adsorption usually only has a small dipole associated with it, and thus only a relatively small change in surface potential would be expected.

Hence any form of adsorption on a surface can cause changes in the surface potential and thus in the work function of the surface. However, surface potential values cannot generally be interpreted in terms of a simple model for the adsorption bond.

Culver and Tompkins (38) in their review of adsorption processes on metals gave an extensive list of the more reliable measurements of changes in surface potential for many substrate-adsorbate combinations. The most important observation from these measurements regarding this work is that oxygen in all the reported cases caused a substantial negative surface potential, indicating that the bonding is largely ionic with negative oxygen ions uppermost on the surface. It is interesting to note that for all physical adsorption measurements cited the surface potential is always positive.

For the metals used in this work (viz gold, silver and aluminium) the adsorbates to be considered are oxygen and water vapour. The effect of these adsorbates on the work function of the metals will now be considered.

i) Gold. From recent work function measurements made at room temperature in vacuum, gold does not chemisorb a significant amount of oxygen (86) (91) (92). However, at elevated temperatures appreciable chemisorption has been found to take place. An increase of 0.70 eV in the work function was reported for a temperature of 500°C. (93). Part of this increase may of course be the result of annealing effects which are known to increase work function values (87). Clark et al (94) attempted to "oxidise" gold then examine the surface by electron diffraction, electron microscopy, X-ray emission spectroscopy and electrochemistry. In agreement with others (95), none of their experiments provided any

evidence for the presence of an oxide of gold, and they suggested that migration of impurities to the surface on heating could explain some of the results obtained, but no actual work function measurements were made. In contrast to these results, Meyer (58) has reported a surface phase of gold which has oxygen adsorbed into hexagonal cells, which he suggests will act to modify the observed work function in different gaseous environments. No work function measurements were made by him to verify this point. The only report of the work function of gold changing considerably in vacuum with oxygen adsorption is given by Dillon and Farnsworth (96). Up to 0.40 eV increases were observed, which Rivière (97) has dismissed as being the result of an unclean 24 ct. gold plated electrode. No report has ever been made of water vapour adsorbing on gold in vacuum. Thus it is concluded that vacuum deposited gold, especially in vacuum at approximately room temperature, does not have its work function significantly changed by adsorption of oxygen or water vapour.

ii) Silver. It is well known that silver reacts chemically with oxygen. Ogawa et al (98) found that a surface potential of 0.60 eV developed when oxygen was allowed to adsorb on a silver surface. This magnitude and polarity of surface potential indicated that the adsorption is most likely ionic with negative oxygen ions uppermost on the surface. Under soft vacuum conditions, for temperatures close to room temperature, the adsorption of oxygen has been reported to be nearly independent of pressure and temperature (99). However, under high vacuum conditions silver

does not appear to readily adsorb either oxygen or water vapour at room temperature. If the work function was effected by low pressure adsorption, then it is thought that Hopkins and Rivière (77) would have observed and reported it during work function measurements of thin films of silver prepared on a variety of substrates. The pressure was not reported with the work function results, but from the apparatus used (100) it is expected that the vacuum chamber used would be at approximately 10^{-9} torr. Scanning electron diffraction work done by Grigson and Dove (101) confirms that face centered cubic metals, especially gold and silver, show little tendency for oxide growth. At pressures greater than 50 mm Hg water vapour is adsorbed onto a bare silver surface at 0° - 100° C. but is adsorbed much more strongly if the surface has been pre-exposed to oxygen so that the surface is occupied by adsorbed oxygen (99). It is concluded that for silver, only under vacuum conditions close to ambient is oxygen or water vapour significantly adsorbed.

iii) Aluminium. Even under high vacuum conditions aluminium is a very reactive metal with oxygen. This can be easily demonstrated by observing the pressure decrease by gettering which often accompanies the evaporation and deposition of aluminium in high vacuum. From section 2.2.5. it appears that the change in the surface potential with oxygen adsorption should be negative i.e. an increase in work function. The finding of several investigators was that the work function in fact decreased (102) (103). Klemperer (103) and others (104) attributed this to oxygen being

bonded just under the metal surface, resulting in a positive surface potential. However Huber and Kirk (29) (105) in a series of well conducted experiments, and later by applying the ultra-high vacuum low energy electron diffraction work of Jona (106), demonstrated that oxygen adsorption causes only a small decrease in the work function up to monolayer coverage - approximately 0.05 eV. Exposure beyond the monolayer region results in an increase in the work function (107). Eley and Wilkinson (39) considered oxygen to be the only gas significantly adsorbed on aluminium in a high vacuum chamber. This idea was radically changed when it was shown in 1966 (29) that water vapour has a very pronounced effect on the work function of a freshly prepared aluminium surface. The effect is accelerated if the surface is firstly pre-exposed, as for silver, to oxygen to monolayer coverage before water adsorption commences. The water vapour causes a decrease in work function of approximately 1.10 eV which is sufficient to explain the earlier decrease in work function which had been accounted for by oxygen adsorption. The decrease in work function with water vapour adsorption is consistent with the results of Ramsey (108) obtained during a study of the emission of electrons from aluminium abraded in air, oxygen, nitrogen and water vapour. It is concluded then, that even in high vacuum, the work function of aluminium surfaces can be significantly modified by the adsorption of oxygen and water vapour.

2.2.6. Metallic Overlayers. The values of work function of two

different metals can vary by as much as 4 to 5 eV if extreme cases are considered. Most commonly occurring metals in polycrystalline form tend to have values in the region of 4.10 eV to 5.30 eV.

Thus, if a clean metal surface is completely covered by a thick layer of a second metal then a change in work function of the surface is expected. From section 2.2.2. a charge double layer exists at the metal/overlayer junction which results in a contact potential between the two materials equal in magnitude to the difference in the work function values. This implies that the final work function of the composite structure surface is that of the overlayer material. If the overlayer is vacuum deposited onto the surface, then exactly how the work function changes as a function of the amount of material deposited depends on the overlayer growth mechanism for the particular combination of substrate/condensate materials under the prevailing experimental conditions.

For vacuum deposition of metals it is often the case that an overlayer growth takes place by a process of adsorption, surface migration and the subsequent spontaneous appearance of atom clusters which have the critical nucleus size as discussed earlier. Well established theories (109) (111) (112) (110) exist for describing such a growth process. However, recent theories of metallic overlayer growth on metal substrates involving changes in work function at the surface (71) (113) are for a different type of growth than that described by the above theories. No nucleation

is considered to occur and the overlayer is assumed to grow as a monolayer structure with the adsorbate appearing as a regular array of atoms located at fixed points with respect to the substrate surface lattice structure. The idea contained in these different theoretical works come together in work reported by Sandejas and Hudson (114), and others (115) (116) where it is suggested that a layer of adsorbate atoms is formed perhaps several monolayers thick, followed by the nucleation and growth of crystallites of adsorbate material on the adlayer. Since this type of growth may occur for many combinations of adsorbate/substrate metals which have large binding energies (116) the form of the work function changes which may occur are now considered. The analysis is conveniently broken down to the two overlayer deposition processes of, firstly the adlayer formation, and secondly that of nucleation with island growth. Levine and Gyftopoulos (71) developed a theory for the change in work function $\Delta\phi$ as a function of adsorbate surface coverage θ , which had some success in explaining experimental results for alkali and rare earth alkali metals deposited on to a refractory substrate (117) (118) (119). The principal equation that they derived is

$$\frac{\Delta\phi}{\phi_2 - \phi_1} = 1 - \zeta(\theta) \left[1 - \frac{0.765 \cdot 10^{-18} \cdot \zeta_f \cdot \theta \cdot \cos \beta}{\left(1 + \frac{\alpha}{4\pi\epsilon_0 R^3}\right) \left(1 + \frac{9\alpha \cdot \zeta_f^{3/2} \cdot \theta^{3/2}}{4\pi\epsilon_0}\right)} \right] \quad (2.2.6)$$

where ϕ_2 = substrate metal work function value.

ϕ_1 = adsorbate metal work function value.

$\zeta(\theta)$ is a function of coverage

$\bar{\sigma}_f$ = density of adsorbate on surface at the completion of one monolayer.

$\cos\beta$ is the cosine of the angle between the surface normal and the line joining an adsorbate and a substrate atom.

α = polarizability of adsorbate atoms.

ϵ_0 has its usual significance.

R = summation of adsorbate and substrate covalent radii r_m and r_f .

Making the same assumptions concerning the adlayer as Levine Gyftopoulos (71) in the derivation of equation (2.2.6), similar equations were derived for the growth of silver on the (111), (110) and (100) planes of a completely regular gold surface. Gold crystal structure is f.c.c. with a cube side length 'a' of 4.0786 Å (120). Because of the small difference between the covalent radii r_m and r_f for gold and silver respectively (120), it was assumed that

$$r_m = r_f = \frac{R}{2} = \frac{a}{2.82} \quad (2.2.7)$$

Thus for the (100) plane present at the surface:-

$$\bar{\sigma}_f = \frac{2}{a^2} \cdot 10^{20} \text{ atoms/m}^2 \quad (2.2.8)$$

$$\text{and } \cos\beta = \frac{1}{\sqrt{2}} \quad (2.2.9)$$

For the (111) plane:-

$$\sigma_f = \frac{3}{\sqrt{3} \cdot a^2} \cdot 10^{20} \text{ atoms/m}^2 \quad (2.2.10)$$

$$\text{and } \cos\beta = \frac{2}{\sqrt{3}} \quad (2.2.11)$$

For the (110) plane :-

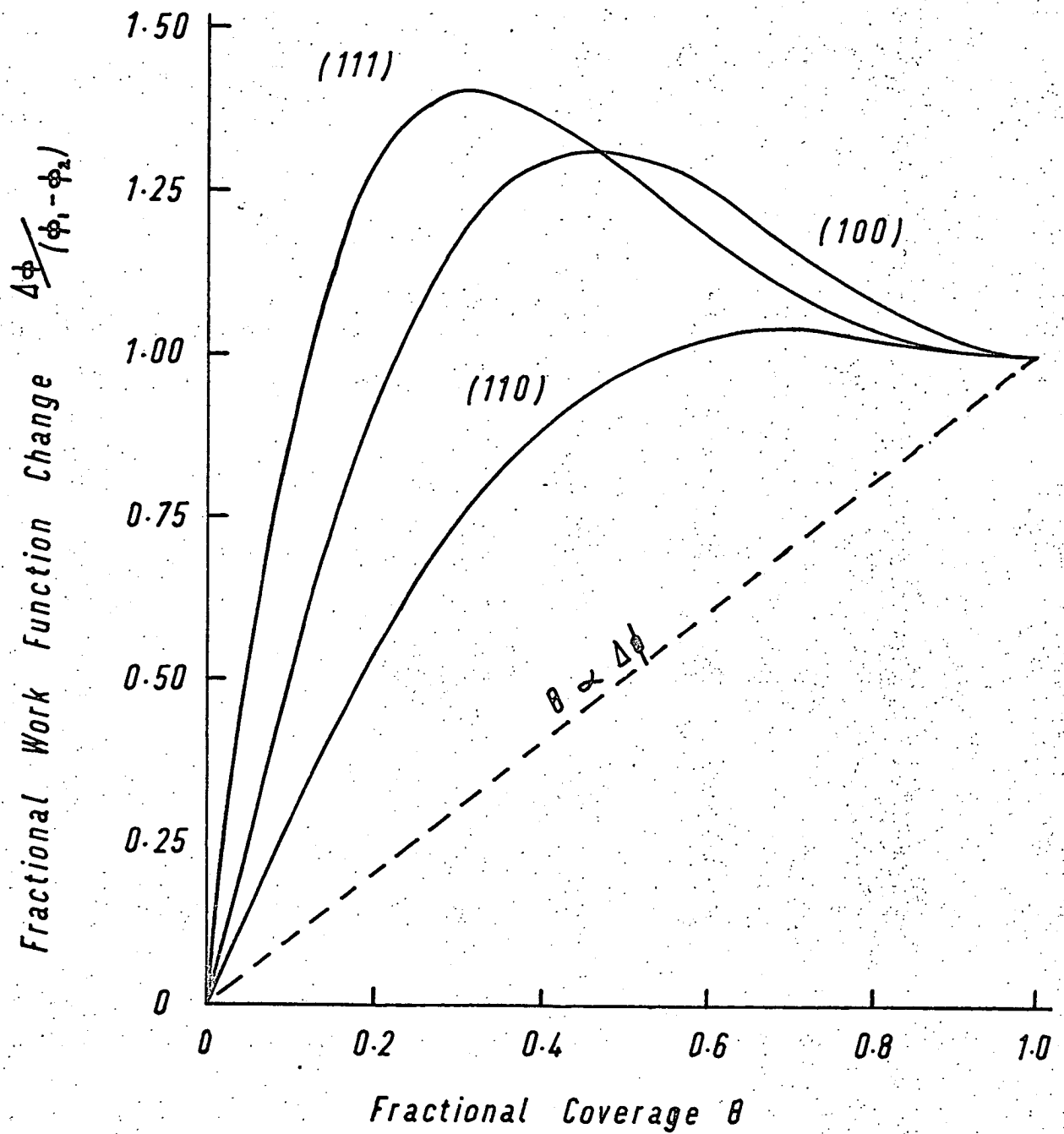
$$\sigma_f = \frac{\sqrt{2}}{a^2} \cdot 10^{20} \text{ atoms/m}^2 \quad (2.2.12)$$

$$\text{and } \cos\beta = \frac{1}{2} \quad (2.2.13)$$

Furthermore, if M_{fm} is the dipole moment per bond-link of the complex adsorbate/substrate molecule, then because a unit cell now consists of three substrate atoms the dipole moment M_o of a single adatom on the (111) face is modified to

$$M_o = 3 M_{fm} \cdot \cos\beta \quad (2.2.14)$$

which makes the multiplying factor $(0.75 \times 0.765 \times 10^{-10})$ instead of (0.765×10^{-10}) in equation (2.2.6).



— Figure 2.2.2 —

— Variations of Work Function with Coverage for Silver —

Figure 2.2.2. shows the fractional change in work function plotted against overlayer coverage for these three planes. The coverage axis goes only to 1.0 i.e. one complete monolayer, since it is explicit in the assumptions of Levine and Gyftopoulos (71) that at $\theta = 1$ the rate of change of work function with coverage is zero. This implies that for all values of θ larger than 1.0 i.e. more than one monolayer coverage, the work function is that of the adsorbate. Macdonald and Barlow (113) have expressed doubts on the validity of the latter assumption, and have put forward a theory which relaxes this constraint. However the form of their derived equation for the surface potential, ΔV , induced with a neutral adsorbate contains factors (effective dielectric constant and the electric field at the metal surface leading to induced polarization) which are difficult to evaluate. Thus, as these authors point out, it is best if these unknown factors can be evaluated by carrying out experiments to determine the dependence of ΔV on coverage and charge on the substrate surface. Also they express understandable concern over the lack of attempts to appreciate the quantum features of such an overlayer. As the theory of adlayers progresses no doubt such considerations will eventually be made.

In order to explain experimental results for the change in surface potential, ΔV , during metallic overlayer formation, Mignolet (121) put forward the empirical relationship of

$$\Delta V = 0.29 (\phi - 3.15. X_a) \quad (2.2.15)$$

Where ϕ is the substrate work function and X_a is the electronegativity of the adsorbate.

Equation (2.2.15) was successfully used by Jones (115) to explain quantitatively the surface potential existing on a tungsten surface covered by an adlayer of Cu atoms. For a silver adlayer on a gold substrate the surface potential can similarly be found as follows. A value of the electronegativity X_s of silver can be found using the empirical relationship of Gordy and Thomas (122).

i.e.

$$X_s = 0.44 \phi_s - 0.15 \quad (2.2.16)$$

Where ϕ_s is the work function of silver.

Substituting 4.30 eV for the work function of silver yields.

$$X_s = 1.74 \text{ eV} \quad (2.2.17)$$

If this value for X_s is substituted for X_a in equation (2.2.10) with a value of 5.30 eV for the work function, representing a gold substrate, then the value obtained for the resultant surface potential is

$$\Delta V = -0.055 \text{ Volts} \quad (2.2.18)$$

Now work function changes expected with adsorbate nucleation and island growth are considered. From the experimental work of Ying and Farnsworth (59) and Mikama and Yasuda (60), and the results of Campbell (24) deduced from the work of Pashley and

Stowell (4) (123), a reasonable relationship, as already put forward in section 2.1., between mean overlayer thickness, t , and surface coverage θ is

$$\theta = (1 - e^{-t/\tau}) \quad (2.2.19)$$

where τ is a constant, dependent on the materials and the experimental conditions employed. Equation (2.2.19) represents an island growth process where the mean thickness of the islands, T , is

$$T = \frac{\tau}{1 - e^{-t/\tau}} \quad (2.2.20)$$

and as shown in section 2.1. the critical nucleus size r_c is given approximately by

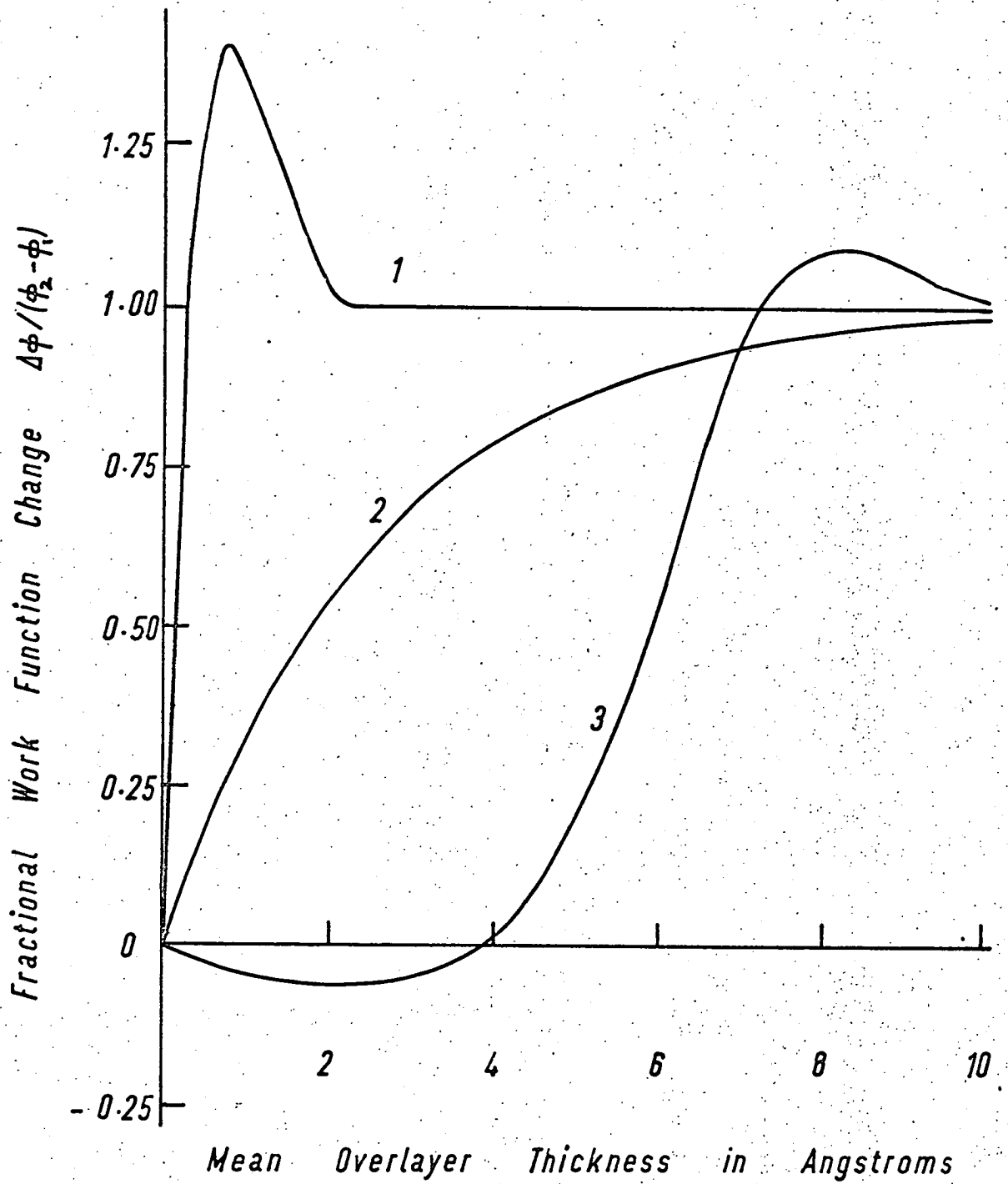
$$r_c \simeq \tau \quad (2.2.21)$$

If, as shown in figure 2.2.2. the work function ϕ is assumed to be a linear function of coverage, then

$$\phi = \phi_2 + \theta(\phi_1 - \phi_2) \quad (2.2.22)$$

where θ , ϕ_2 and ϕ_1 are as defined previously, and substituting for θ in equation (2.2.22) from equation (2.2.19) yields

$$\phi = \phi_2 + (1 - e^{-t/\tau})(\phi_1 - \phi_2) \quad (2.2.23)$$



— Figure 2.2.3 —

— Possible Work Function Variations for Silver Overlayers on Gold —

Alternatively, a fractional change in work function can be expressed as a function of mean thickness, t , as

$$\frac{\Delta\phi}{\phi_1 - \phi_2} = (1 - e^{-t/\tau}) \quad (2.2.24)$$

Where $\Delta\phi = \phi_1 - \phi_2$ is the surface potential as the result of the adatoms.

On figure 2.2.3. is shown for comparison purposes the different forms that the work function versus mean overlayer thickness might take for the different growth processes considered, using as the example the growth of silver on a gold substrate. Curve 1 is for the (111) plane using the theory of Gyftopoulos and Levine (71) assuming that the mean thickness of a monolayer is approximately 2.38\AA . Curve 2 is for equation (2.2.24) with $\tau = 2.50\text{\AA}$. Curve 3 is obtained by using equation (2.2.15) to predict the surface potential at monolayer coverage, after which the work function decreases to that of silver as the adlayer is formed to a thickness of several monolayers, and finally nucleation of silver crystallites is assumed to occur. The slight increase in the work function before dropping to a constant value is attributed, after Jones (115), to the onset of the nucleation process. As already discussed in section 2.2.4. the more crystalline a deposit is, the higher its work function value tends to be.

The characteristics of each of these curves are:-

For curve 1. A rapid change in work function with a noticeable

overshoot before reaching a constant value at monolayer coverage.

For curve 2. A monotonic exponential rise.

For curve 3. A slight decrease before increasing to overshoot the final constant value of work function change at a thickness of several monolayers.

Thus from an experimentally found relationship between work function change and overlayer thickness it should be possible to identify the type of growth process involved.

2.2.7. Oxide Growth. Of the three metals gold, silver and aluminium, gold, as discussed in section 2.2.5., does not form an oxide, whereas in contrast aluminium readily oxidises to a depth of many monolayers with sufficient exposure. Silver does form an oxide, but the growth of the oxide of aluminium has been studied in more detail, and hence will be considered first.

Two theoretical models exist for the oxidation of aluminium. The first is due to Cabrera and Mott⁽¹²⁴⁾, and secondly there is the theory of Lanyon and Trapnell⁽¹²⁵⁾. The theory of Cabrera and Mott⁽¹²⁴⁾ predicts a pressure independent, inverse logarithmic time law for oxide growth, which has been found to hold for experiments at atmospheric pressure⁽¹⁰⁸⁾ ⁽¹²⁶⁾. That of Lanyon and Trapnell⁽¹²⁵⁾ predicts a pressure dependent and direct logarithmic time law, and has been found to hold for pressures of 1 to 10^{-3} torr⁽¹⁰⁷⁾ ⁽³⁹⁾. A direct logarithmic work function versus log (time) and log

(oxygen pressure) dependence has also been found for oxide growth beyond the completion of the first adsorbed oxygen monolayer (107). This incorporation of the oxygen into the bulk of the metal results in a Volta potential, which changes as the oxide thickness increases (37). The magnitude of this potential can be as great as 0.5 to 0.6 volts (126) which is of the same order as the value of 0.6 volts reported for the incorporation of oxygen into a nickel surface (128). If both oxygen and water vapour are present then the expected sequence of events occurring at an aluminium surface are, firstly, the rapid adsorption of oxygen to monolayer formation followed by the adsorption of polar groups from H_2O molecules, and finally the slow incorporation of oxygen into the aluminium to form an oxide (29). The sequence is consistent with the electron emission measurements of Ramsey (108) made in various gaseous environments. The work function during the sequence firstly increases by approximately 0.05 eV, then decreases by over 1 eV as the polar groups adsorb and finally increases as the oxide layer grows in thickness.

Silver does react with oxygen to form an oxide, but insufficient experimental evidence is available to predict actual work function changes during oxidation.

2.2.8. Work Function Complications. The following are further complications which can exist when measuring the work function, or surface potential, of metals.

i) Impurities - If impurities are present in the metal sample

then the surface will not be 'clean' since the impurities will exist at the surface as well as in the bulk, especially if the sample is subjected to elevated temperatures. A 2% surface concentration of rhenium on a tungsten surface caused a measured change of 0.04 eV in the surface work function (129). This change is more than 2% of the difference between the work function values of rhenium and tungsten. Impurities exist preferentially at faults on crystal faces and hence clusters of impurities forming projections at the surface are liable to appear.

ii). Temperature Effects. - Thin films formed by vacuum deposition can be as much as 400° - 500° K higher than the substrate temperature (130). This large increase is attributed to exothermic heat of condensation and radiation heating from the evaporation source. Thus it is possible that deposited atoms are frequently in a more mobile state on the substrate surface than the nominal substrate temperature would suggest, resulting in larger agglomerates of condensate forming. A numerical example given by Belous and Wayman (130) is that for a source 19cm from a mica substrate nominally at 300° K, a deposition rate of 10^6 Å/sec of gold results in a film temperature of about 600° K. The work function of a surface is somewhat temperature dependent, described by several authors (73) (131) (132) (133) in the form

$$\phi = \phi_0 + \alpha T \quad (2.2.)$$

Where ϕ_0 is the work function at 0°K

α is a linear temperature coefficient

T is the absolute temperature in $^\circ\text{K}$

Although α is usually small, obviously with potentially large temperature changes possible care must be taken to minimise temperature variations. Some metals change structure at elevated temperatures with an attendant change in work function. Such a case is uranium which can be orthorhombic (below 938°K), tetragonal (938°K to 1043°K) and b.c.c. (1043°K) with work functions of 3.47, 3.25 and 3.39 eV respectively (134) (135). No such structural changes are expected for gold, silver and aluminium in the experiments carried out during this work.

- iii). Non-Uniformity of Surface - For overlayer growth the size of islands formed during the growth process may influence the effective work function (136) (79) (116). Vladimirov (137) has calculated the size that patches of different work function can be before present emission theory is inadequate. The effect of patches of different work function will be discussed again in the next chapter when different techniques for measuring

work function are considered.

- iv). Surface States - These only occur in semiconductors. However, silver oxide has been described as a p-type semiconductor (138) and from the results obtained during this work aluminium oxide, perhaps in an excess oxygen state, also acts as a semiconductor. Surface states can pin the Fermi level at a semiconductor surface, and hence mask work function variations which would otherwise have taken place (139).
- v). Alloying - Of the materials used, the combination of a silver substrate with aluminium as adsorbate will result in the alloy Ag_2Al being formed to a depth of several monolayers (63). Pashley (4) presented evidence to suggest that a phenomenon similar to alloying occurs when metal atoms are deposited onto a metal substrate. It is that they can penetrate the substrate surface, forming a layer consisting of a mixture of condensate and substrate atoms several monolayers deep.

2.3. Electrical Conductivity and Work Function Interdependence.

2.3.1. Value of relating Work Function to Conductivity. Few attempts have been reported of experimental work carried out in order to relate electrical conductivity (or resistance) to effective work function (or surface potential) for thin metal films. Bryla and Feldman (140) in 1962 recorded the change in

surface potential as a function of resistance during the growth of thin films of gold and silver prepared by vacuum deposition on fused silica substrates nominally at room temperature. No significant variation in contact potential with respect to a platinum reference electrode occurred over the sheet resistance range 10^9 to $10 \Omega / \text{sq.}$ These results imply that for a single uncontaminated metal deposited onto an insulating substrate, no relationship exists between electrical resistance and effective work function which helps elucidate the conduction process in the metal. However, as will now be shown, when gas adsorption, oxidation or metallic overlayers are present at a metallic film surface, then monitoring the effective work function of the surface can yield valuable information concerning the electrical conduction in the thin film. This of course will only apply under conditions where the film is sufficiently thin for surface effects to be significant.

2.3.2. Adsorption and Oxidation. Of the metals studied in this work only aluminium and silver are considered to have any reaction with oxygen and water vapour. The relationship for oxygen and water adsorption on freshly prepared aluminium thin films can be conveniently considered for five separate cases. They are;

- i). Low oxygen exposure up to monolayer coverage. The electrical resistance R is given by

$$R = A(1 - e^{-(B \cdot \theta)}) \quad (2.3.1)$$

where A, B are constants

and θ is the fractional coverage.

Equation (2.3.1) follows from the work of Huber and Kirk (29) with the assumption that the mass of gas adsorbed, M, is directly proportional to θ . Also from the work of these authors the change in work function, $\Delta\phi$, is related to θ by

$$\Delta\phi \propto M \quad (2.3.2)$$

and hence

$$\Delta\phi \propto \theta \quad (2.3.3)$$

Thus to a first approximation substituting for θ using equation (2.3.3), equation (2.3.1) yields

$$R = A \left(1 - e^{-D \Delta\phi} \right) \quad (2.3.4)$$

where D is a constant.

ii). Oxygen exposure beyond monolayer coverage. The mean thickness of oxide, t , is related to the mass of oxygen incorporated by,

$$t \propto M \quad (2.3.5)$$

Hence the change in resistance, ΔR , with an oxide of thickness t , provided the thickness, t , is small compared to the initial film thickness, is related to M by

$$\Delta R \propto M \quad (2.3.6)$$

but $M \propto \log(\text{time}) \times \log(\text{pressure})$

and $\Delta\phi \propto \log(\text{time})$ at constant pressure

$\Delta\phi \propto \log(\text{pressure})$ at constant time

so that it follows that

$$\Delta\phi \propto \Delta R \quad (2.3.7)$$

iii). Water vapour exposure up to monolayer coverage on a clean surface. The resistance change is the same order of magnitude as for oxygen adsorption, and the corresponding work function change is very small as for case (i) i.e.

$$\Delta\phi \approx 0.06 \text{ eV} \quad (2.3.8)$$

iv). An aluminium surface exposed to water vapour which has been pre-exposed to oxygen up to monolayer coverage. The resistance is virtually insensitive to the water vapour adsorption i.e. $R = 0$, and the work function

Type of Exposure	Variation of R	Variation of ϕ	Relation between R & ϕ
Oxygen up to monolayer coverage	$\Delta R = A(1 - e^{-B.M})$	$\Delta\phi = f_A(\theta)$	$\Delta R = A(1 - e^{-C.\Delta\phi})$
Oxygen beyond monolayer coverage	$\Delta R \propto M$	$\Delta\phi \propto \log(t) \times \log(p)$	$\Delta R \propto \Delta\phi$
Water vapour up to monolayer coverage	$\Delta R \propto (1 - e^{-\gamma.M})$	$\Delta\phi = 0.06$	—
Water vapour on oxygen pre-exposed surface	$\Delta R = 0$	$\Delta\phi = 1 \text{ eV}$ (for $> 10^{-6}$ torr.min.)	—
Water vapour beyond monolayer formation	$\Delta R \propto M$	$\Delta\phi = 1 \text{ eV}$ (for $> 10^{-5}$ torr.min.)	—

— Figure 2.3.1 —

— The Effect of Oxygen and Water vapour on Aluminium —

decreases by approximately 1 eV during the formation of a polar sheet on the surface of the oxygen covered metal between 10^{-7} and 10^{-6} torr-min of water vapour exposure. This same drop in potential occurs for water vapour on a fresh aluminium surface in case (iii) beyond monolayer exposure.

- v). Oxygen and water vapour both present in significant quantities. It is expected that firstly there is oxygen adsorption as for case (i), secondly water vapour adsorption as for case (iv) and finally oxidation or incorporation of oxygen into the bulk of the aluminium takes place according to case (ii).

With the exception of the combined oxygen and water vapour classification (v), the above are shown in tabular form in figure 2.3.1. It is assumed in this section that adsorption and oxidation have no effect on the electron scattering mechanisms or the degree of specular or diffuse scattering which takes place at the film surface. This is reasonable since the films in this work were not to be specifically annealed, and several authors, as discussed in section 2.2.2., have at least gone some way towards demonstrating that unannealed thin metallic films can be thought of as having completely diffuse electron scattering at their surfaces. The formation of oxide at the surface would not help 'smooth' the surface as required for less diffuse scattering. However, if any specular scattering is present before gas

adsorption takes place, then it is possible that increases in resistance are the result of changes in the electron boundary scattering.

For silver, only general statements can be made relating work function and electrical conductivity measurements. As for aluminium, Benton and Elgin (99) have reported that oxygen promotes the adsorption of water vapour on silver surfaces, but no work function or resistance measurements were made. It appears that this is the only observation reported in the literature of the dependence of water vapour adsorption on pre-exposure to oxygen for silver surfaces. It is expected that the reaction with oxygen which is known to occur with silver can be described by the first two lines of table 2.3.1. for aluminium. However, the absolute values for the constants in these various relationships will in all probability be significantly different from those for aluminium.

2.3.3. Overlayer on Low Conductivity Thin Film Metallic Substrates.

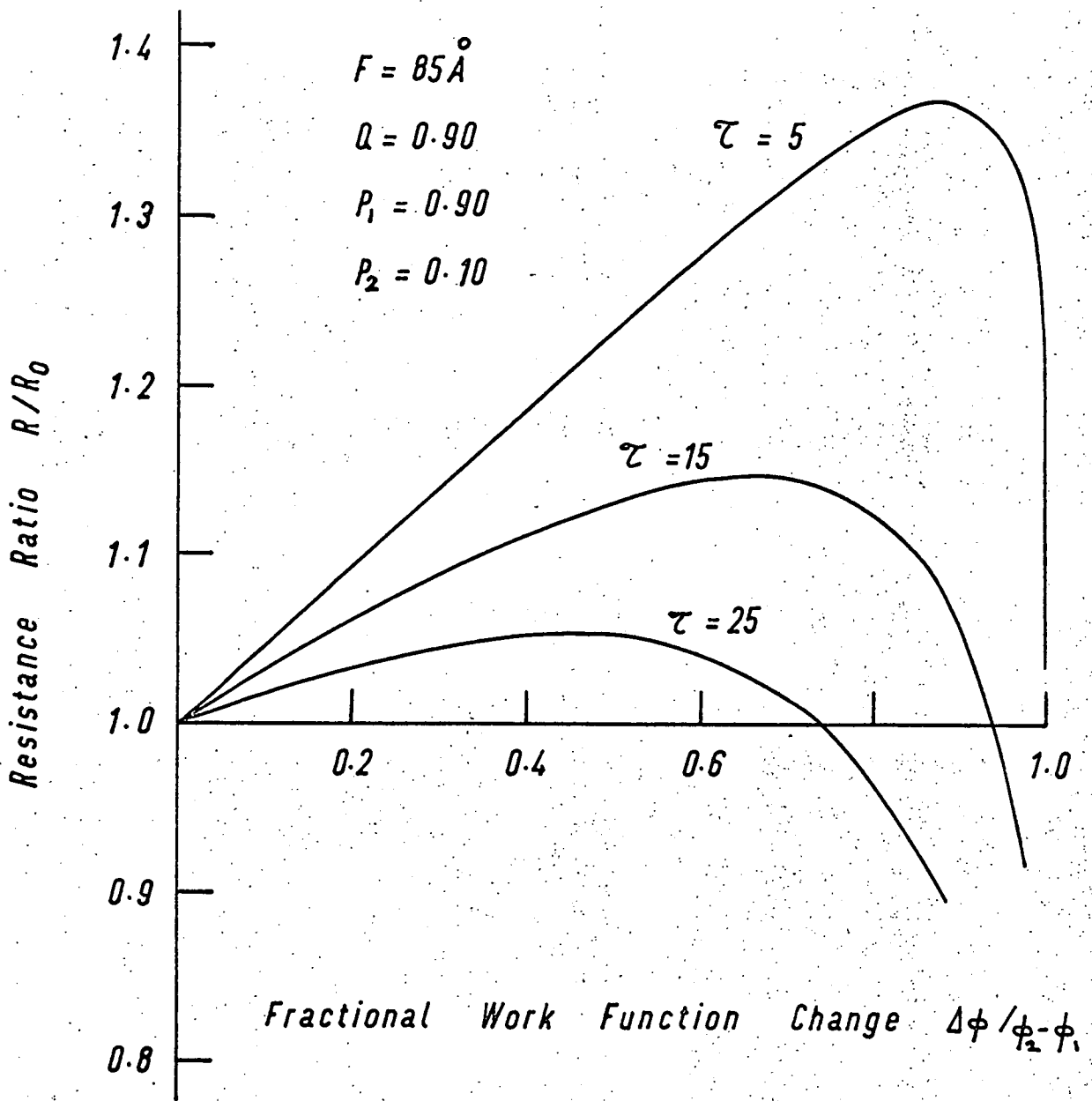
A metallic film of sheet resistance say 10 to $10^1 \Omega$ /sq. may have a positive temperature coefficient of resistance, but there are still many discontinuities in it. These discontinuities largely determine the resistance, where there is an activated electron transfer process between separated or isolated crystallites constituting the film in the direction of an applied electric field. When a metallic overlayer is deposited onto such a film, then provided the growth process of the composite film is similar

to that of the underlayer, a resistance versus mean thickness plot will have approximately the same form before and after the overlayer deposition. This is because it is predominantly the reduction of the size of the discontinuity gaps and not the value of the bulk conductivity of either the underlayer or overlayer material which determines the overall sheet resistance. The work function will vary with surface coverage, or mean overlayer thickness, in one of the three ways already discussed in section 2.2.6. Monitoring the work function of high resistivity films can thus assist in the identification of the overlayer growth process, which helps in the qualitative, if not quantitative, explanation of the conduction process.

2.3.4. Overlayers on High Conductivity Thin Metallic Films. For thin films having conductivity values approaching that of the bulk material, then more explicit forms of work function and conductivity relationships can be derived than for the films considered in section 2.3.3.

Consider a thin metallic film which is of uniform thickness and consists of large crystallites so that grain boundary scattering in the bulk of the film is insignificant compared to surface effects. If a metallic overlayer is deposited onto such a film, then assuming the same growth process as described in section 2.1.2., the resistance change from equation (2.1.19) is

$$\frac{R_T}{R_0} = (1 - \theta^2)^{1/2} + \left\{ \frac{\theta^{1/2}}{(1 - \theta^{1/2}) + \theta^{1/2} \frac{\rho_u}{\rho_T} \left(\frac{F+T}{F} \right)} \right\} \quad (2.3.9)$$



— Figure 2.3.2 —

— Predicted Variations of Work Function with Resistance —

where the symbols are as defined previously in section 2.1.2. Note that in equation (2.3.9) R/R_0 is a function of the surface coverage θ . (This θ is not to be confused with the surface coverage which is occasionally assumed to be the number of monolayers of overlayer on the surface equivalent to the mean thickness, t , of the deposit. The latter interpretation of surface coverage is not used in this work). Work function has been shown in section 2.2 to be a function of coverage θ , and hence a functional relationship exists between the fractional change of work function $\Delta\phi/\phi_1 - \phi_2$, where ϕ_2 and ϕ_1 are the work function values of overlayer and substrate respectively, and the resistance ratio R/R_0 during the formation of a metallic overlayer. Assuming the following values in the evaluation of the ratio R/R_0

$$F = 85 \text{ \AA}$$

$$P = 0.90$$

$$Q_1 = 0.90$$

$$Q_2 = 0.10$$

for a thin film of gold, with a work function ϕ_2 , having an overlayer of a metal with the same bulk conductivity, but with a work function ϕ_1 ; the variations of R/R_0 with $\Delta\phi/\phi_1 - \phi_2$ for three different values of t is shown graphed in figure 2.3.2. Obviously similar graphs could be obtained for any reasonable values of F , Q_1 , Q_2 and t for different overlayer materials. In the evaluation of equation (2.3.9) it is assumed that the work function change is directly proportional to the surface area covered by the overlayer material, i.e.

$$\Delta\phi \propto \theta$$

(2.3.10)

which is a reasonable approximation for an overlayer growth process involving nucleation and crystallite formation at the substrate surface. However, if considered necessary, a work function and coverage interdependence different from equation (2.3.10) can be employed, e.g. that of Levine and Gyftopoulos (71) described in section 2.2.6.

Thus for metallic overlayers it is shown that, just as for the case of adsorption and oxidation of thin metal films, work function values can be employed to explain resistance changes which occur as a result of surface effects. Care must however be taken to ensure that the work function complications in section 2.2.8. are given due consideration before measured work function values are used to explain conductivity changes.

CHAPTER 3.WORK FUNCTION MEASUREMENTIntroduction.

Several comprehensive reviews of the techniques for measuring work function have been written (76) (141) (38) (142). These reviews make it unnecessary to give in this work a complete discription of all the techniques currently available. However, a list of techniques is given explaining the basic principles of each one, and citing relevant references for more detailed theoretical and experimental works. From all of these different methods of measurement the one most suited for this work is selected and its theory developed. The instrumentation necessary for the realisation of the technique to be developed is then considered, and the chapter is concluded with an ewaluation of the measuring systems actually constructed.

3.1. Methods of Measuring Work Function.

Not all the methods considered yield absolute values of work function, but instead some only monitor changes which take place with respect to a reference electrode which may or may not have a known work function. Such techniques are still applicable since it is changes in work function, and not absolute values, which are more important in the experiments to be carried out. With very few exceptions all the various methods of monitoring work function can be thought of as belonging to one of the following.

- i) Contact potential.
- ii) Thermionic emission.
- iii) Field emission.
- iv) Photoelectric emission.
- v) Ion emission.

Each of these five types will now be considered in turn.

3.1.1. Contact potential. It was explained in section 2.2.2.

that when metals are in contact, or are connected by an external circuit, then a contact potential exists between them. This potential, V_{cp} , is equal in magnitude to the difference in the effective work function values ϕ_2 and ϕ_1 , of the metals, i.e.

$$V_{cp} = \phi_2 - \phi_1 \quad (3.1.1)$$

If the two metal bodies are separated, and have a capacitance C , then the charge q which flows round the external circuit in order that the bodies reach equilibrium is given by

$$q = C \cdot V_{cp} \quad (3.1.2)$$

or from equation (3.1.1)

$$q = C \cdot (\phi_2 - \phi_1) \quad (3.1.3)$$

From equation (3.1.3) if the capacitance C is caused to change by ΔC , then there is a corresponding change Δq in the

charge q , i.e.

$$\Delta q = \Delta C (\phi_2 - \phi_1) \quad (3.1.4)$$

By making C a periodic function of time, $f_c(t)$, and applying a D.C. voltage, V_a , across the bodies making up the capacitor in the opposite sense to the contact potential, then the charge q is a function of time given by

$$q = f_c(t) [(\phi_2 - \phi_1) - V_a] \quad (3.1.5)$$

Equation (3.1.5) when differentiated with respect to time represents the current i in the external circuit, i.e.

$$i = [(\phi_2 - \phi_1) - V_a] \frac{d(f_c(t))}{dt} \quad (3.1.6)$$

Assuming $[(\phi_2 - \phi_1) - V_a]$ is a constant.

The current i is reduced to zero when

$$(\phi_2 - \phi_1) = V_a \quad (3.1.7)$$

Thus when the condition of equation (3.1.7) is satisfied the difference in the effective work functions is found by measuring the applied D.C. potential V_a .

Equation (3.1.6) is the basis for the celebrated Kelvin ⁽¹⁴³⁾ capacitor method for measuring contact potential. Zisman ⁽¹⁴⁴⁾,

<i>Technique*</i>	<i>Accuracy</i>	<i>Response</i>
<i>Vibrating capacitor</i>	$\pm < 1\%$ (165)	<i>0.1 Volts/sec.</i> <i>0.5 sec.</i>
<i>Static capacitor</i>	$\pm 1\%$ (149)	
<i>Rotating capacitor</i>	$\pm 1\text{ mV}$ (148)	
<i>Oatley magnetron</i>	$\pm 20\text{ mV}$ (153)	
<i>Saturated diode</i>	$\pm 10\text{ mV}$ (132)	
<i>Breakdown field</i>	$\pm 30\text{ mV}$ (150)	
<i>Electron beam method</i>	$\pm 30\text{ mV}$ (181)	
<i>Space-charge limited diode</i>	$\pm 10\text{ mV}$ (152)	
<i>Thermionic emission</i>	$\pm 40\text{ mV}$ (129)	
<i>Field emission</i>	$\pm 10\text{ mV}$ (84)	
<i>Photo-electric emission</i>	$\pm 7\text{ mV}$ (89)	
<i>Ion emission</i>	$\pm 5\text{ mV}$ (133)	

* Note that all of the first group come under the general heading of 'contact potential methods.'

— Table 3.2.1 —

— Typical Accuracy for each Measurement Technique —

in 1932, at the suggestion of Professor Max Noble, made the technique more sensitive by making the capacitance vary at audio frequency, and detecting the current so generated by a valve amplifier. By employing negative feedback Simon (145), and later Petit-Clerc and Carette (146) and the author et al (147), made the Kelvin method more versatile by allowing a continuous recording of contact potential. Other methods which depend for their operation on the existence of contact potential are, the rotating dynamic capacitor (148), static capacitor (149), dielectric breakdown field (150), saturated diode (151), space charge limited diode (152), Oatley magnetron (153) and the electron beam method (154). Of these methods several have been suitably modified so that a map of contact potential variations over a surface can be obtained (155) (146) (156). Table 3.1.1. shows for ease of comparison typical accuracies reported for the different methods of measurement, and also the reported time response of the systems with feedback. For reference later, typical accuracies reported using techniques not based on contact potential measurement are included in the table. Using contact potential methods the effective work function values of silver (77) gold (84), and aluminium (29) have all recently been derived.

3.1.2. Photo-electric. Electrons can be emitted from a metal surface by the irradiation of light as a result of the absorption of photon energy. As the frequency ν of the light decreases, a value of ν_0 is eventually reached when electrons are only just emitted from the surface. This limiting frequency ν_0 is then related to the work function, ϕ_{ph} , of the metal surface by

$$h \cdot \nu_0 = e \cdot \phi_{ph} \quad (3.1.8)$$

where h and e have their usual significance.

Any real surface however, because it is at a non-zero temperature and the work function is unlikely to be constant over the entire surface, cannot have equation (3.1.8) applied directly to it for accurate work function determinations. For a uniform surface at a non-zero temperature, T , Fowler (157) derived the following relationship between photo-current i_p and irradiation frequency ν

$$\log \frac{i_p}{T^2} = K + f \left(\frac{h\nu - h\nu_0}{kT} \right) \quad (3.1.9)$$

where h and k have their usual significance.

K is a constant.

and $f \left(\frac{h\nu - h\nu_0}{kT} \right)$ is a complicated function of $\frac{h\nu - h\nu_0}{kT}$.

When using photo-electric emission as a means of measuring

work function care must be taken to allow for the electric fields which may exist, intentionally or unintentionally, at the surface (158). Riviere (76) has given suitable forms of equation (3.1.9) for the extreme cases where the electric field at the surface is much greater and much less than the patch fields on a non-uniform surface. An apparently rarely used method of work function measurement by photo-electric means is based on Planck's radiation law, from which it is possible to derive a useful equation very similar to the Richardson equation for thermionic emission (159). Using Fowler's theory recent work function measurements have been made for silver (160) and gold (84).

3.1.3. Field Emission. On the application of a high electric field of 10^7 Volts/cm, or larger, at a metal surface the probability of an electron being emitted increases considerably. The Fowler-Nordheim (161) (162) theory of field emission related the current density, J , to the applied electric field strength E and work function, ϕ_{fe} , by

$$J = \left(\frac{K_1 \cdot E^2}{\phi_{fe}} \right) \cdot e^{\left[\frac{-K_2 \cdot \phi_{fe}^{3/2} \cdot \Theta(x)}{E} \right]} \quad (3.1.10)$$

where $\Theta(x)$ is the Nordheim elliptic function with:-

$$x = \frac{K_3 \cdot E^{1/2}}{\phi_{fe}} \quad (3.1.11)$$

and K_1 , K_2 and K_3 are known constants.

Difficulty in relating the voltage applied between the metal and a counter electrode to the field strength at the metal surface makes the practical application of equation (3.1.11) difficult. As has been pointed out in proof of this difficulty (76) "It is no coincidence that all published measurements of the work function by field emission have referred to individual crystal planes." More recent theoretical treatments of field emission (163) (164) appear to lead to more reliable ways of deriving work function values from field emission measurements.

3.1.4. Thermionic Emission. The Richardson-Dushman equation is the basis for evaluating work function using thermionic emission. The equation relates the current density, J , from a heated emitter at temperature T to the work function value, ϕ_t , by

$$J = A(1 - \bar{r}_e) T^2 \cdot e^{\left(\frac{-e\phi_t}{kT}\right)} \quad (3.1.12)$$

where A is a constant.

e, k , have their usual significance.

\bar{r}_e is the electron reflection coefficient.

Complications arise in the application of equation (3.1.12) as a result of work function temperature dependence, patch field effects and electric fields at the emitting surface (69) (76) (141) (73). Hensley (73) has given a good discussion on thermionic emission with particular emphasis on what quantities are actually measured by this method. Because of the temperatures required for a

reasonable emission current density this method is best suited for metals with high melting points, such as the refractory metals tungsten and molybdenum.

3.1.5. Ion Emission. This method is based on the Saha-Langmuir equation which in modified form ⁽¹⁴²⁾ relates the ratio, α , of the number of ions to the number of atoms desorbed from a surface at temperature T to the work function, ϕ_i , by

$$\alpha = \frac{g_+}{g_0} \left[\frac{1 - r_i}{1 - r_0} \right] \exp \left[\frac{e(\phi_i(T) - 1)}{kT} \right] \quad (3.1.13)$$

where r_i is reflection coefficient for ion.

r_0 is reflection coefficient for atom.

g_+ is statistical weight of ionic states.

g_0 is statistical weight of atomic states.

e and k have their usual significance.

and $\phi_i(T)$ is the work function as a function of temperature.

Just as for the other work function measurement techniques described, this one has similar complications for the effect of applied electric fields and patch fields at the surface ⁽¹⁴²⁾ (76).

3.2. Selection of Contact Potential Method.

It is required in this work to investigate the work function of thin metal films under various experimental conditions. It was discussed in section 2.2.8. that temperature effects can have

a considerable influence on the work function of thin metal films. Also, it is well known that applied electric fields at the surface of high conductivity films during their formation can have a marked effect on the film structure. Thus it is undesirable to employ high temperatures or high electric fields for the work function measurements, which are a necessity for the application of the thermionic and high field emission techniques respectively. Hence, these two techniques are unsuitable. The following experiments require that the work function can be monitored during vacuum deposition, which for most practical cases means a process of evaporation then measurement being repeated many times. This being so, any work function monitoring techniques which critically depend on very accurate geometric alignment will not be suitable since the substrate (or counter electrode) would have to be moved many times during the experiments. The only measurements not requiring applied electric fields or high temperatures at the surface, and satisfy the alignment considerations, are several of the contact potential type. Of the methods discounted for the above reasons, the photo-electric is perhaps the best suited for this work, but just as the ion emission method gives an indication of the highest work function value present (142), so the photo-electric method gives an indication of the lowest work function value present for crystallites in a polycrystalline surface. The static and dynamic capacitor methods at the point of measurement have no net electric field applied at the surface, and do not require temperatures above

ambient. Furthermore, no magnetic fields are required as for some of the methods based on contact potential (153) (151). Two contact potential techniques remain to be considered. They are the breakdown field method and Anderson's electron beam method. The first of these is not applicable when it is the work function of an exposed surface which is to be monitored, and the second is undesirable since an electron beam can modify the structure of a very thin metallic film, especially when it has high resistivity and is grown on an insulating substrate. Gas adsorption is important in this work, and hence a technique that is capable of monitoring surface work function changes up to atmospheric pressure is preferred. This is satisfied only by the static and dynamic capacitor methods. However, although the static capacitor is eminently suitable for studies in rapid gas adsorption, it will become clear from the next section that a variation of the Zisman dynamic capacitor system is preferable in this case, especially since long term work function changes, and changes during vacuum deposition are to be investigated. In section 2.2.4. the average work function, $\bar{\phi}$, of a surface was defined. It is this average value, $\bar{\phi}$, that is measured by contact potential methods (77) (78). This is an advantage since work function measurements made by many of the alternative methods depend on complicated weighting functions of the crystallite type and size present at the surface (76), and are hence difficult to interpret except in simple cases when single crystal planes only are present. Also from table 3.1.1. it is evident that the

accuracy to be expected from the dynamic capacitor technique compares very favourably with the others.

3.3. Proposed System for Measuring Contact Potential.

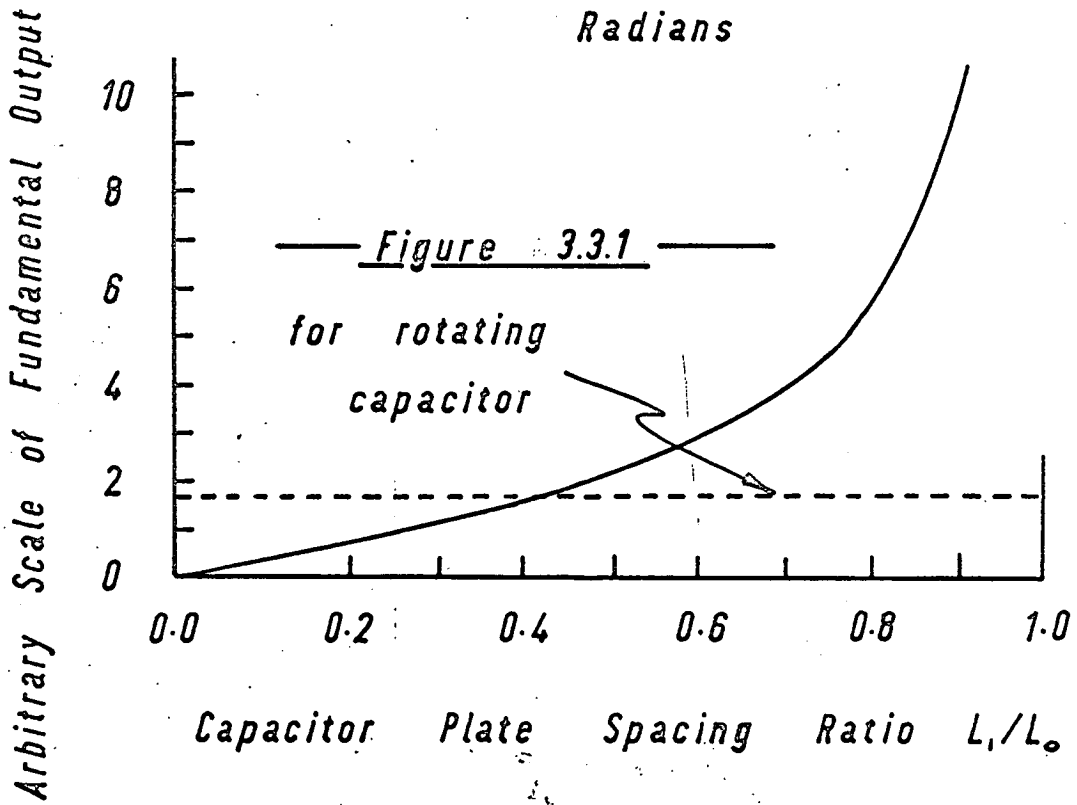
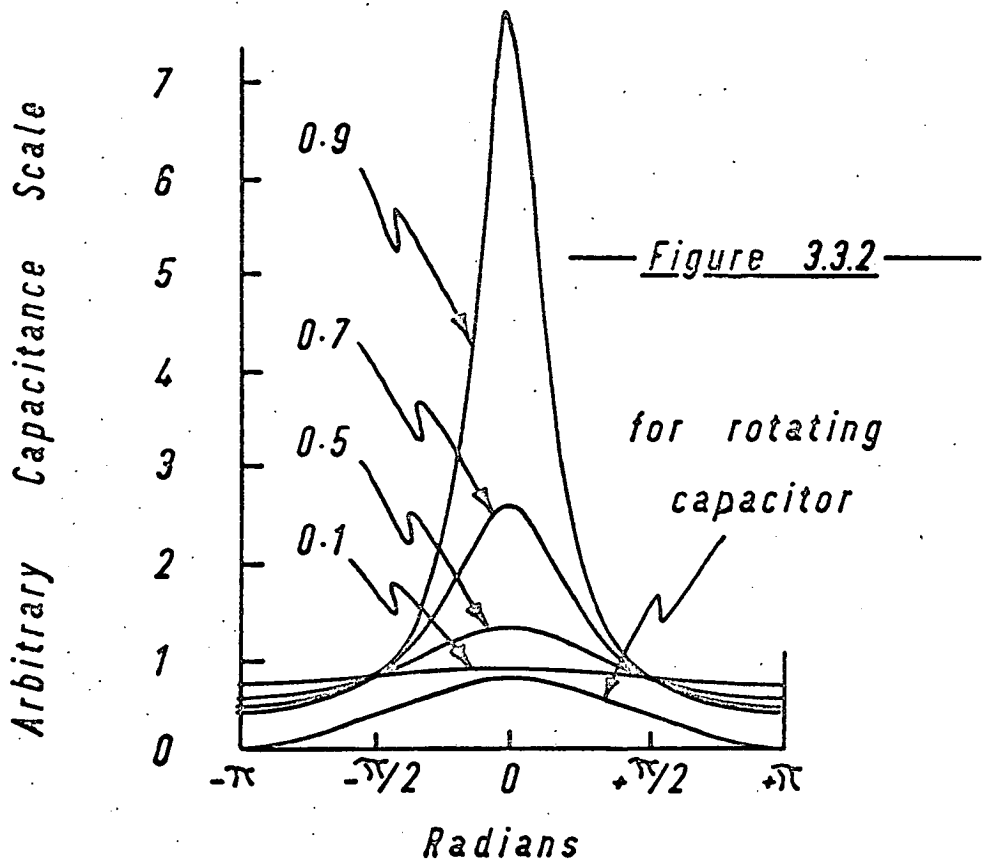
This section is divided into three parts. The first concerns the theoretical analysis of the action of dynamic capacitors, with particular emphasis on the rotating variation (148). The second part considers what instrumentation is required for the realization of a rotating system, and finally the third part examines the performance of the actual system constructed to monitor contact potential.*

3.3.1. Theory of Operation. Consider a conventional parallel plate capacitor with plates of area A spaced a distance L_0 apart. Assume that one plate is caused to vibrate sinusoidally in a direction perpendicular to the plane of the plates through an amplitude L_1 at angular frequency ω_0 , and let V_{cp} denote the contact potential difference between the plates. Then the magnitude of the charge, q , on the plates is given at time t by

$$q = V_{cp} \left[\frac{\epsilon_0 \epsilon_r A}{L_0 + L_1 \cos \omega_0 t} \right] \quad (3.3.1)$$

Assuming that during any period of measurement that $\frac{\partial V_{cp}}{\partial t}$ can be considered zero, then the current, i , generated by the dynamic capacitor is

* Footnote - Subject of UK Provisional Patent number 7323/70.



Dependence of Dynamic Capacitor Output on (L/L_0)

$$i = V_{cp} \frac{d}{dt} \left[\frac{\epsilon_0 \epsilon_r A}{L_0 + L_1 \cos \omega_0 t} \right] \quad (3.3.2)$$

or carrying out the differentiation.

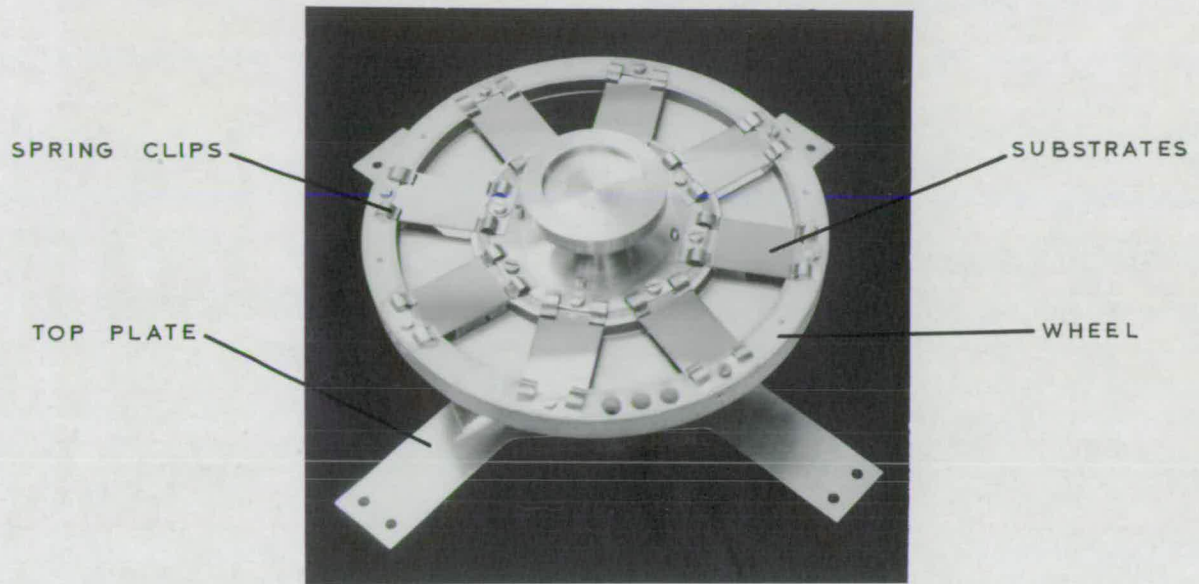
$$i = V_{cp} \left[\frac{L_1 \omega_0 \epsilon_0 \epsilon_r A \sin(\omega_0 t)}{(L_0 + L_1 \cos(\omega_0 t))^2} \right] \quad (3.3.3)$$

If an internal D.C. voltage, V_a , is applied to the plates with the correct polarity, then

$$i = (V_{cp} - V_a) \left[\frac{L_1 \omega_0 \epsilon_0 \epsilon_r A \sin(\omega_0 t)}{(L_0 + L_1 \cos(\omega_0 t))^2} \right] \quad (3.3.4)$$

and if the value of V_a is adjusted until the current, i , is zero, then from equation (3.3.4) V_a is equal in magnitude and opposite in sign to the contact potential difference, V_{cp} , between the plates.

For a fixed frequency ω_0 , equilibrium electrode spacing L_0 and contact potential V_{cp} , the fundamental component of current, i , generated is dependent only on the ratio $\frac{L_1}{L_0}$. Figure 3.3.1. shows how the fundamental component of the current signal varies with $\frac{L_1}{L_0}$, and figure 3.3.2. shows the capacitance variation for one complete cycle of vibration for various values of $\frac{L_1}{L_0}$. It is apparent that the Q value of the vibrating system increases rapidly with $\frac{L_1}{L_0}$ for $\frac{L_1}{L_0} > 0.5$. Atlas Autocode computer programs were employed in the drawing of figures 3.3.1. and 3.3.2.



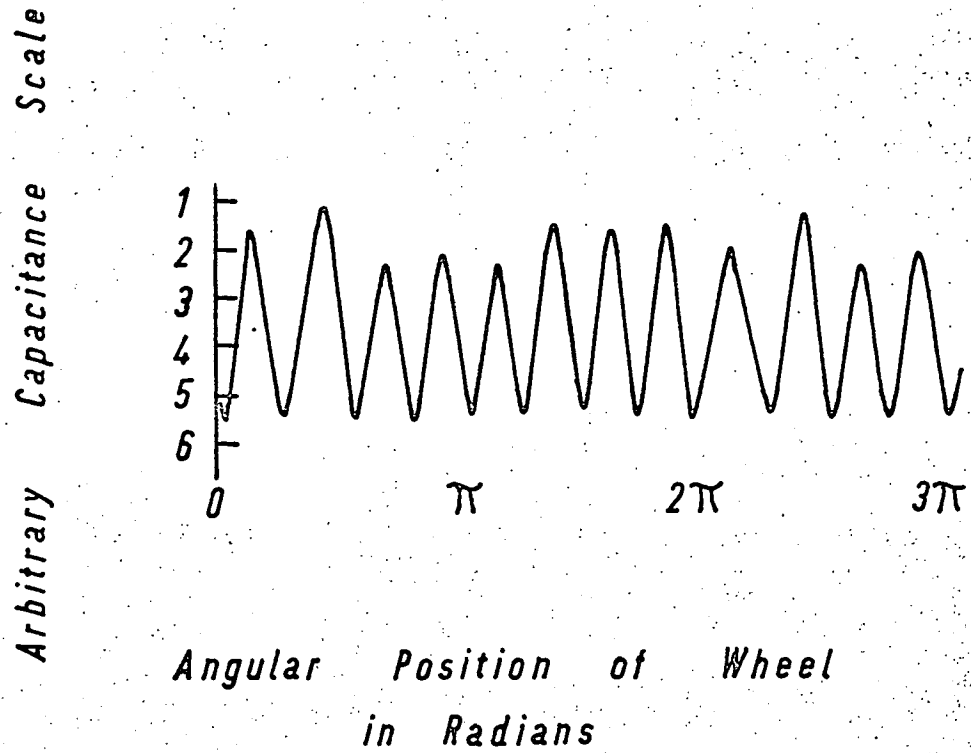
— Figure 3.3.3 —

— Eight Substrates mounted on Wheel —

Consider now a capacitor which has a spacing of L_0 between the plates, but one plate is swept across the other as shown in figure 3.3.5. For a series of n such electrodes mounted on a wheel, as shown in the photograph in figure 3.3.3. and in figure 3.3.5., and rotated at N revolutions per second, the output current signal is at angular frequency

$$\omega_0 = 2\pi n N \text{ rads./sec.} \quad (3.3.5)$$

The harmonic content of the A.C. current generated by this rotating dynamic capacitor is dependent on the shape of the electrodes. It can be shown (see Appendix 1.) that a series of rectangular plates rotating over a circular electrode generate a current with a high proportion of fundamental component. These shapes are also suitable for the practical reasons that glass substrates are readily available in rectangular form, and that a circular electrode gives the minimum periphery-to-surface ratio which is desirable from edge effect considerations. Other parameters being equal, the fundamental component of the output of the rotating capacitor is approximately the same as for a corresponding vibrating capacitor with $L/L_0 = 0.5$. For comparison a line is drawn on figure 3.3.1. at the appropriate output level of a rotating system with the plate dimensions and equilibrium spacing, L_0 , similar to those for the vibrating system. The two lines on figure 3.3.1. can be seen to intersect at $L/L_0 \approx 0.5$. The rotating capacitor which was constructed had



— Figure 33.4 —

— Dynamic Capacitance Variations —

the following leading dimensions:-

radius of reference electrode $R_1 = 0.95$ cm.

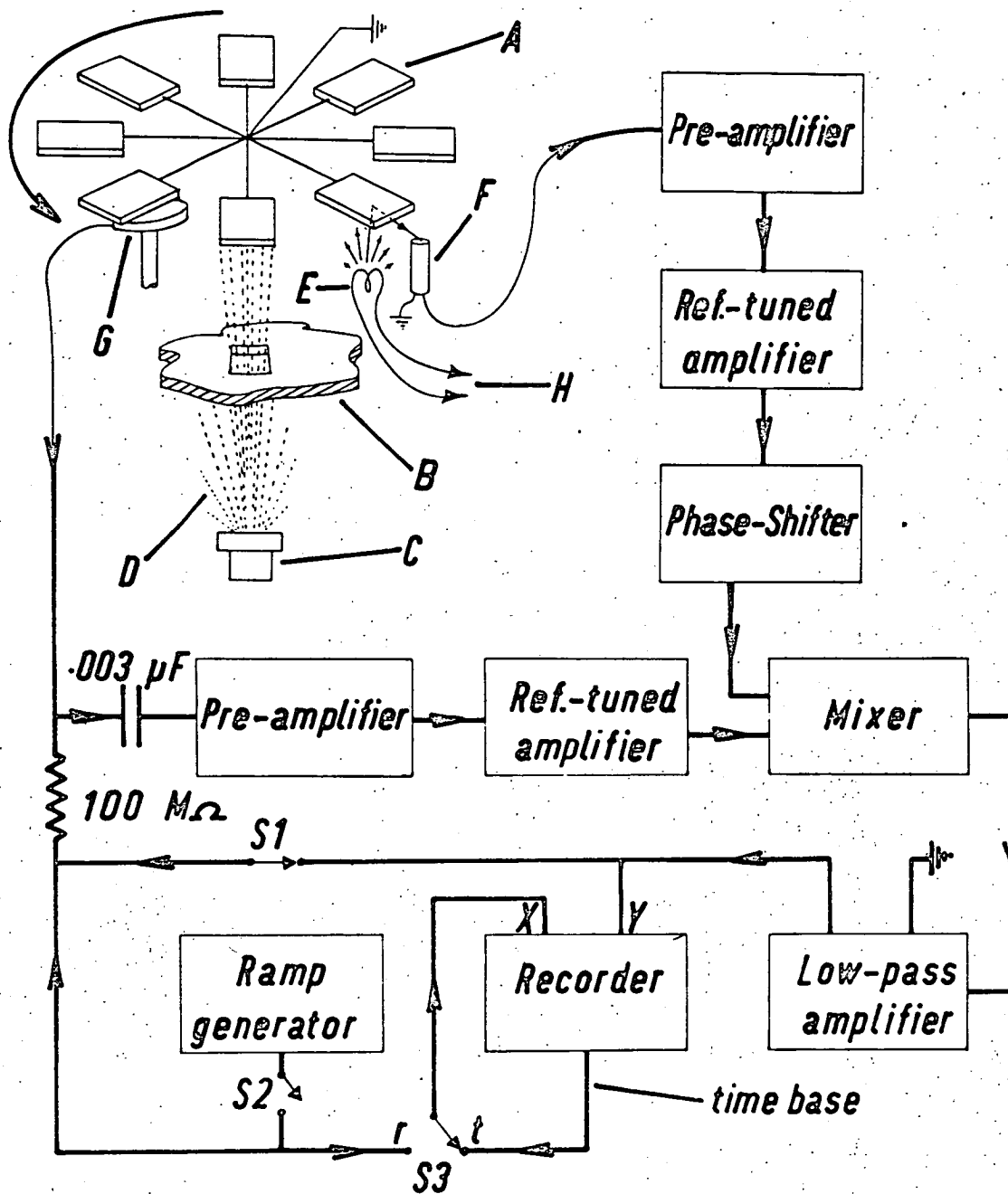
difference between centre of electrodes and point of rotation $R_2 = 5.1$ cm.

and from figure 3.3.3. it is seen that the number of rotating electrodes $n = 8$.

One complete revolution of actual capacitance variations is shown in figure 3.3.4. The method of capacitance measurement used for figure 3.3.4. resulted in the angle scale not being completely linear, however it is apparent that this approximates much more closely to a pure sinusoid of frequency ω_0 than does the capacitance variations shown in figure 3.3.2. for a vibrating system. This is important since it is the amplitude of the fundamental component and not the whole current signal, $\dot{\lambda}$, which is detected by the instrumentation employed. This is a consequence of a very narrow effective bandwidth which is necessary because of the small values expected for the current $\dot{\lambda}$. Typically the current $\dot{\lambda}$ is 10^{-12} to 10^{-11} amps r.m.s. for realistic values of capacitance, and for contact potential values of 10 to 100 millivolts. A useful quality parameter of a dynamic capacitor is the 'conversion efficiency' defined as

$$V_e = \frac{\text{r.m.s. volts of fundamental of input into instrumentation}}{\text{D.C. voltage existing across capacitor plates}}$$

Typically V_e is of the order of 1 to 10^{-3} .



— System for measuring contact potential —

— Figure 3.35 —

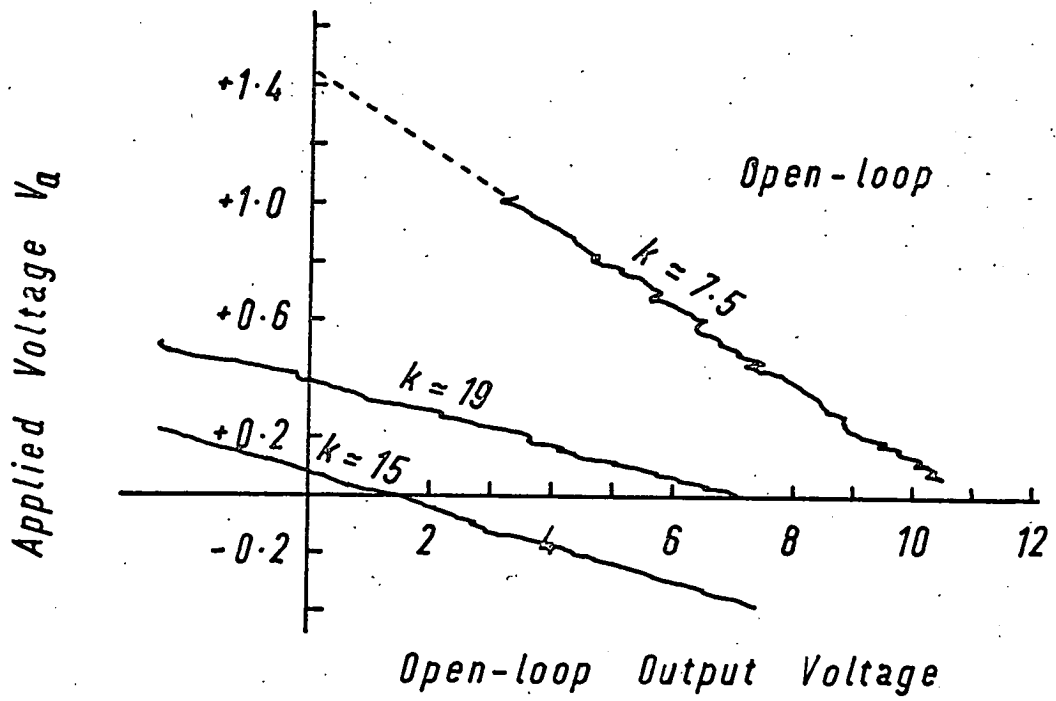
3.3.2. Instrumentation Required. Block diagrams of the instrumentation required for use with the vibrating type of dynamic capacitor, using negative feedback, have been reported by several authors (145) (146). However for the rotating system no similar closed loop system has been reported. Figure 3.3.5. shows the block diagram of a rotating system which is not substantially different from that given by Delchar and Ehrlich (165) when describing Simon's (145) instrumentation.. The most important difference is that no frequency divider is required with the rotating system, and that the circuit in figure 3.3.5. makes provision for applying a ramp voltage to the capacitor electrodes. In figure 3.3.5. A is one of eight earthed substrates rotated so as to pass over a reference electrode G and through an evaporation stream D. B is a baffle between the evaporation source C and the substrates. A lamp E is connected to a D.C. power supply H. The light from the lamp is reflected by the substrates and picked up by the photo-diode F in order to provide a synchronous input to the instrumentation. The output from the reference electrode is A.C. coupled to the instrumentation input, and can be D.C. coupled through a high voltage resistor to the instrumentation output in a closed loop configuration with negative feedback. With switch S3 in the 't' position, S1 closed and S2 open, the recorder trace follows changes in the contact potential difference between the reference electrode and the substrate surfaces. In this way work function changes during vacuum deposition can be continuously monitored, which would be

difficult to arrange with a conventional vibrating capacitor. Furthermore, the half revolution that the wheel has to travel to carry the substrates from the point of deposition to the point of measurement of contact potential allows a finite time lapse, during which ions deposited onto the substrate have sufficient time to be neutralised. If this was not done such charge effects could easily swamp the quantities which are required to be measured. After proving the technique by constructing an instrument according to a circuit designed previously (166), which was used in conjunction with a vibrating system to carry out a series of measurements on CdS thin films (167), a lock-in amplifier unit was acquired. It was an HR8 Princeton Applied Research Corporation (U.S.A.) unit, which performed the function of all the amplifiers, phase shifters and mixer on figure 3.3.5. with the exception of the pre-amplifier for the photo-diode.

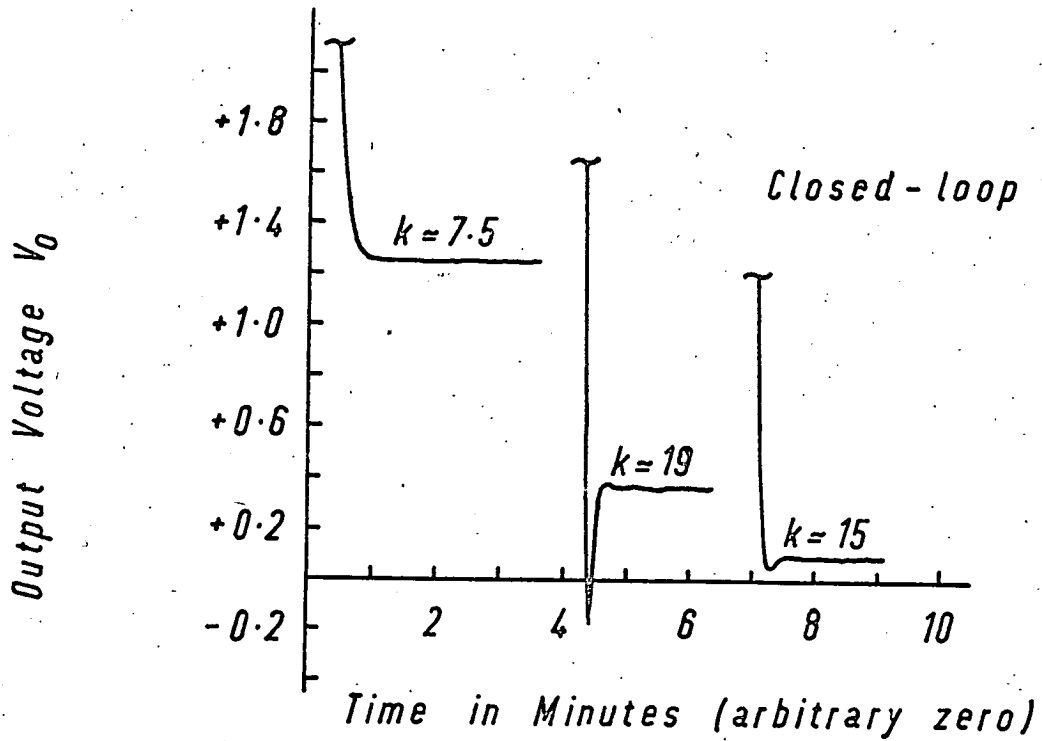
3.3.3. Performance of system. For the closed loop system shown in figure 3.3.5. with S1 closed, S2 open and S3 in position 't', the output voltage, V_o , is related to V_{cp} by the steady-state open loop gain, (k), thus

$$V_o = \left(\frac{k}{k+1} \right) \cdot V_{cp} \quad (3.3.6)$$

A common approximation is to make k sufficiently high to be able to regard V_o as approximately equal to V_{cp} . It is well-known, however, that the transient stability of a closed loop system is



— Figure 3.3.7 —



— Figure 3.3.6 —

— Dynamic Capacitor System Output —

highly dependent on the open loop gain. Figure 3.3.6. shows how the output of this particular system varies with k for a time constant of approximately five seconds. It is evident that the gain for critical damping should be approximately 15. This value is not high enough for $V_o = V_{cp}$ to be a valid approximation, but allowance can be made for this since k is a known constant. In any practical system there is a tolerance on k which will cause an error in the measured value of V_o . Figure 3.3.6. shows the open loop output of the rotating system when a sweep voltage is applied across the capacitor plates. (Figure 3.3.5. with S1 open, S2 closed and S3 in position 't'.) Figure 3.3.6. is for three different values of contact potential and gain k (corresponding to those of figure 3.3.7.). k is calculated from figure 3.3.6. by dividing the intercept on the x axis by that on the y axis

i.e.

$$k = \frac{\text{open loop output for no applied voltage}}{\text{contact potential}}$$

By fitting the best straight line to each of the traces on figure 3.3.6. it can be shown that variations in k are not greater than 10%. In the rotating system, however, the average value of k remains constant and can be accurately set since it is a direct function of L_o . Allowance can therefore be made for the fact that $k \gg 1$ since the value of k is known. Hence, if a quantity V_o/k is added to the output voltage, the result is exactly equal to V_{cp} , allowing for no random fluctuations in k .

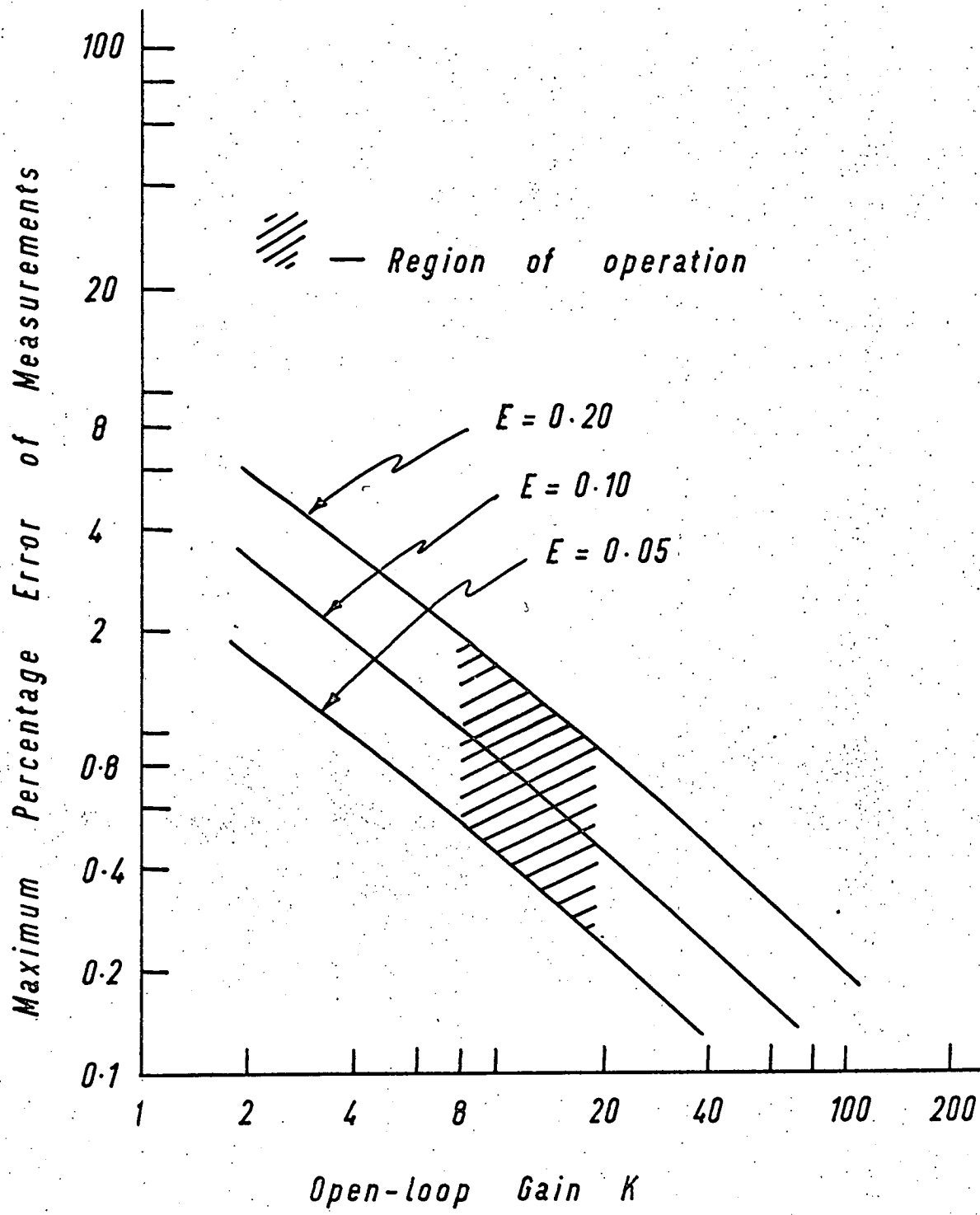


Figure 3.3.8

Accuracy of Dynamic Capacitor Output

If the output voltage is V_o from a contact potential difference V_{cp} with k set to a value k_s which fluctuates through $\pm \Delta k_s$, and V_{cp} is taken as $((k+1)/k)V_o$, the error, ξ , in V_{cp} can be shown to be

$$\xi = V_{cp} \cdot \frac{\frac{\Delta k_s}{k_s}}{k_s \left(\frac{1}{k_s} + 1 + \frac{\Delta k_s}{k_s} \right)} \quad (3.3.7)$$

If $\Delta k_s/k_s$ has a maximum value E , the, as a percentage,

$$\xi = 100 \cdot \frac{E}{k_s \left(\frac{1}{k_s} + 1 + E \right)} \quad (3.3.8)$$

Figure 3.3.8. shows this function plotted for $E = 0.05$, 0.10 and 0.20 for a wide range of k_s . The shaded region is bounded by $E = 0.05$, $E = 0.20$, $k = 8$ and $k = 20$. This is the region of operation of the system for reasonable transient response compatible with a steady-state measurement error of better than 2% and normally less than 1%. To this must be added the zero drift error which in the present system is ± 5 mV, but this could be reduced by better screening of the electrodes.

Furthermore, if it is required to change L_o , this is much more readily done on the rotating system with much less risk of the plates touching. One problem that is eliminated by employing a rotating rather than a vibrating dynamic capacitor is that the latter in practice usually depends on a mechanical resonance for a reasonable value of conversion efficiency, which may make the interpretation of results difficult if, as has been reported (168),

the contact potential difference is frequency dependent. Unlike the vibrating system, the operation of the rotating capacitor is not dependent on the medium between the plates and requires no adjustment for changes in pressure. This allows the facility of operation to be exploited to the full as the surface potential of films can be measured not only during high vacuum deposition, but also with equal accuracy under any subsequent changes of the gaseous environment. Also, within the experimental error of the technique, the deduced values of contact potential were found to be independent of the electrode spacing, L_0 , within operating limits.

CHAPTER 4.DESIGN AND CONSTRUCTION OF APPARATUS.Introduction.

This chapter in the first section presents a justification for a U.H.V. work chamber, followed by a specification of the requirements of such a system. A description of the actual vacuum system employed, with the expected pumping performance is then presented. In the second section details are given of the design and construction of the apparatus to be installed in the vacuum chamber. Finally, in the third section, the instrumentation employed to monitor and measure the various required parameters during the experiments is described and illustrated.

4.1. Vacuum Chamber.

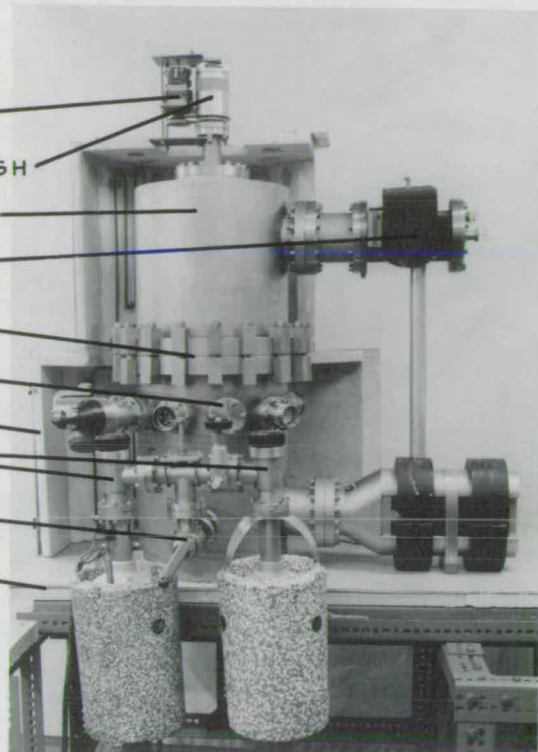
4.1.1. Vacuum Chamber Required. It is required that thin metal films are prepared by vacuum deposition. Furthermore, it is well known that residual gases present during deposition, especially water vapour, can significantly influence crystal growth^{(169) (170)} (29). However, even if the total gas pressure is sufficiently low that growth is not noticeably effected by residual gases, surface effects as a result of adsorption can become evident in a few minutes at pressures as low as 10^{-7} torr, e.g. that of oxygen on aluminium⁽²⁹⁾. In the extreme case of unity sticking

coefficient a metal surface in a gas pressure of 10^{-8} torr becomes covered with a monolayer of adsorbed gas molecules in a few minutes. Thus it is apparent that a vacuum system having a base pressure of 10^{-9} torr, or better, is required for this work. With a pressure of this order the residual gas composition can be better controlled since gases can be bled into the vacuum system without resulting in a pressure which is too high to allow investigations in the onset of surface effects of these gases. Hence, provision is to be made for mounting a leak valve on the chamber. Other feedthroughs required in the chamber walls are;-

- i) A high speed rotary feedthrough for rotating the 'wheel' with eight substrates mounted on it.
- ii) High power feedthrough for taking power to the evaporation sources.
- iii) Slow speed rotary or linear motion feedthrough for changing evaporation sources.
- iv) Multi-way instrumentation feedthrough for low power electrical connections to within the vacuum chamber.
- v) Precise linear motion feedthrough for positioning the reference electrode with respect to the wheel mounted substrates.
- vi) Viewing ports for making various visual checks.
- vii) Suitable mounting point for a mass spectrometer in order to analyse residual gases in the chamber.

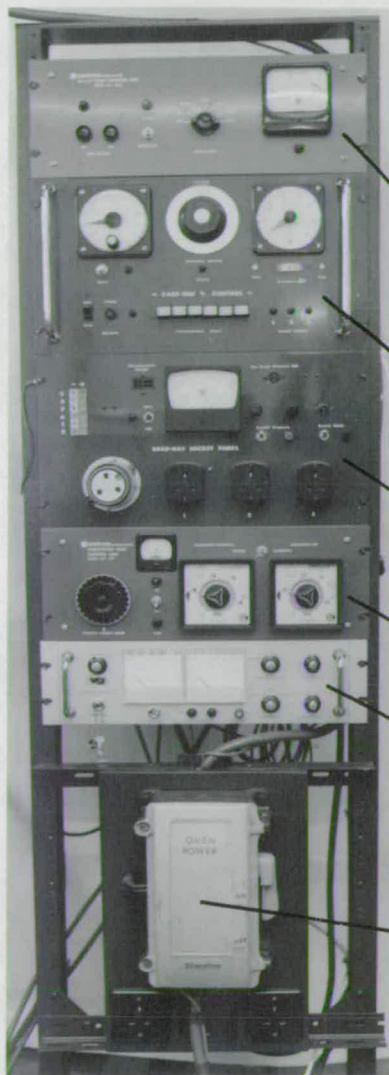
All of these feedthroughs are readily obtainable

ELECTRIC MOTOR
 HIGH SPEED ROTARY FEEDTHROUGH
 STAINLESS-STEEL VACUUM CHAMBER
 MASS SPECTROMETER HEAD & MAGNET
 WHEELER FLANGE
 TEN 1½" I.D. PORTS
 ONE SECTION OF OVEN
 VITON SEAT VALVES
 BAKEABLE VALVE
 INSULATING BASE



— Figure 4.1 —

— Vacuum System —



ION PUMP CONTROL UNIT

BAKE-OUT CONTROL PANEL

BAKE-OUT SOCKET PANEL

T.S.P. CONTROL UNIT

VACUUM MEASUREMENT

OVEN POWER CONTACTOR

— Figure 4.2 —

— Vacuum System Instrumentation —

for fitting to a stainless steel vacuum chamber using Conflat flanges.

Also, a stainless steel chamber is suitable since stainless steel has a slow surface degassing rate, especially after being baked at high temperatures under vacuum, which is necessary for obtaining U.H.V. conditions; and that very robust, large stainless steel vacuum chambers can easily be obtained which are readily accessible. The all-dry pumping systems normally used with steel work chambers do not suffer from the surface contamination effects that diffusion pumps are known to have. (85). In fact, triode ion pumps of the Vac-Ion type help clean surfaces in the chamber since a glow discharge occurs until the pressure is reduced to below $\sim 10^{-3}$ torr, and it is well known that such discharging serves to clean surfaces. Electrical screening is made easier with an all metal chamber than for a glass one, since it is usually necessary to paint the outer surface of the latter with a conducting layer which is then connected to earth. The only serious disadvantage of present day vacuum systems constructed from stainless steel is one of expense, which was not a problem for this work since an all-stainless steel system was made available.

4.1.2. Vacuum System Employed. The system is a modified VI-220 Varian vacuum system, and is shown in figure 4.1.1. It is pumped by two Varian 941-5610 sorption pumps, a 50 litre per second Vac-Ion pump and a three element titanium sublimation pump (T.S.P.).

A bakeable valve isolates the roughing pumps from the chamber, and two non-bakeable valves allow the sorption roughing pumps to be operated alternately. By working in this way a roughing pressure suitable for starting the ion pump is reached in a relatively short time (171). The base pressure expected with the combination of the pumps described above is of the order of 10^{-10} torr provided the system is given a bake at, say, 200°C . for several hours, and that the chamber contents are made of good vacuum materials. A good vacuum material is one that has a very low vapour pressure, does not have foreign substances on its surface which outgas significantly, and can withstand the bake-out temperature without changing its characteristics. The time taken to reach the base pressure will be largely determined by the duration of the bake and the considerable period that the system and contents will take to return to approximately room temperature. Hence, the time from starting to chill the roughing pumps to reaching the base pressure will be of the order of 15 hours. The chamber is 12" diameter and is in two parts, the top being held to the base part by a Wheeler flange. As seen in figure 4.1.1. the top part has fitted to it the high speed rotary feedthrough and the mass spectrometer head. The lower part has ten $1\frac{1}{2}$ " I.D. ports fitted at regular intervals round the circumference of the chamber, as well as the two pumping ports and the T.S.P. element cartridge. All of the flanges used are of the Conflat type. During the bake-out period the roughing pump system is removed at the bakeable valve joint. Also various parts of the feedthroughs are removed

For key to
numbers - see next page.

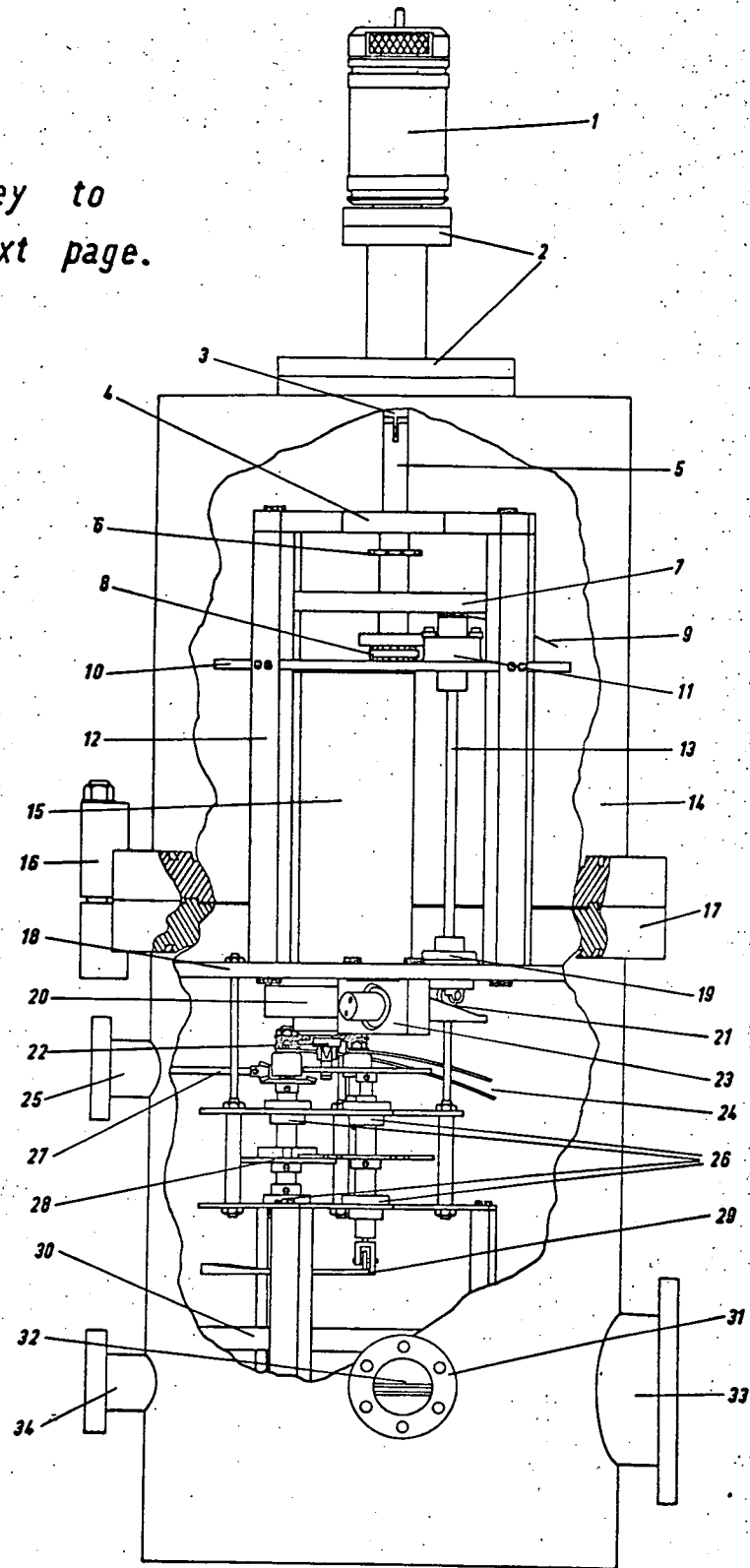


Figure 4.2.1

Exploded Diagram of Vacuum System

Key To Figure 4.2.1 (on Previous Page).

1. Varian high speed rotary feedthrough.
2. Conflat flanges (bolts are not shown).
3. Adaptor piece from rotary-feedthrough shaft to wheel shaft.
4. Top plate of wheel assembly.
5. Shaft for wheel.
6. Milled teeth to give dynamic capacitor synchronous pick-up signal (not used).
7. Wheel holding 8 substrates.
8. End race set for shaft.
9. Electrical output from reference electrode.
10. Bottom plate of wheel assembly.
11. Rotolin bearing and housing to allow vertical movement of reference electrode.
12. Legs (4) of wheel frame assembly.
13. Push-rod connected to reference electrode.
14. Stainless-steel vacuum chamber wall.
15. Baffle for evaporation source.
16. Wheeler flange clamp assembly (1 of 25).
17. Wheeler flange with only one bolt assembly shown.
18. Base plate for wheel assembly.
19. Rotolin bearing for guiding connecting rod.
20. Electron beam evaporator head containing filament and electron optics.
21. Inclined plane to convert from horizontal to vertical motion.
22. Source crucible.
23. Stainless steel block/

23. Stainless steel block housing Rotolin bearing for horizontal push rod.
24. Electrical input for electron beam evaporator.
25. One of 10 ports with $2\frac{3}{4}$ " diameter Conflat flanges positioned round the chamber.
26. Rotolin bearings of assembly for changing sources.
27. Rotary motion drive shaft for changing sources.
28. Geneva mechanism for changing sources.
29. Castor running on an inclined plane on a wheel to give vertical positioning of the crucibles.
30. Titanium sublimation pump guard.
31. Roughing port.
32. Titanium sublimation pump elements (3).
33. Ion pump port.
34. Port for titanium sublimation pump power feedthrough.

including the mass spectrometer magnet, the high speed rotary feedthrough magnet and motor, the plastic pieces of the precise linear and slow motion rotary feedthroughs and all external electrical connectors except the H.T. lead to the ion pump. The whole vacuum system is mounted on an insulating base of Sindanyo board, which is an asbestos filled cement made by Turners Asbestos Cement Co., on 1" thick asbestos. In order to reduce dust from the asbestos it was treated with several coats of potassium silicate. An oven made of 1" thick asbestos covered with aluminium sheeting completely enveloped the vacuum system. The oven was in sections, one of which was shown in figure 4.1.1., and had on its inside heating elements with a total heating power of 6 kilowatts. Instrumentation was such that the power to the oven could be switched on or off depending on the pressure in the chamber, the duration of bake required, and the temperature as measured at set points by chromel-alumel thermocouples. Figure 4.1.2. shows the front panels of the bake-out control instrumentation together with the other electronics concerned with the creation, control and measurement of the low pressure in the vacuum chamber.

4.2. Design of Vacuum Chamber Contents.

4.2.1. Dynamic Capacitor. The starting point for the design of the wheel dimensions is that 2 cm by 3 cm. 7059 Corning glass substrates are to be used. From section 33, the instrumentation gain is proportional to the frequency of the A.C. current generated

by the dynamic capacitor, i.e. to the number of substrates mounted on the wheel, and the gaps between successive substrates should be approximately equal to the substrate width for high fundamental component of the current generated. From these considerations, 8 substrates, as shown in figure 3.2.3., is a convenient number consistent with a wheel size which is not too large to result in appreciable wobble during rotation. The wheel is made of Fluorosint, manufactured by G.H. Bloore & Co., which is a glass filled P.T.F.E. with a low vapour pressure and an almost linear temperature coefficient of expansion, unlike most plastic based materials. It is a very good insulator and is easily machined, although it is relatively expensive (£40 per square foot for $\frac{1}{2}$ " thick sheet). Recesses are machined in the wheel in order to locate the substrates, which are held in place by beryllium copper spring clips as shown in figure 3.2.3. The wheel is mounted on a non-magnetic stainless steel shaft which is located at two points by ball bearing sets, see figure 4.2.1. Referring to figure 4.2.1., the shaft (5) mates with a drive shaft (3) rotated by the magnetically coupled high speed rotary feedthrough (1). By having a magnetically coupled drive no actual shaft has to penetrate the vacuum chamber wall. The ball bearing sets are mounted on the top plate (4) and on the baffle plate (10). Four legs (12) are securely fixed to these plates and screwed to a $\frac{3}{8}$ " thick base plate (18). The base plate is bolted to three small fixing platforms which are welded to the chamber wall, see figure 4.2.2. The plates and legs are of stainless steel

with all of the blind screw holes having relief holes drilled into them so that no pockets of gas in these blind holes could limit the pressure by outgassing over a prolonged period. Still referring to figure 4.2.1., the reference electrode is mounted on the top end of the push rod (13). The rod is located in the horizontal plane with Rotolin bearings (11 and 19) housed in the baffle plate (10) and base plate (18) respectively, and in the vertical plane by the bearing (21) running in an inclined slot. The reference electrode can then be raised and lowered by horizontal movement of the plunger moving in the bearing housing (23), causing the bearing (21) to run up and down the inclined slot. The plunger is fixed to the precise linear feedthrough via the push bar see figure 4.2.2. By the use of this mechanism the reference electrode can be set in the vertical plane to within approximately $\pm .01$ mm., and a measure of its position is obtained directly from a dial on the linear feedthrough. However, considerable backlash in the mechanism has to be allowed for. Reference electrodes which are spherical (156), cap shaped (29) and planar have all been used in contact potential studies. In this work a round reference electrode of stainless steel, was used having an optical finish, and coated with $\sim 1500\text{\AA}$ of gold deposited in a vacuum system with an oil diffusion pump. The electrode is separated from the push rod by a disc of Fluorosint, and electrical connection is made by having a thin foil of beryllium copper protruding from the electrode/fluorosint junction which was made with a layer of Silastoseal vacuum leak sealant. Capacitance

variations between the reference electrode and the wheel mounted substrates, as shown earlier in figure 3.3.4. for a typical measurement, could be repeated very easily using the mechanism described above for controlling the electrode-to-substrate gap. For the capacitance variations on figure 3.3.4., assuming the arbitrary scale represents picofarads, then the extremes of amplitude variation are approximately 3 and 5 pf. Thus the variation in gap width, assuming an electrode area of $2.84 \cdot 10^{-4}$ sq. m. and no fringing effects, is

0.85 mm to 0.51 mm.

i.e. a difference of 0.34 mm.

This represents the combined effects of uneven substrate mounting, substrate thicknesses which may vary a few thousandths of an inch, and the wobble of the wheel as it rotates. The wobble however would be somewhat exaggerated at the very low speed of rotation used for making the capacitance measurements.

A reasonable approximation to the capacitance C variations on figure 3.3.4. is

$$C = C_0 + 2 \cos(\omega_0 t) \cdot 10^{-12} \text{ Farads} \quad (4.2.1)$$

where C_0 is the background capacitance

ω_0 is the frequency of the capacitance variations in radians per second

and t is the time in seconds

If ω_0 is say 60π radians per second, then differentiating equation (4.2.1) with respect to time yields

$$\frac{dc}{dt} = -2 \cdot 10^{-12} \cdot 60 \cdot \pi \cdot \sin(\omega_0 t) \quad (4.2.4)$$

Substituting for $\frac{dc}{dt}$ in the equation for the A.C. current, i , generated by a dynamic capacitor

$$\text{i.e.} \quad i = V_{cp} \cdot \frac{dc}{dt} \quad (4.2.3)$$

yields

$$i = -2 \cdot 10^{-12} \cdot 60 \cdot \pi \cdot V_{cp} \cdot \sin(\omega_0 t) \quad (4.2.4)$$

or as an r.m.s. value

$$i_{\text{r.m.s.}} \simeq 0.7 \cdot 2 \cdot 10^{-12} \cdot 60 \cdot \pi \cdot V_{cp} \quad \text{amps r.m.s.} \quad (4.2.5)$$

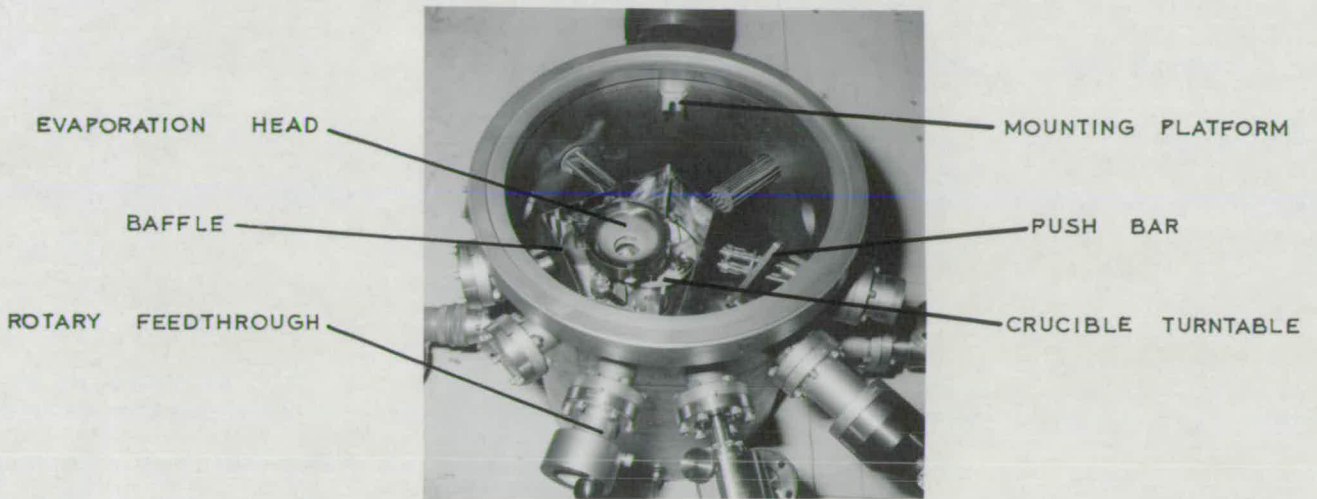
If the input impedance of the pre-amplifier is $10^7 \Omega$, then the input voltage, V_e , as an r.m.s. value is

$$V_{e \text{ r.m.s.}} \simeq 10^7 \cdot 0.7 \cdot 2 \cdot 10^{-12} \cdot 60 \cdot \pi \cdot V_{cp} \quad \text{volts r.m.s.} \quad (4.2.6)$$

Hence the conversion efficiency, as defined previously in section 3.4.1., is given by

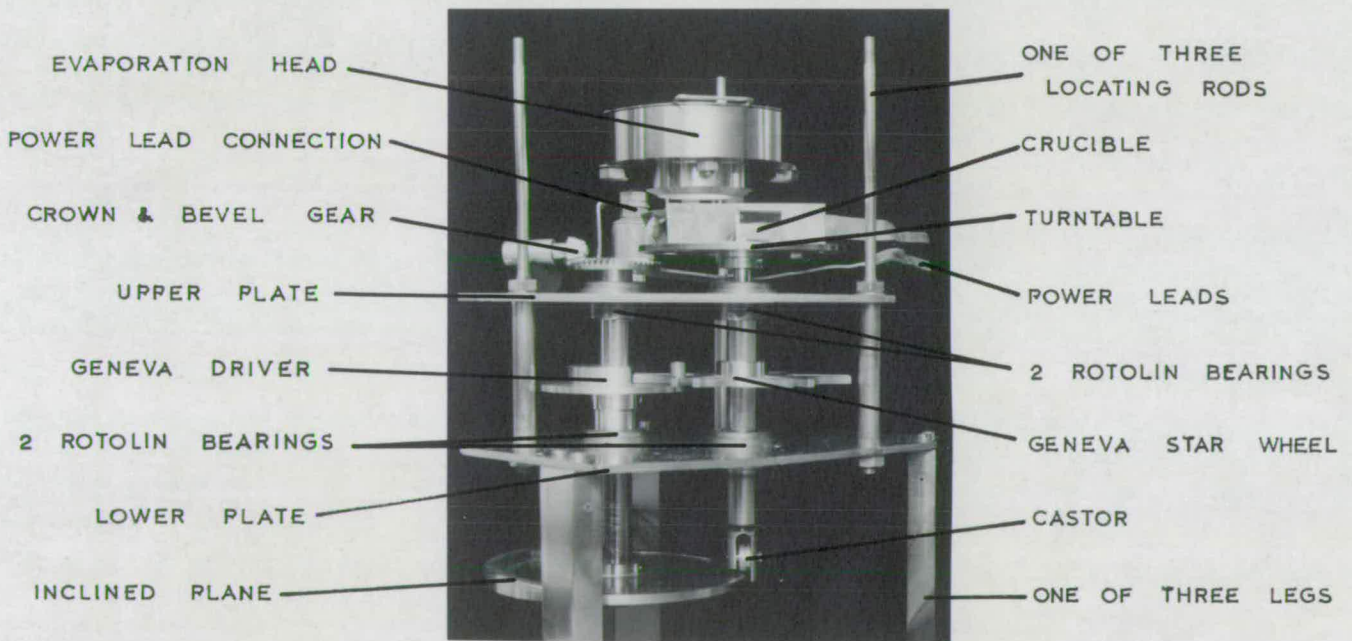
$$V_e \simeq \frac{V_{\text{r.m.s.}}}{V_{cp}} = 0.0025 \quad (4.2.7)$$

i.e. for 1 millivolt of contact potential there is an input



— Figure 4.2.2 —

— Evaporator unit in Vacuum Chamber —



— Figure 4.2.3 —

— Electron beam Evaporator —

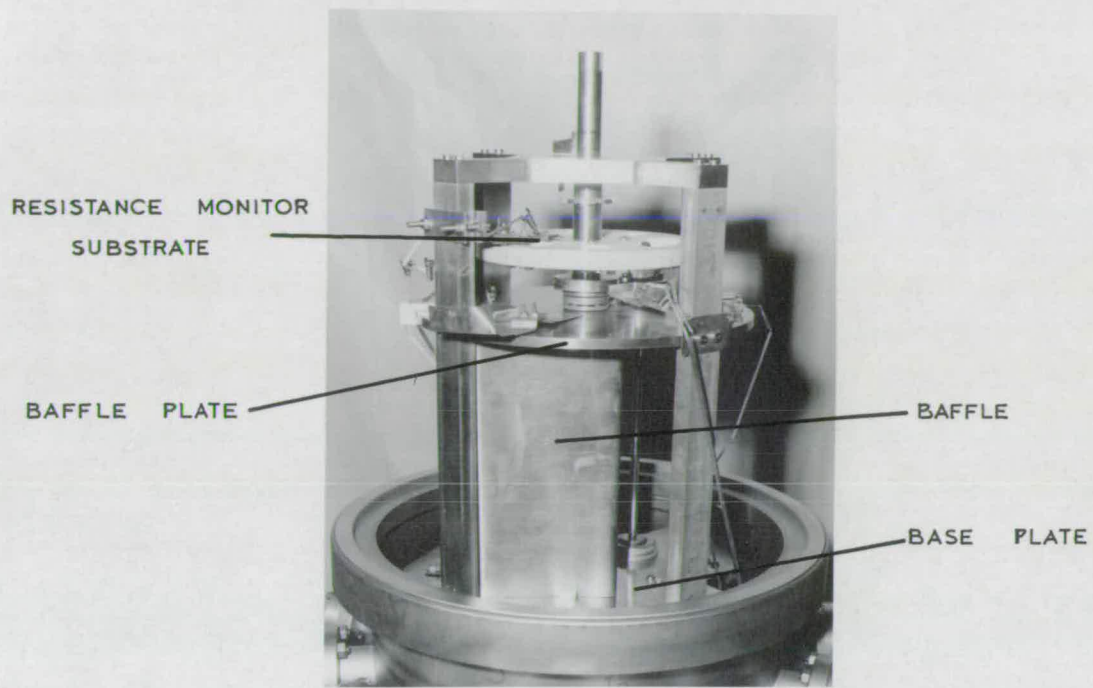
to the instrumentation of 2.5. micro-volts r.m.s. at the fundamental frequency.

Capacitance variations of the rotating dynamic capacitor are very much independent of shock and vibration in the vicinity of the apparatus. When a 160 lb weight was dropped from a height of two feet, a few feet from the chamber, onto the suspended concrete floor supporting the apparatus no change was observed in capacitance measurements. For vibrating capacitors located on the same floor and subjected to the same treatment, very noticeable changes in capacitance took place.

The synchronous signal input is obtained, as explained previously, from a photo-diode which receives the chopped light beam reflected from a quartz lamp. On figure 4.2.5. the photo-diode and lamp can be seen separated by a baffle. The light received by the photo-diode is reflected by the substrates from the lamp, and hence is at the same frequency as the current signal at the reference electrode. The diode is a LS400 (Texas Instr. Co.), and the lamp is a Wotan type 6.4625 NHD quartz source.

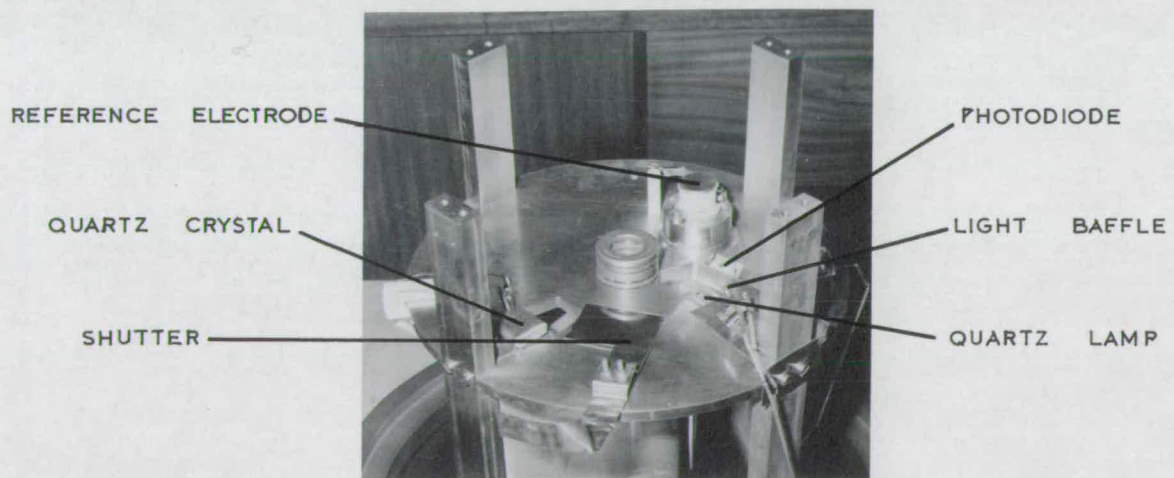
4.2.2. Evaporator. A multi-source electron beam evaporator unit suitable for U.H.V. was designed and constructed for use with the Birvac type RG1 Ring Gun console. Figures 4.2.2. and 4.2.3. show the various parts of the unit. An electron beam evaporator was chosen in preference to other types because only two high power feedthroughs are required to operate, in this case, up to six different sources, each one of which is located in the same

position when being evaporated. Furthermore, the evaporation stream passes up through the electron beam, and hence will have a relatively high ion density. These ions will help to clean the substrate, and also the charge of the ions will result in the deposited films being continuous at a lower mean thickness than for a thermal source ⁽¹⁷²⁾. An indication of the minimum possible ion density can be got from the report by Chopra ⁽¹⁷³⁾ that a silver source at about 1200°C when being deposited at a rate of 50Å per minute has one out of every 2000 silver atoms with a net positive charge. The evaporator filament is of tantalum and emits electrons in the temperature limited mode. Operating in this mode means that once the gun has reached an equilibrium state, with a fixed current passing through the filament, then the emission current is relatively insensitive to changes in the H.T. voltage between the filament and evaporation source which can hence be used as a fine control over the evaporation rate. If instead, the filament current is used as the fine control, then a long time lag occurs before equilibrium conditions are reached, which will usually result in an overshoot of the desired evaporation rate. Such variations in the evaporation process are not desirable since the film growth is dependent, at least to some extent, upon the evaporation rate. Referring to figures 4.2.2. and 4.2.3. a brief description of the source changing mechanism, which is thought to have some unique features, is now given. The turntable holding the crucibles is secured to the shaft carrying the driven star wheel of a Geneva mechanism.



— Figure 4.2.4 —

— Wheel-frame Assembly —



— Figure 4.2.5 —

— Wheel-frame Assembly with Wheel removed —

The Geneva driver is on a shaft which is rotated through a crown and bevel gear by the slow speed rotary feedthrough. Four revolutions of the feedthrough shaft represents one complete revolution of the driver shaft, and one crucible shift of the turntable. In order that the crucibles are positioned well into the neck of the evaporator head a circular inclined plane is screwed onto the bottom of the driver shaft. A castor arrangement at the foot of the driven shaft runs on the inclined plane and causes the crucibles to be raised and lowered at the appropriate times. The two shafts are located by four Rotolin bearings housed in the upper and lower plates of the assembly. Three legs supporting the plates reach to the chamber floor, and in order to prevent the whole assembly from moving in the chamber, three locating rods are bolted to the base plate, see figure 4.2.1. The evaporation stream from the crucibles reaches the rotating substrates through holes in the base and baffle plates. To confine the evaporation stream, baffles are fitted round the evaporator and between the baffle and base plates, as shown in figures 4.2.2. and 4.2.4. respectively. A shutter, which can be moved with a magnet from outside the vacuum chamber, as shown in figure 4.2.5., allows the evaporation stream to be prevented from reaching the substrates. The power leads to the evaporator head are self-supporting copper strips which are slotted into the high power feedthrough and bolted to the evaporator unit. Insulating parts required were machined from a ceramic material (Alsil), and with the exception of the bearings, filament, and copper leads

all parts were of non-magnetic stainless steel. All blind screw holes had relief holes drilled, and the bearings and Geneva mechanism were dry lubricated with molybdenum disulphate powder. This was found to be an excellent way of lubricating all of the bearing used in the apparatus for use at the U.H.V. provided that all excess powder was removed, and that the bearings were run-in for several minutes before use. The crucibles used were shaped from double layer molybdenum sheet, except for use with aluminium when carbon crucibles retained by steel clips were employed. The latter was done because aluminium is known to react with molybdenum at high temperature.

4.2.3. Film Thickness. A quartz crystal resonating at a nominal frequency of 6 MHz is used with an Edwards type F.T.M.1 film thickness monitor. The rate of evaporation and the thickness of deposit can be obtained by suitable calibration of the frequency change for a known thickness of film. The crystal is located in an earthed casing, as shown in figure 4.2.5., with a $\frac{1}{4}$ " diameter hole located under the centre of the crystal in the crystal casing and the baffle plate. The crystal is thus exposed to the evaporation stream continuously and can hence be used for setting up outgassing and evaporation conditions without evaporant reaching the substrates. Also the crystal, because of its location, receives approximately sixteen times the area density of source material than the substrates do. This makes the crystal more sensitive to very thin deposit measurements provided complete

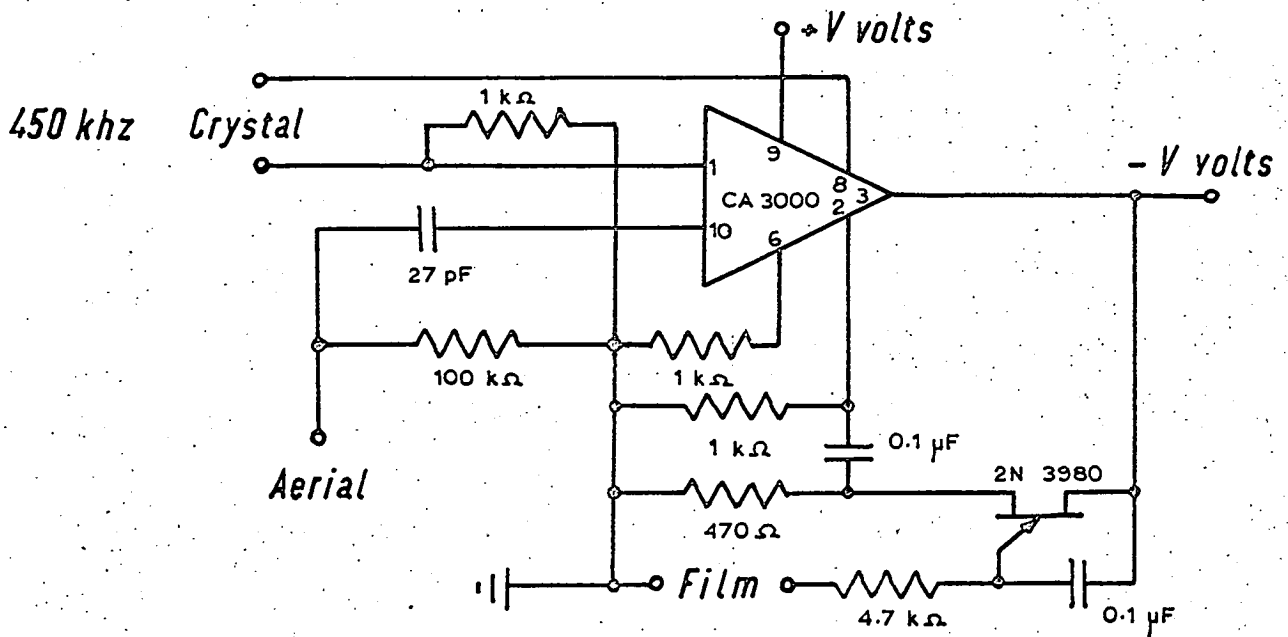


Figure 4.2.6

Circuit Diagram of Oscillator and Modulator

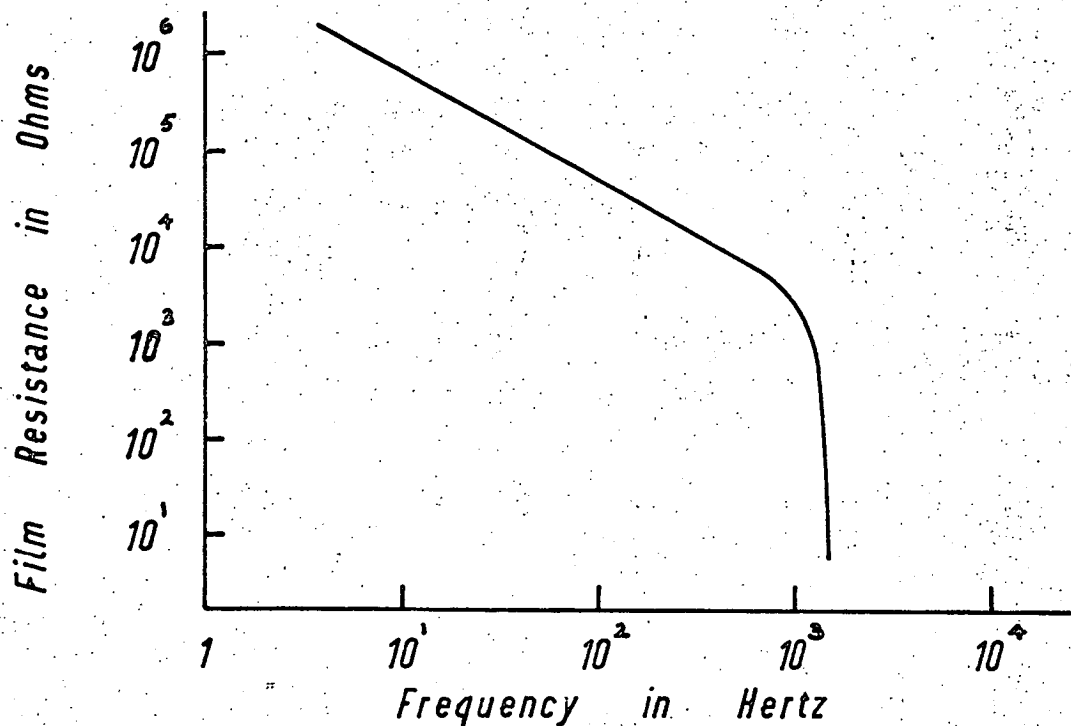
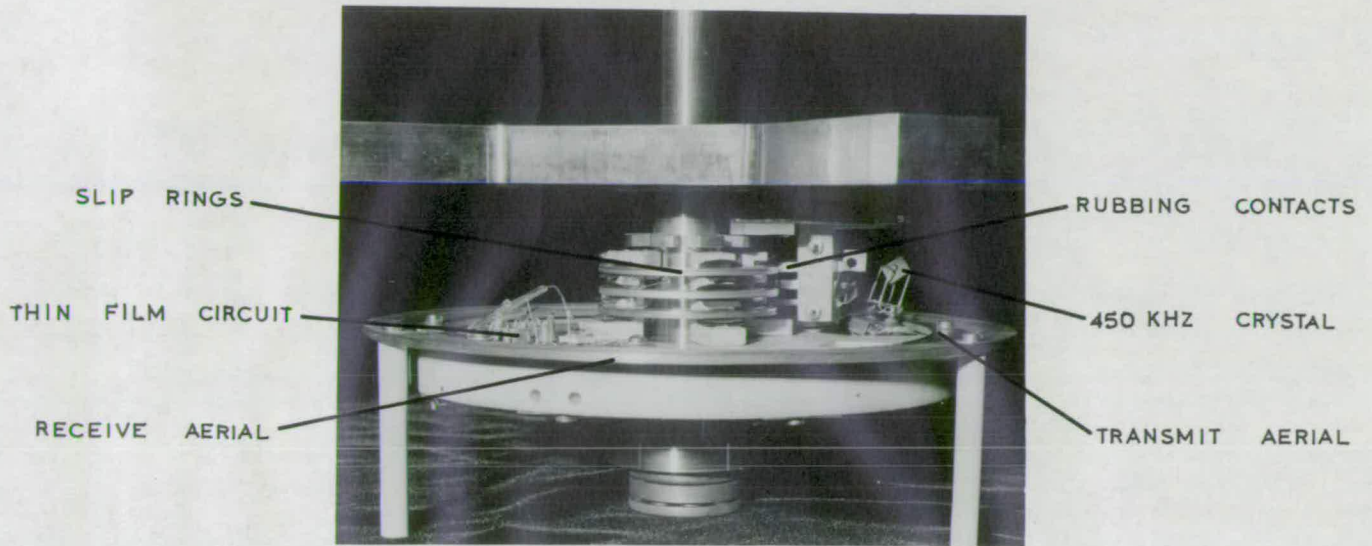


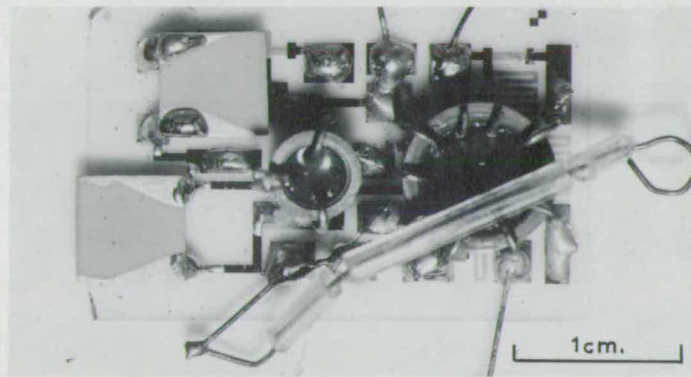
Figure 4.2.7

Calibration of Resistance versus Frequency



— Figure 4.2.8 —

— Thin Film Circuit mounted on Wheel —



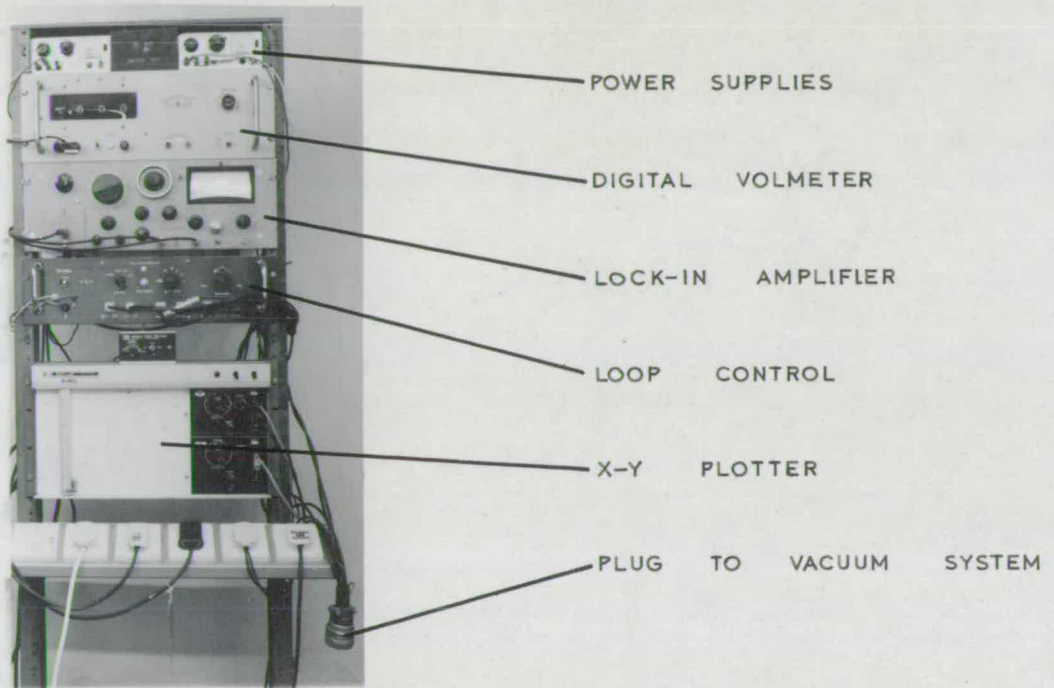
— Figure 4.2.9 —

— Thin Film Circuit —

condensation of the evaporant can be assumed to take place on both the crystal and the rotating substrates. Considering the distance of these faces from the source, the shielding from radiation that they have, and that the substrates are nominally at room temperature, this is a reasonable assumption. However, allowance will have to be made for the frequency shift of the crystal as a result of heating by the source for all measurements taken.

4.2.4. Electrical Resistance of Films. It is required that the electrical resistance of metal films be monitored during the formation of various condensed and adsorbed layers. The obvious way to do this, since the substrates are rotating, is to mount the measuring circuitry on the wheel and allow it to rotate with the substrates. This way no rubbing electrical contacts are required. The power necessary can be supplied from a wheel mounted battery. The circuit shown in figure 4.2.6. allows the resistance to be measured as a calibrated function of the frequency of the signal obtained by a radio receiver on demodulating the 450 khz A.M. modulated signal transmitted across the aerial system. A calibration of film resistance versus frequency is shown in figure 4.2.7. Unfortunately no battery power source could be obtained which would withstand the planned bake-out temperature of approximately 200°C. Thus rubbing contacts had to be employed for supplying the necessary power to the circuit. As shown in figure 4.2.8. the contacts, made of beryllium copper .

strip, made contact to the wheel at slip rings constructed from used U.H.V. copper gaskets. Although perhaps not essential, a rubbing earth contact was made, together with the necessary positive and negative supply lines. The circuit on figure 4.2.6. was constructed on a 3 cm. x 2 cm. glass substrate in thin film form with discreet capacitors and active components. Figure 4.2.9. is a photograph of this actual circuit. The substrate was coated with nichrome and gold, and the resistors and connection pattern were formed in the usual manner by photographic and etch techniques. A high temperature solder was used to secure the components added, and gold wire one thousandth of an inch diameter was used to wire the circuit to the slip rings, crystal, thin film and aerial system. The circuit components all had a storage temperature rating of 200°C or higher, and it was considered, and later confirmed, that the components would operate at U.H.V. without being significantly detrimental to the pressure. Figure 4.2.8. shows the aerial system, which was constructed from four and six inches diameter U.H.V. copper gaskets, and the microcircuit and crystal mounted on the wheel. Unfortunately, although it is considered worthwhile to report this technique for resistance measurement, its sensitivity was not good enough, and an alternative method of measuring the film resistance was adopted. Why it was not successful can be seen in figure 4.2.7., which shows that for a film resistance of less than say 1 k Ω , a $\pm 1\%$ accuracy in frequency measurement is required for a $\pm 10\%$ accuracy in resistance. With the rubbing contacts employed



— Figure 4.3.1 —

— Instrumentation for monitoring Contact Potential —

frequency measurements did not consistently agree to better than $\pm 10\%$. The alternative is to have a substrate mounted directly above the wheel in the path of the evaporation stream, as shown in figure 4.2.4.. One of the recessed gaps between successive substrates on the wheel was removed in order to allow the same quantity of evaporant to reach this substrate as the other eight. This substrate is subjected to exactly the same cleaning and coating procedures as the wheel mounted substrates, which should ensure that it behaves electrically in a similar manner. Electrical contact is made to it by spring terminals onto evaporated metal lands at each end, and a thermocouple is mounted on it at one end to give an indication of temperature changes taking place. However a current must be passed through the film on the substrate in order to measure its electrical resistance and hence care must be taken that this current does not influence or change the structure of the film. Using this technique resistance changes can be accurately followed even when the absolute value is small.

4.3. Instrumentation.

4.3.1. Contact Potential Recording. Figure 4.3.1. shows the rack of electronics used for measuring and recording the contact potential. The digital voltmeter gives a direct reading of the output voltage V_o which is related to the contact potential, V_{cp} , by

$$V_o = \left(\frac{k}{k+1} \right) \cdot V_{cp} \quad (4.3.1)$$

where k is the open loop gain.

V_o can be recorded on the y axis of the xy plotter as a function of time with the x axis driven by a Hewlett Packard type 17108-A time base. The time base is also used as a ramp generator since it is battery operated and can give very slowly varying ramp voltage signals. All of the electrical connections from the contact potential instrumentation to the vacuum chamber are made by a twenty-way Canon connector, shown on figure 4.3.1., which fits directly onto the multi-way electrical feedthrough.

The following is the procedure adopted for making the instrumentation ready for measurements to be taken. Firstly a static capacitor measurement as described in section 3.3.1. is carried out, using a Wayne Kerr type 2B 01 universal bridge, and the capacitor gap is set to give a capacitance variation of approximately 5 pF from peak to peak. For the time constants used an open loop gain of ~ 15 is required, as shown in section 3.3.3. The type HR8 lock-in amplifier gives an output of ± 10 volts D.C., with the requisite synchronous input signal having zero phase difference from the input signal, for full scale input over all of the voltage ranges. Hence, since the conversion efficiency, \sqrt{e} , can be calculated knowing the peak to peak capacitance variation and the frequency that the wheel is to be operated at, the input voltage setting should be

$$\frac{10}{15} \cdot \sqrt{e} \text{ volts r.m.s.}$$

if $\sqrt{v_e}$ is, say, about 0.002 as calculated previously, then a suitable setting for the lock-in amplifier is 1 millivolt r.m.s. A fine control over the gain K is provided by the precise linear feedthrough controlling the capacitor gap. Having decided upon the input voltage setting on the lock-in amplifier, the lamp for the synchronous signal is switched on and the wheel is rotated by energising the motor driving the high speed rotary feedthrough. The wheel speed is increased slowly until it is rotating at about 4 revolutions/second. The speed of the wheel is monitored by rotating the frequency tune of the lock-in amplifier until a maximum reading is obtained on its meter when monitoring the r.m.s. voltage from the photo-diode. Once the synchronous signal maximum is steady at ~ 30 hz its amplitude is set according to the HR8 manual using an amplifier in the loop control box and the attenuator in the lock-in amplifier. The minimum lamp intensity consistent with sufficient signal level is used in order to minimise the chance of the lamp burning itself out in the vacuum chamber. A further reason for the low intensity is to minimise the temperature rise of the wheel-mounted substrates as a result of being heated by the radiation from the lamp. Having set the synchronous signal input level and decided upon the amplifier settings, the next step is to use the phase-shifter of the HR8 to make the synchronous input and the signal input enter the mixer stage with the correct phase relationship. This is done by monitoring the D.C. output of the lock-in amplifier for

phase shift settings of 0° to 360° in convenient steps, and determining where the maximum output is with the correct polarity. The correct polarity is determined by considering the polarity of the voltage across the dynamic capacitor. The angular setting for this maximum output represents the required condition of no phase difference between the two signals. The open loop gain k is then measured accurately by applying a sweep voltage across the dynamic capacitor as explained in section 3.3.3. All of the lock-in amplifier settings are noted, and the feedback loop closed by a switch on the loop control box. The digital voltmeter now gives a reading of V_0 , and the XY plotter, with a suitable time base, records V_0 as a function of time.

4.3.2. Other Quantities Recorded. The other quantities recorded during the experiments were:-

- i) Evaporator Settings. The H.T. current to the crucibles, H.T. voltage between filament and crucibles, the current through the filament, and which crucible is employed are all noted for each evaporation in order to allow repeatability.
- ii) Electrical Resistance. The electrical resistance of the stationary substrate located above the wheel is measured and noted at regular intervals of time using a Keithley type 610 B electrometer. For some early experiments a constant current source was employed

which allowed the resistance to be recorded directly on a chart recorder, however this method was discontinued in favour of the electrometer since, as will be seen later, high current density effects became troublesome.

- iii) Temperature. Several thermocouples had their e.m.f. variations monitored on a Honeywell-Brown potentiometric recorder. These thermocouples, with one exception, were positioned at various points inside the oven, but outside the vacuum chamber, during the bake-out period. Only one thermocouple was positioned inside the vacuum chamber, and was used not only during the bake-out period, but also during evaporations.
- iv) Film Thickness and Deposition Rate. The D.C. output voltage from the Edwards type F.T.M.1 crystal monitor control, which is proportional to the frequency of the quartz crystal, was recorded on the Brown recorder. Thus a record of mean film thickness was kept. Also as a check the rate of frequency change was noted directly from the front panel meter on the Edwards control box.
- v) Pressure. The D.C. voltage from the 'pressure record' output of the control box for the Varian Vac-Ion pump was connected to an input of the Brown recorder. Although the D.C. output is not a linear function of pressure, the manufacturers do supply a calibration

chart which allows it to be converted to a pressure reading.

CHAPTER 5.

EXPERIMENTAL PROCEDURES AND RESULTS.

Introduction.

The first section in this chapter is concerned with cleaning, assembling and testing the apparatus installed in the vacuum chamber. This is followed by a brief description of the procedures used to obtain the required low pressure in the vacuum chamber. In sections 3, 4 and 5 the experimental results obtained are reported and shown in graphical form. The chapter ends in section 6 with the results of examinations of the thin metallic films carried out by various techniques after venting the vacuum chamber to atmospheric pressure and then removing the films from the chamber.

5.1. Preparing Apparatus.

5.1.1. Cleaning Procedures. In order to obtain ultra-high vacuum conditions it is necessary to thoroughly clean, and then maintain clean, all parts of the vacuum apparatus. Parts made of different materials are usually cleaned in differing ways, but the principally used methods are

Immersion in various solvents.

Mechanical polishing.

Ultrasonic cleaners and vapour degreasing baths.

Once all of the apparatus has gone through the cleaning

process it is important that no organic stains, such as fingerprints, subsequently appear on it, and that dust in the vicinity of the chamber is kept to a minimum when it is open to the atmosphere. These potential limitations on the pressure are minimised by taking the precautions of wearing nylon gloves when handling pieces of apparatus, and of working in clean-room conditions respectively. After being cleaned, any parts of the apparatus which are not installed immediately in the chamber are stored in a clean air cabinet. The chamber itself is cleaned when empty, firstly with a vacuum cleaner and then wiped with a tissue (Kimwipe) soaked in isopropyl alcohol. After a blast of nitrogen with a high pressure cylinder to remove any foreign particles, which might result in bad seating of the copper gaskets, all gasket seats are given a similar wipe. All of the stainless steel parts are subjected to the following cleaning and polishing steps:-

- i) Mechanically polished using carborundum stone, fine carborundum grinding powder, emery cloth and Brasso.
- ii) Immersed in a warm solution of Decon 2 for several hours.
- iii) Immersed in a shallow vessel of concentrated detergent solution for several hours with a constant supply of water entering the vessel until no trace of the detergent could be observed.
- iv) If too large to fit into the ultrasonic cleaner container (3" diameter by 3" deep) the part is

suspended in a vapour degreasing bath (constructed from a tea urn with water cooling coils installed at the top) for several hours.

- v) If the part is small enough, it is ultrasonically cleaned for several hours in isopropyl alcohol.
- vi) Each part is taken from the ultrasonic cleaner, or the urn, to the clean air cabinet ready to be assembled with the other parts.

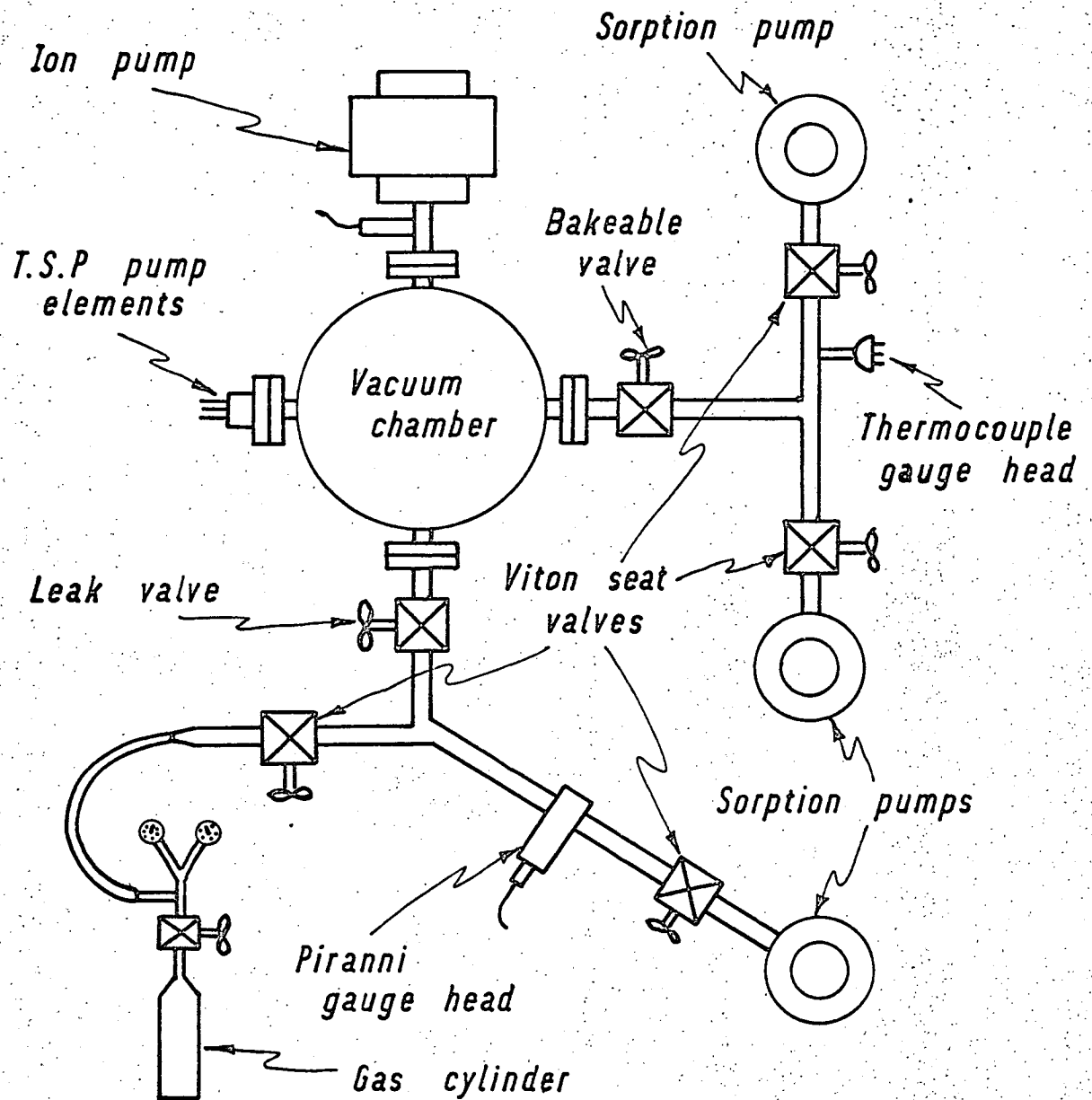
All of the smaller parts which did not require mechanical polishing such as the bearings, substrate clips, electrical stand-offs, nuts, bolts, etc., etc., were immersed in isopropyl alcohol in the ultrasonic cleaner for several hours. The large piece of Fluorosint making up the wheel was mounted on its shaft and secured to the top plate by the ball bearing set and housing which had a light interference fit onto the shaft and top plate recess. This sub-assembly was placed in the vapour degreasing bath for several hours before the eight substrates were mounted on it. The 7059 Corning glass substrates themselves were cleaned in the following way:-

- i) Immersed for several minutes in a solution of R.B.S. 25 (Chemical Concentrates Ltd.) in the ultrasonic cleaner.
- ii) Washed in distilled water.
- iii) Immersed for several minutes in isopropyl alcohol in the ultrasonic bath.
- iv) Placed for several hours in a vapour stream of a

cycling condenser containing Analar isopropyl alcohol.

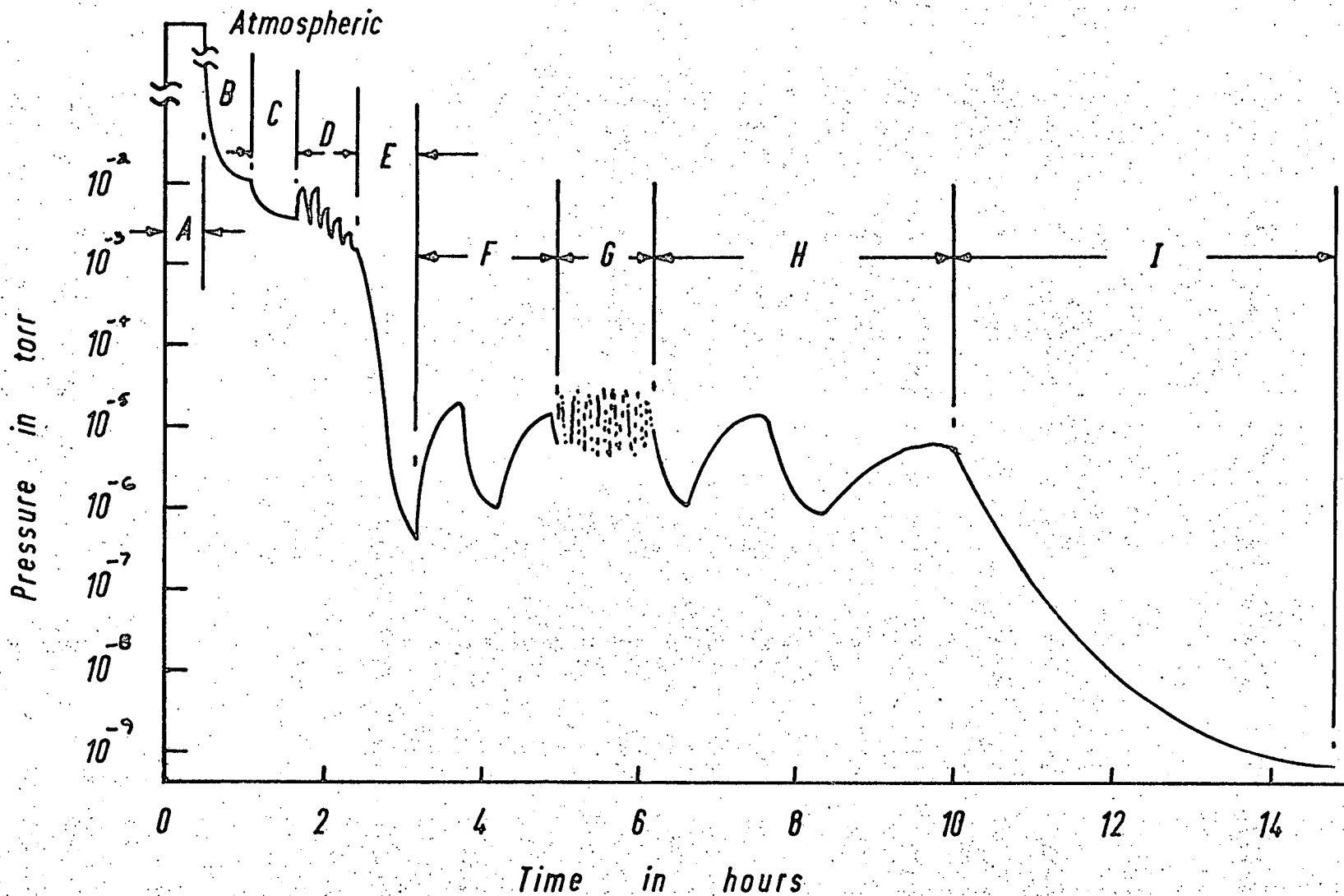
Before being installed in the chamber the two principal assemblies of the electron beam evaporator and the apparatus mounted on the base plate, as shown in figures 4.2.3. and 4.2.4. respectively, were placed in the vapour degreasing urn for several hours. They were then transferred directly from the urn to the chamber.

5.1.2. Assembling and Testing. A list of procedures to be followed were drawn up for assembling the apparatus in the vacuum chamber. This was done to minimise the time required and the risk of evacuating the chamber only to find that some part of the apparatus was not functioning properly as a result of incorrect assembly or faulty electrical wiring. The list had approximately fifty items in it, commencing with cleaning the chamber, and finishing at evaporating from the sources. Great care was taken during this period not to damage the copper gasket seats on the flanges, especially on the Wheeler flange which is in a very vulnerable position. New copper gaskets were used each time a flange was loosened off, except for the Wheeler flange where the cost of gaskets (£5 for three) made it worthwhile to risk using one gasket for several evacuations of the chamber. A test that was always made before closing the chamber was to ensure that the electrical contacts onto the gold-land areas deposited onto the substrates were of low resistance. This test is essential because even one substrate



— Figure 5.2.1 —

— Valve and Pump Arrangement on Vacuum Chamber —



— Figure 5.2.2 —

— Pressure versus Time for an Evacuation of the Vacuum Chamber —

with a bad contact can be very troublesome since charge may build up on the substrate surface resulting in spurious, if not completely useless, contact potential measurements. Between successive experiments it is important that the reference electrode is not scratched or otherwise changed because it is required that it has a constant effective work function throughout the experiments. Figures 3.3.3., 4.2.3., 4.2.2., 4.2.5., 4.2.4., 4.2.1. and 4.1.1. show the apparatus in successive stages of assembly.

5.2. Evacuating Chamber.

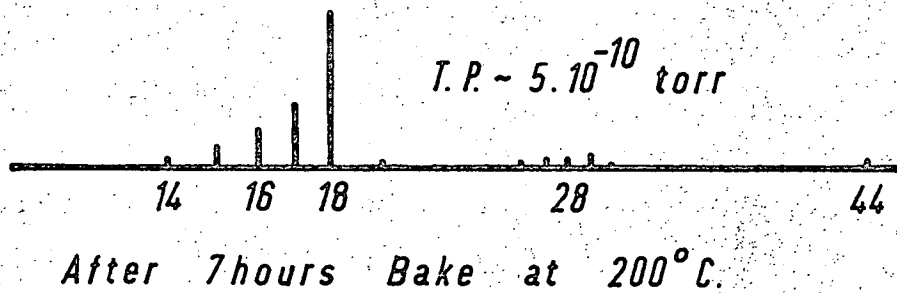
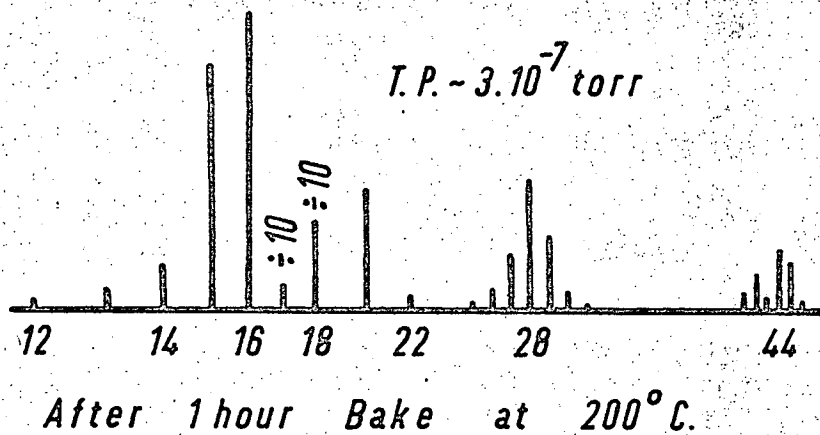
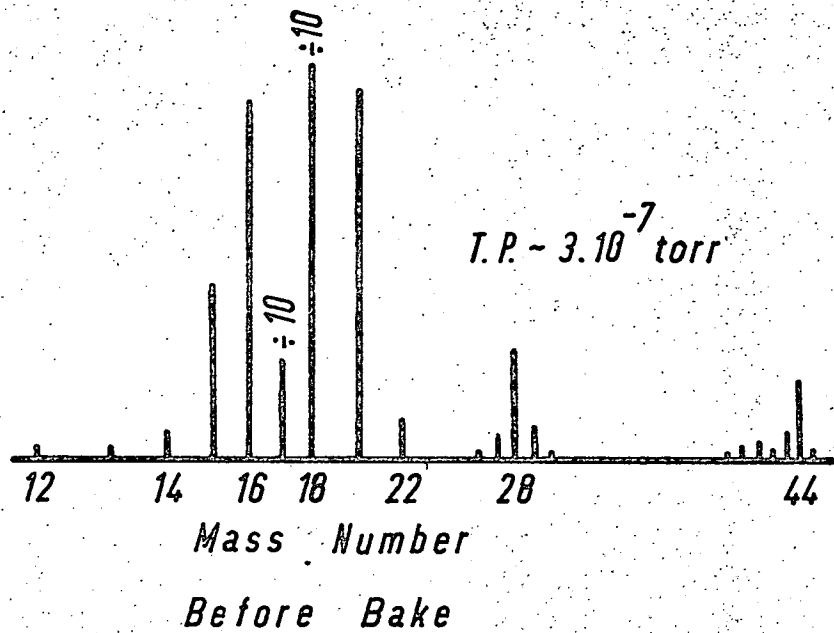
5.2.1. Pumping. Between successive evacuations of the chamber the sorption roughing pumps were baked using specially fitted heating elements in order to regenerate their sieve material. After the check list of procedures is complete, baking of the sorption pumps is stopped and they are then chilled with liquid nitrogen to their operating temperature. At this stage both of the Viton seat valves in the bakeable valve roughing line, and the bakeable valve itself, are closed. Figure 5.2.1. shows the valve and pump arrangement on the vacuum chamber. When the pumps are considered to be at approximately liquid nitrogen temperature the two Viton seat valves are opened alternately and the pressure for each pump measured using the thermocouple gauge, corresponding to region A on figure 5.2.2. On reaching a pressure of 1 micron or better the bakeable valve is opened fully with one of the Viton seat valves closed. The chamber then takes thirty to forty minutes

to reach a pressure of about 10 microns, after which the Viton seat valve which is open is closed, and vice versa. Within thirty minutes the pressure falls to less than 5 microns. Roughing with the sorption pumps corresponds to regions B and C on figure 5.2.2. Before starting the ion pump, the leads from the quartz crystal of the thickness monitor are made open circuit, and those of the photo-diode are shortcircuited to earth. These precautions prevent destroying the input transistor on the thickness monitor instrumentation and the photo-diode respectively. No such precautions were taken the first time that these devices were used, and as a consequence both had to be replaced. The whole vacuum chamber and the ion pump itself become very hot, and remain so, from the time that the ion pump is switched on until the pressure is reduced to less than $5 \cdot 10^{-5}$ torr, which corresponds to a pump power dissipation of approximately 20 watts. The peak power dissipation, of over 300 watts, occurs at 1.8 to 2.0×10^{-3} torr. While the bakeable valve is still open to the roughing pumps the T.S.P. elements are outgassed, and the T.S.P. timer is set to give a short duty cycle to help the ion pump to pass quickly to a low pressure. The bakeable valve is closed with a torque wrench to a torque of 45 lbs/ft. when the pressure reaches 1.5 to 2.0 microns. During the period when the chamber is hot, electric fans are employed to aid cooling, but usually even they cannot prevent the chamber from reaching temperatures that cause the pressure to increase. When this happens the ion pump and T.S.P. are switched off for several minutes, and if the pressure

rises to more than $2 \cdot 10^{-3}$ torr the bakeable valve is reopened in order to allow the roughing pumps to contain the pressure rise. Typical times are, three quarters of an hour from starting the ion pump to closing the bakeable valve for the last time, and a further three quarters of an hour before the chamber reaches a pressure of $5 \cdot 10^{-3}$ torr. These times correspond to regions D and E on figure 5.2.2. Once the chamber pressure is below 10^{-5} torr there is no further risk of a discharging occurring, and the various electrical circuits within the chamber are tested for malfunction. Assuming the circuits are all found to be in order, then the chamber is prepared for a bake, or as it is usually called, a 'bake-out.'

5.2.2. Bake-out. The chamber is prepared for the bake-out as described in section 4.1.2. The thermocouple for controlling the oven power switch is positioned inside the top of the oven, but outside the chamber, and 200°C is set on the bake-out control panel as the switching level. The pressure level for controlling the oven power switch is set at 10^{-5} torr, i.e. for a pressure of $>10^{-5}$ torr the oven power is switched off but is automatically resumed when the pressure goes below about 10^{-6} torr. The timer that determines the duration of the bake-out is set to two hours, after which the power is switched on and the bake can commence. At the end of the two hour period, corresponding to region F on figure 5.2.2., the oven is opened up in order to outgas the evaporation sources, and to further outgas the T.S.P. elements.

Amplifier Range Factor — x 10



— Figure 5.23 —

— Mass Spectrometer Recorder-output Traces —

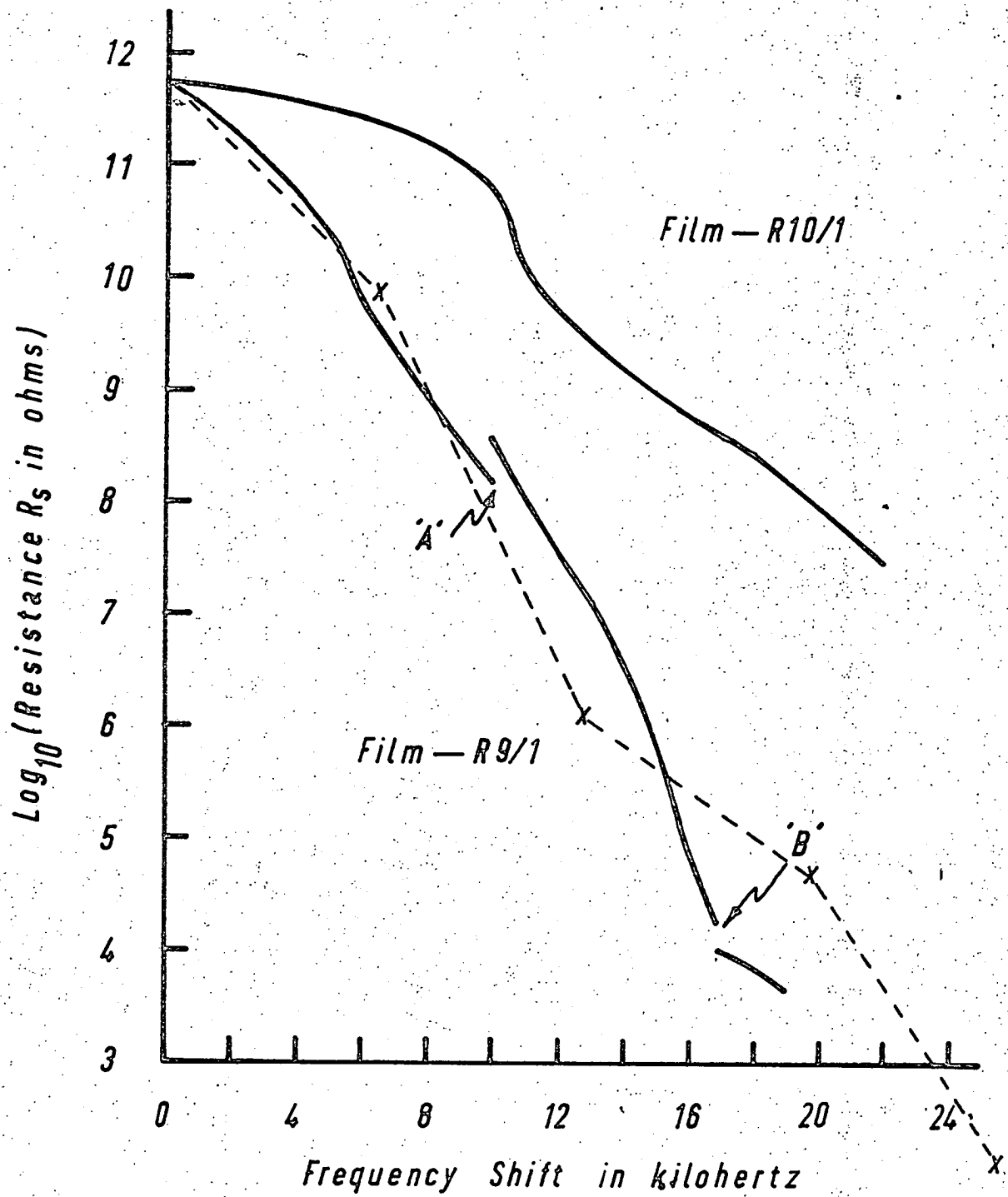
The crucibles are considered to be sufficiently outgassed when ten minutes at red heat with the crucible contents on the point of evaporation (as observed with the quartz crystal monitor) does not appreciably raise the pressure in the chamber. The three T.S.P. elements are outgassed once again so that when they are used at U.H.V. they reduce, and not increase the pressure, because if the latter occurred all of the benefits gained from the bake-out could be lost. Before further baking commences all of the sets of ball bearings are rotated as a precaution against pockets of air being trapped, which could be detrimental to the pressure in the chamber when they are used after the bake-out is complete. Region G on figure 5.2.2. corresponds to the outgassing stage of the evacuation procedures. The chamber is then baked for at least a further three hours at 200°C, corresponding to region H on figure 5.2.2. Region I on figure 5.2.2. represents the final stage which is the cooling down of the chamber to room temperature after the completion of the bake-out, when the base pressure of the chamber is reached within a period of four to five hours. The base pressure is normally expected to be $< 10^{-9}$ torr, and a higher pressure would suggest an air leak at one of the flanges. At the base pressure the T.S.P. timers are set to give a duty cycle of thirty minutes OFF and one and a half minutes ON.

Figure 5.2.3. shows mass spectrometer measurements taken before, during and after the bake-out. On the top diagram it is

seen that before the baking commences the amplitude corresponding to mass number 18 is very much larger than any other. After even a slight bake of one hour at 200°C the middle diagram shows that the amplitudes corresponding to mass numbers 17 and 18 are very much reduced, indicating that the proportion of water vapour in the chamber has been decreased. When baked for seven hours at 200°C, as seen in the bottom diagram, the proportion of water vapour is further decreased, but it still remains the single most prevalent residual gas present in the vacuum chamber. The other predominant peaks on the diagrams are at mass numbers 14, 28, 20, 16 and 15, and 14 corresponding to the gases CO₂, N₂ and CO, Ne, CH₄, and N₂ and CH₄ respectively.

5.3. Growth of Gold Films.

The first layer deposited in the Varian vacuum chamber for each of the films made was of 99.999% purity gold. The films were prepared on 3 cm x 2 cm 7059 Corning glass substrates which, before deposition took place, had a measured resistance of $\approx 5 \cdot 10^8 \Omega$ /square. The substrates were nominally at room temperature, and the area of substrate used for resistance measurement was approximately 2 cm x 2 cm. The thermocouple mounted on the front of the substrate used for monitoring the electrical resistance indicated that no appreciable rise in temperature occurred, which may not be a true representation of the actual thin film temperature rise since the thermocouple wires would act as heat sinks resulting in only a small temperature rise at the thermocouple



— Figure 5.3.1 —

— Resistance of Gold Films During Initial Growth Period —

EXPERIMENT NUMBER	WHEEL-MOUNTED SUBSTRATES (8)	RESISTANCE MONITOR SUBSTRATE
7	<p>a) CONTACT LANDS OF Au APPROX. 1500 Å THICK WERE DEPOSITED AT THE ENDS OF THE SUBSTRATES IN THE EDWARDS 19E COATING UNIT.</p> <p>b) ALL SUBSEQUENT DEPOSITIONS TOOK PLACE IN THE VARIAN U.H.V. SYSTEM AS PER TEXT.</p>	<p>SAME AS FOR WHEEL-MOUNTED SUBSTRATES.</p>
8, 9, 10	<p>a) APPROXIMATELY 1000 Å OF Au WAS DEPOSITED OVER ENTIRE SURFACE OF SUBSTRATES IN EDWARDS 19E COATING UNIT.</p> <p>b) ALL SUBSEQUENT DEPOSITIONS TOOK PLACE IN THE VARIAN U.H.V. SYSTEM AS PER TEXT.</p>	<p>a) Au CONTACT LANDS APPROXIMATELY 1000 Å THICK WERE DEPOSITED IN THE EDWARDS 19E COATING UNIT.</p> <p>b) ALL SUBSEQUENT DEPOSITIONS TOOK PLACE IN THE VARIAN U.H.V. SYSTEM AS FOR THE WHEEL-MOUNTED SUBSTRATES OF THE CORRESPONDING EXPERIMENT.</p>

junction. During the deposition of these gold layers no contact potential measurements were taken until the eight substrates mounted on the wheel had a resistance of less than $10^7 \Omega$ / square because the instrumentation cannot operate correctly until the resistance falls to about this value. The pressure during depositions remained at or below 10^{-8} torr, and the rate of deposition was approximately $45 \text{ \AA}/\text{minute}$. All Talysurf thickness measurements were found to agree, within the stated experimental error, with film thickness values deduced from the frequency shift of the quartz crystal monitor using the following relationship for gold.

$$32 \text{ khz} \equiv 100 \text{ \AA} \pm 20\%$$

In order to allow the measurement of contact potential from the start of depositions, the wheel mounted substrates for experiments 8, 9 and 10 were coated with approximately 1000 \AA of gold in an Edwards 19 E coating unit from a 99.9% purity source at a pressure of about 10^{-6} torr and a rate of $100 \text{ \AA}/\text{minute}$. The table opposite shows all coatings done in the Edwards 19E coating unit.

Figure 5.3.1. shows the resistance changes during the deposition of 60 \AA to 70 \AA of gold for experiments 9 and 10. For film R9/1[†] the resistance changes can be approximated by

$$\log_{10} R = 11.5 - 0.14 \times F \quad (5.3.1.)$$

[†] Footnote. All of the films beginning with the identification R8/ are for experiment 8, R9/ for experiment 9 and R10/ for experiment 10.

where R is the film resistance in Ω /square.

and F is the film thickness in Angstroms.

On differentiating equation (5.3.1) the relationship is obtained

$$\frac{dR}{R} = - 0.14 \frac{dF}{F} \quad (5.3.2)$$

or using the approximation that $\Delta R \approx dR$ and $\Delta F \approx dF$, it follows that the fractional change in resistance for a further small increase in thickness, t , is given by

$$\frac{\Delta R}{R} = - 0.14 \frac{t}{F} \quad (5.3.3)$$

The resistance changes for film R10/1 do not follow a straight line so closely as for R9/1, however the changes have an approximate gradient of -4 decades of resistance/50 Angstroms which yields a relationship similar to equation (5.3.3) with the form

$$\frac{\Delta R}{R} = - 0.08 \frac{t}{F} \quad (5.3.4)$$

Points A and B for film R9/1 are where the evaporation was stopped for several minutes. At point A the resistance increased on cessation indicating a negative temperature coefficient, but at point B a positive temperature coefficient is evident. The points joined by the dotted line are from the work published by Reate (174)

and will be discussed in the next chapter.

The contact potential between the reference electrode and the gold films of experiemnt 7, which were about 170\AA thick and were deposited entirely in the Varian vacuum chamber, was - 165 millivolts \pm 5 millivolts. This indicates that the effective work function $\bar{\phi}_{g^v}$ of the gold films was

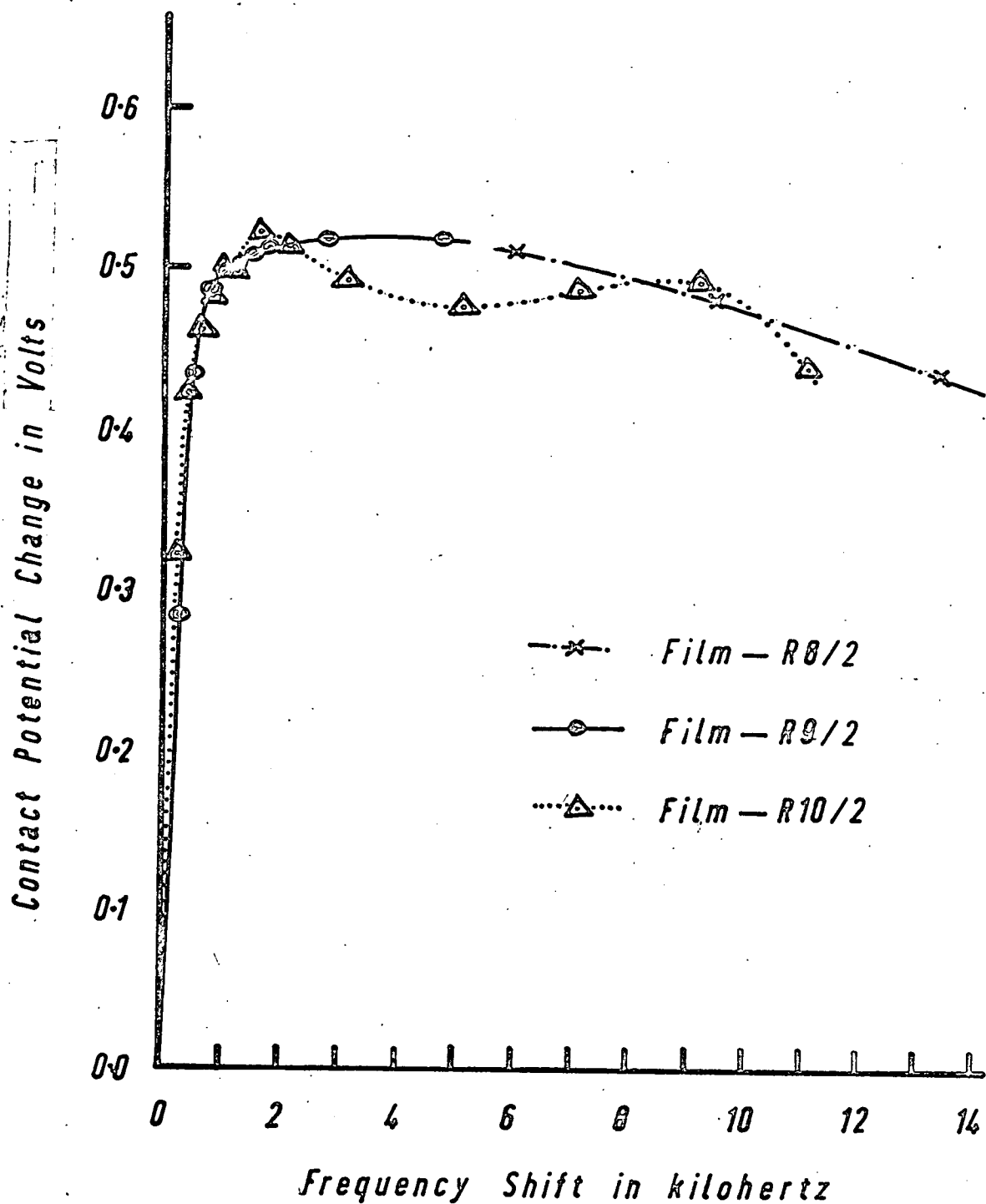
$$\bar{\phi}_{g^v} = (\bar{\phi}_r + 0.165) \text{ eV} \quad (5.3.5)$$

where $\bar{\phi}_r$ is the effective work function of the reference electrode in electron volts.

The gold films prepared in the Edwards vacuum chamber, which were subsequently mounted on the wheel in the Varian system, however, had measured contact potentials of + 235 \pm 5 millivolts (R9/1) and +240 \pm 5 millivolts (R8/1) before any further deposition took place. This indicates an effective work function $\bar{\phi}_{g^e}$ of

$$\bar{\phi}_{g^e} = (\bar{\phi}_r - 0.240) \text{ eV} \quad (5.3.6)$$

Thus the effective work function values for the gold films prepared in the Edwards (pumped with oil diffusion and rotary pumps) and the Varian (pumped with all dry pumps) vacuum systems differ by approximately 400 millivolts.



— Figure 5.4.1 —

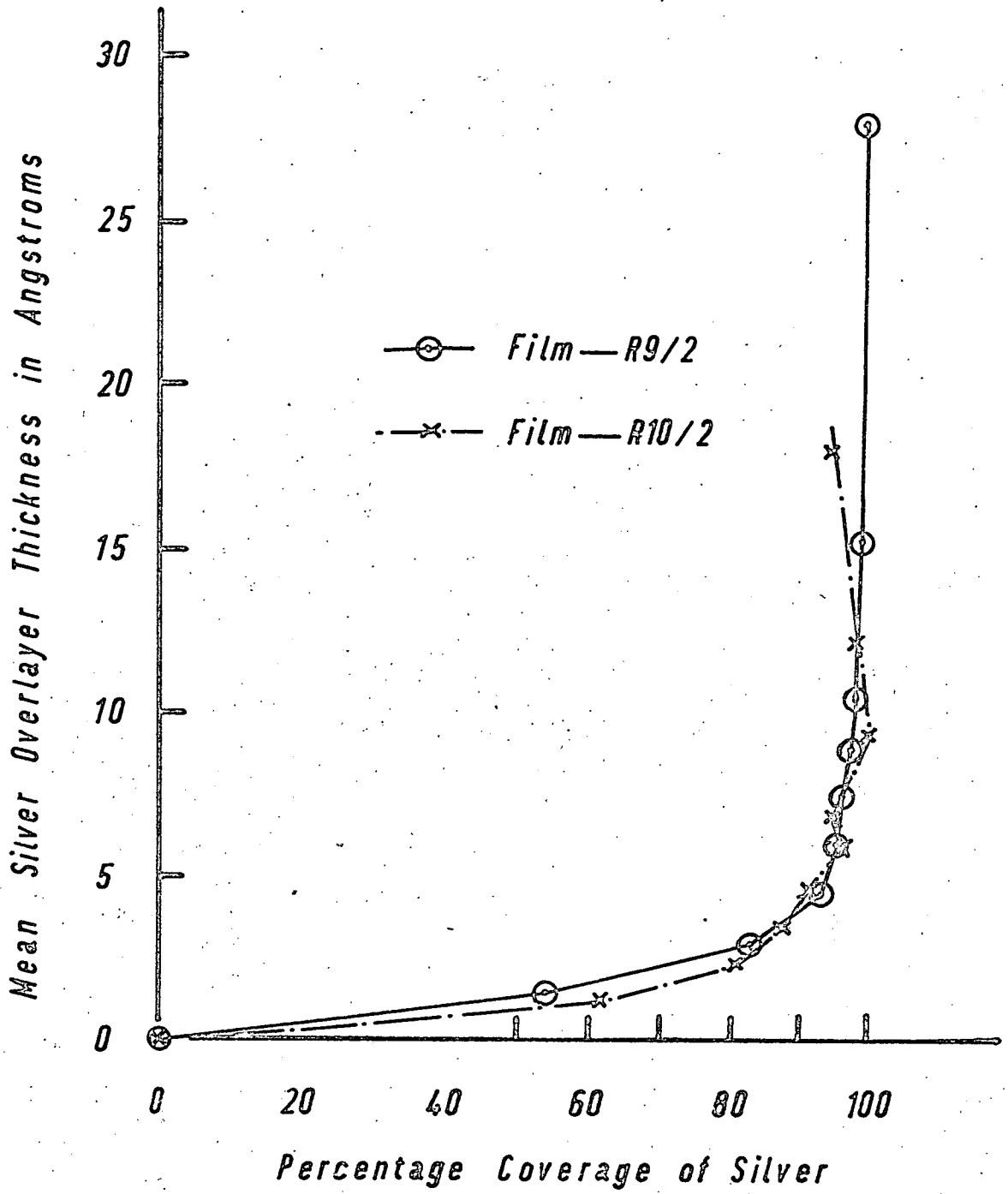
— Contact Potential Change with Silver Overlayer —

$$\text{i.e. } \bar{\phi}_{g^v} - \bar{\phi}_{g^e} = 0.400 \pm 0.01 \text{ electron volts} \quad (5.3.7)$$

Repeated evaporations of gold in the Varian system onto the gold films prepared in the Edwards system reduced the contact potential with respect to the reference electrode, but not by the whole 0.4 volts. Film R9/1 showed the largest change of three different sets of films, with the contact potential decreasing from + 235 millivolts to + 50 millivolts when a 60\AA overlayer was deposited at 10^{-8} torr and a rate of $50\text{\AA}/\text{minute}$. Furthermore, although the reference electrode surface was prepared by depositing a layer of gold ($\sim 1000\text{\AA}$ thick) onto a stainless steel disc in the Edwards system, its effective work function is about 240 millivolts higher than the value for gold films prepared on glass substrates in the same manner.

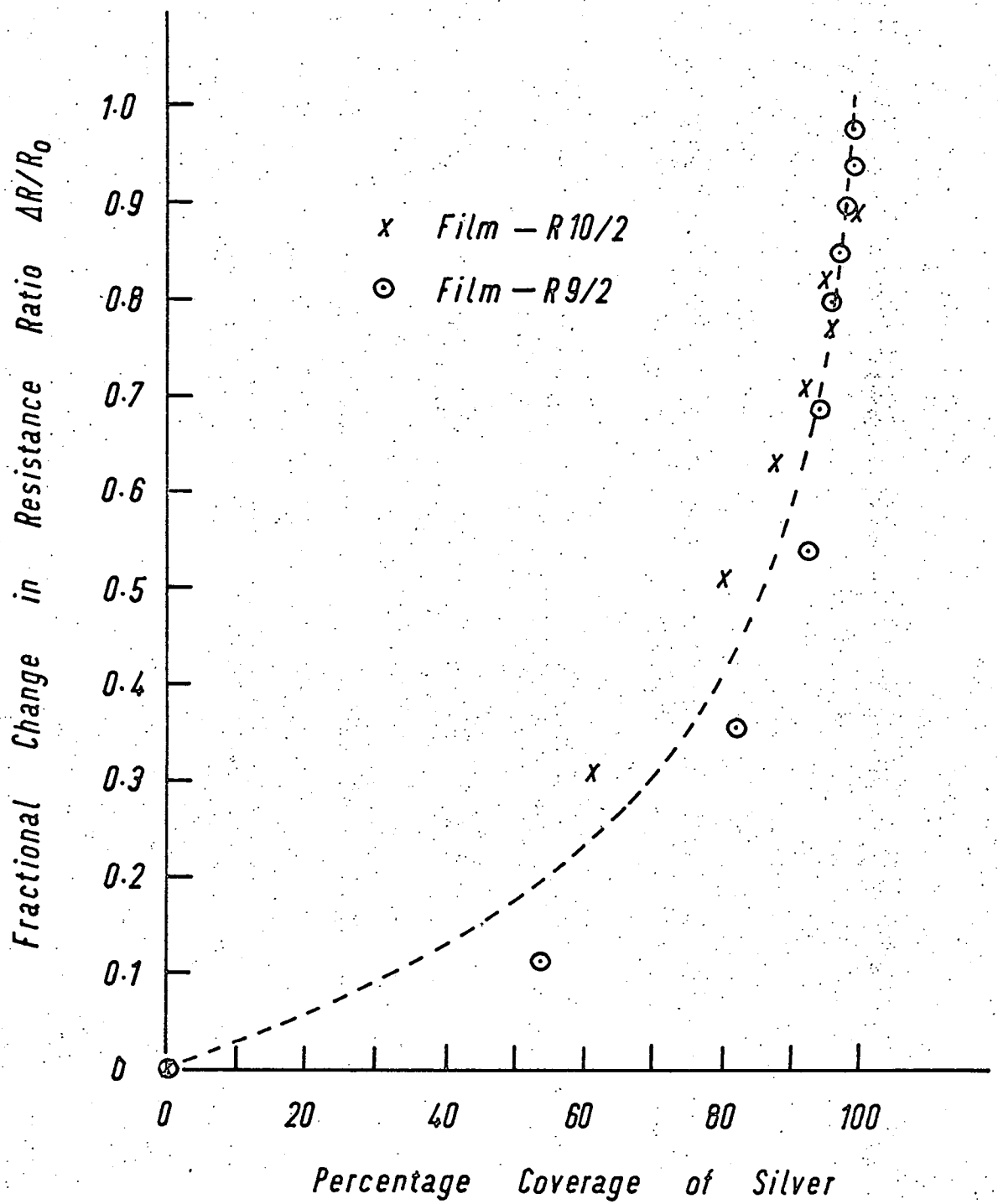
5.4. Silver and Gold Overlayers.

5.4.1. Silver Overlayers. Figure 5.4.1. shows three curves of contact potential versus quartz crystal frequency shift for 99.999% purity silver deposited onto thin gold films on glass substrates. The three films R8/2, R9/2 and R10/2 were deposited at a pressure of better than 10^{-8} torr with a rate of approximately $100\text{\AA}/\text{minute}$. All three have a maximum contact potential value of 0.51 to 0.52 volts, and films R8/2 and R10/2 show a decrease in contact potential as the thickness increases. Using the following



— Figure 5.4.2 —

— Variation of Mean Thickness with Coverage —



— Figure 5.4.3 —

— Resistance Changes with Silver Overlayers —

calibration of the quartz monitor for silver

$$17.5 \text{ khz} \equiv 100\text{\AA} \pm 20\%$$

and by assuming that the fractional change in contact potential, $\frac{\Delta\phi}{\phi_2 - \phi_1}$, is proportional to the surface coverage, θ , as discussed in section 2.2., then figure 5.4.2. was plotted showing the variations of mean silver film thickness versus percentage coverage for films R9/2 and R10/2. A good approximation to the mean of the two curves on figure 5.4.2. is

$$\theta = 1 - e^{-(t/2)} \quad (5.4.1)$$

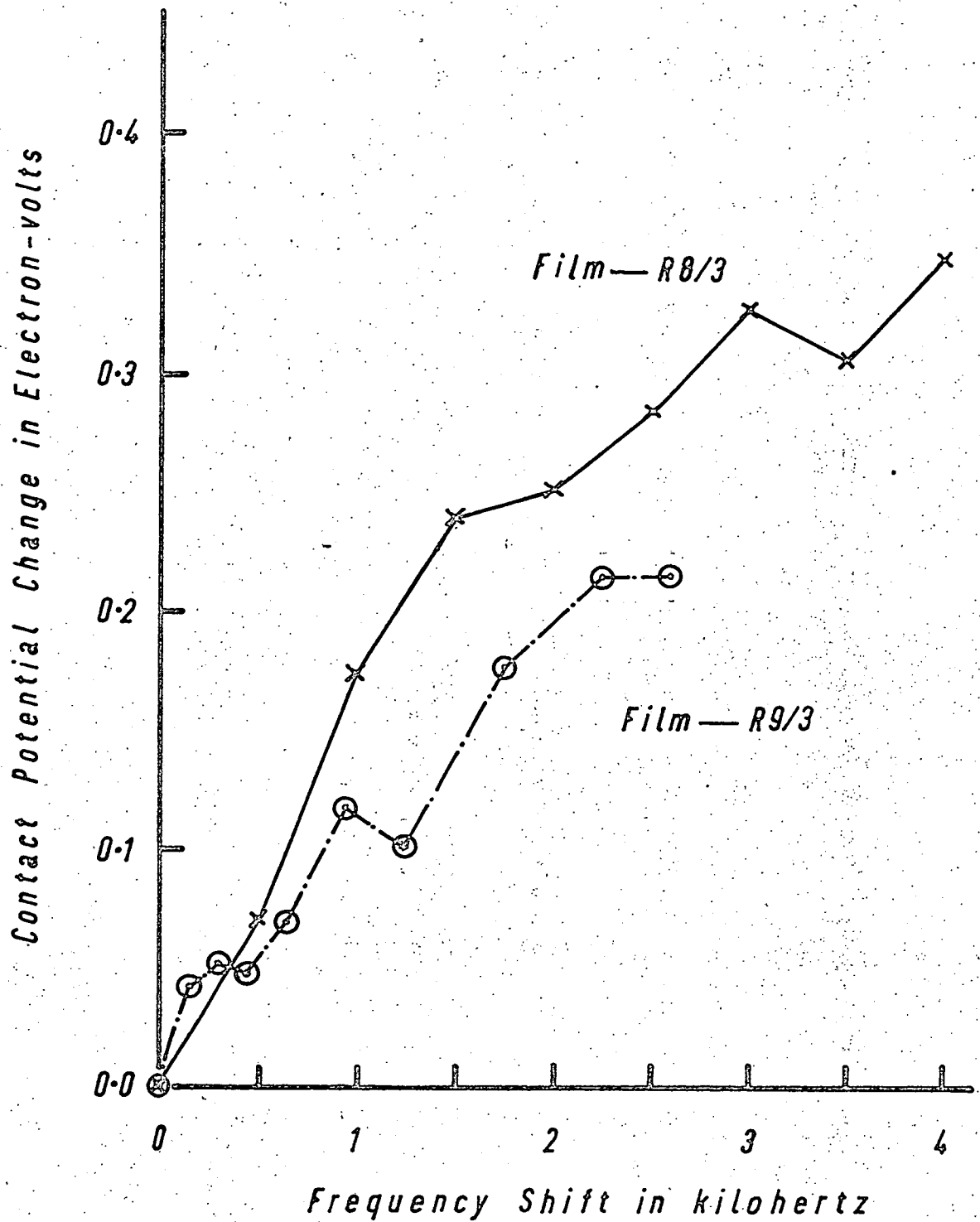
where t is the mean silver overlayer thickness in Angstroms.

The fractional resistance changes as a function of coverage for films R10/2 and R9/2 are shown plotted on figure 5.4.3. The fractional resistance is expressed as the ratio of the resistance change ΔR to the resistance R_0 before commencing deposition of the silver. The dotted line on figure 5.4.3. has the form

$$\theta = \left(1 - e^{-\left(\frac{\Delta R/R_0}{0.25}\right)} \right) \quad (5.4.2)$$

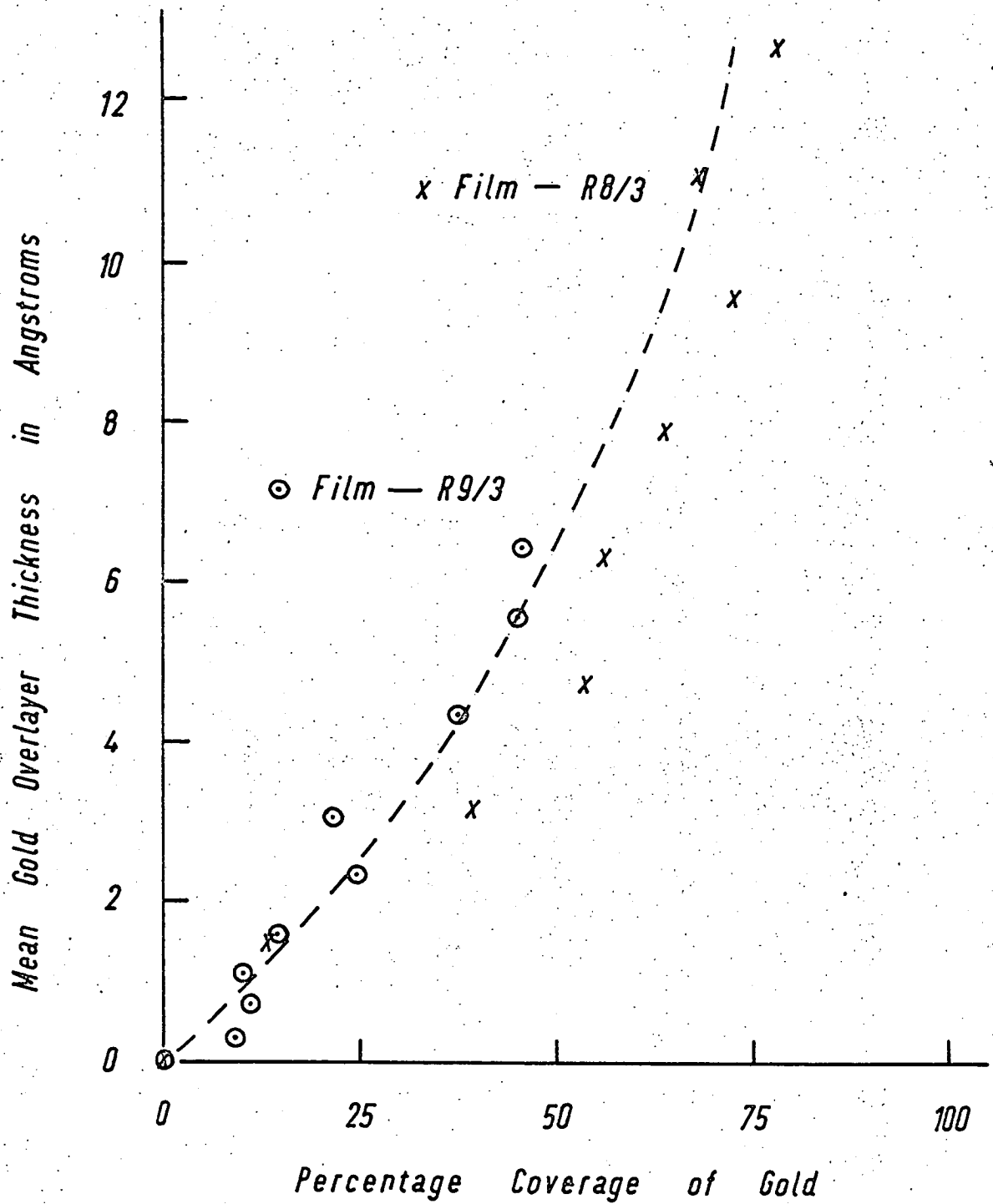
which is seen to be a reasonable approximation to the experimental points.

When equations (5.4.1) and (5.4.2) are equated, the result



— Figure 5.4.4 —

— Contact Potential Change with Gold Overlayer —



— Figure 5.4.5 —

— Variation of Mean Thickness with Coverage —

is obtained

$$\frac{\Delta R}{R_0} = 0.125.t \quad (5.4.3)$$

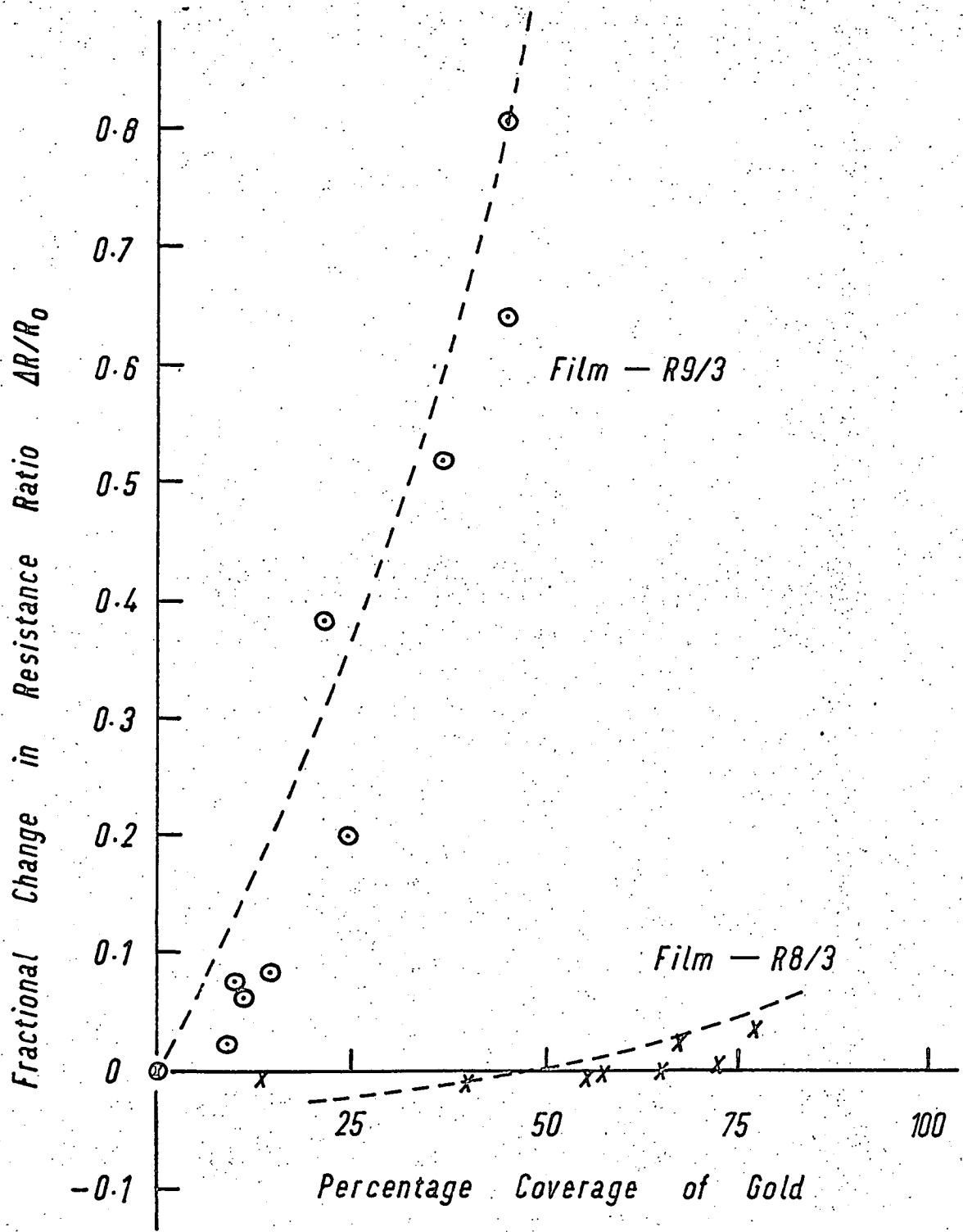
and since it is assumed that $\theta = \frac{\Delta\phi}{\phi_2 - \phi_1}$, then equation (5.4.2) yields

$$\frac{\Delta\phi}{\phi_2 - \phi_1} = \left(1 - e^{-\left(\frac{\Delta R/R_0}{0.25}\right)}\right) \quad (5.4.4)$$

5.4.2. Gold Overlayers. Figure 5.4.4. shows the variations in contact potential with quartz crystal frequency shift for two gold films, (R9/3 and R8/3), deposited onto silver films prepared as described in the previous section. The gold was deposited at a pressure of 10^{-8} torr, or better, at a rate of about $20\text{\AA}/\text{minute}$. Just as for the films deposited previously, the glass substrates were nominally at room temperature. Using the quartz crystal frequency calibration for gold, and again assuming that $\theta = \frac{\Delta\phi}{\phi_2 - \phi_1}$, then the points on figure 5.4.5. were plotted showing the mean gold overlayer thickness versus percentage coverage. A reasonable approximation to the experimental points on figure 5.4.5. is the line drawn dotted which is represented mathematically by the equation

$$\theta = \left(1 - e^{-\left(t/9.5\right)}\right) \quad (5.4.5)$$

The resistance changes taking place in the film on the



— Figure 5.4.6 —

— Resistance Changes with Gold Overlayers —

resistance sample substrate are shown plotted in figure 5.4.6. as a function of coverage. It is obvious that there is a large discrepancy between the two sets of points plotted, which can be explained on the basis of the different techniques used to measure the resistance of films R8/3 and R9/3, as discussed later in section 6.2.2. The points of film R9/3 can be approximated by the line shown dotted which is represented by the equation

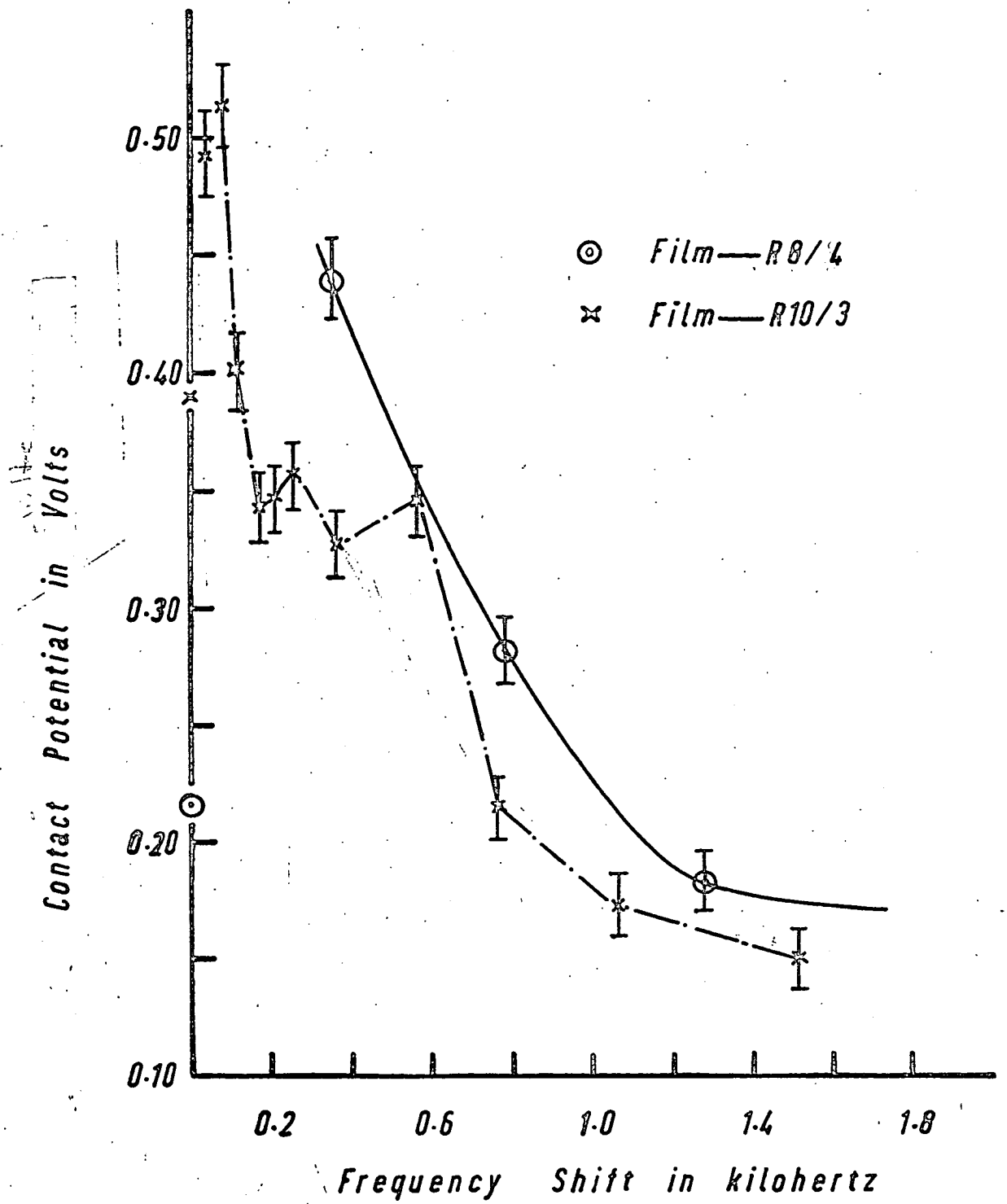
$$\theta = \left(1 - e^{-\left(\frac{\Delta R/R_0}{1.5}\right)} \right) \quad (5.4.6)$$

The resistance of film R8/3 changes only very slightly over the complete coverage range measured. The resistance at first increases slightly, then decreases by approximately 5% from the maximum to the final value at just over 75% coverage. The dotted line drawn through the points of film R8/3 represents the combination of a resistance increase as a result of a temperature rise of the film, and the shunting effect of an overlayer assuming the theory of section 2.2.2. to be relevant. The principal equation needed from the theory is

$$\frac{R_T}{R_0} = (1 - \theta^{1/2}) + \frac{\theta^{1/2}}{(1 - \theta^{1/2}) + \theta^{1/2} \left(\frac{\rho_u}{\rho_c}\right) \left(\frac{F+T}{F}\right)} \quad (5.4.7)$$

with the symbols having the same significance as before.

As a simplification ρ_u is made equal to ρ_c , and the required relation between θ and T is obtained from figure 5.4.5. For film R8/3 the film thickness F is equal to $130\text{\AA} \pm 20\%$ as deduced from



— Figure 5.5.1 —

— Contact Potential Change with Aluminium Overlayer —

the frequency shift of the quartz crystal monitor. In order that equation (5.4.7) can yield a curve to fit the experimental resistance changes for film R8/3 on figure 5.4.6 the required fractional change in resistance with the temperature rise is + 0.04, which can be considered to represent a temperature coefficient of $0.002/^{\circ}\text{C}$. and a temperature rise of 20°C . Any reasonable temperature rise to give the product of temperature rise and temperature coefficient a value of + 0.04 is of course possible, with the constraint that the coefficient cannot be greater than the bulk value.

From equations (5.4.5) and (5.4.6) above it follows that the relationship between fractional resistance change and overlayer film thickness, t , in Angstroms is

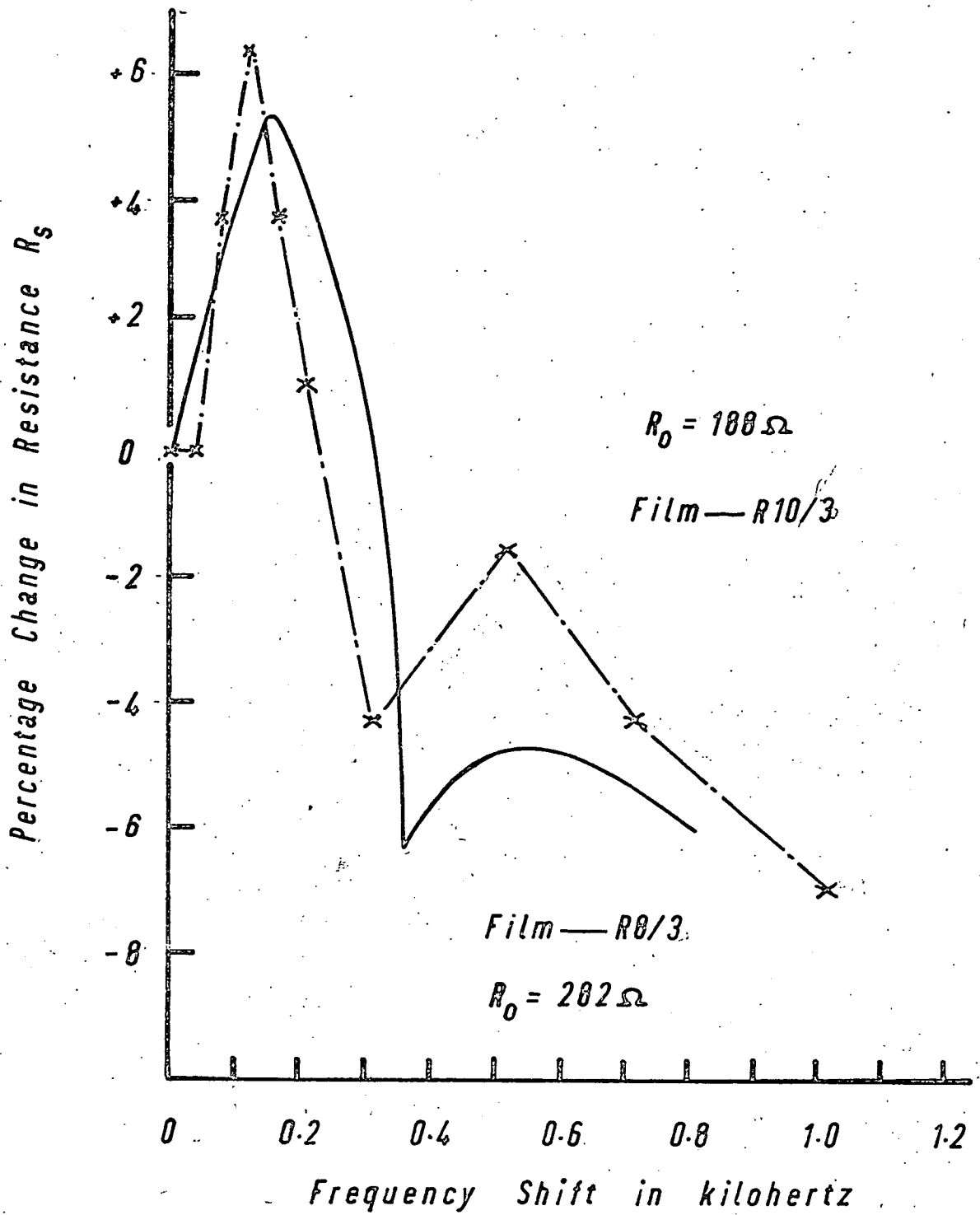
$$\frac{\Delta R}{R_0} = 0.158.t \quad (5.4.8)$$

which obviously can only apply up to

$$t = \frac{1}{0.158} \text{ \AA}$$

5.5. Aluminium Overlayers.

Figure 5.5.1. shows contact potential changes measured during the growth of aluminium overlayers onto a polycrystalline silver thin film surface. Film R:10/3 was grown on a surface with greater than 99% coverage of silver, and R8/4 on a film with approximately 50% of silver and 50% of gold present at the surface.



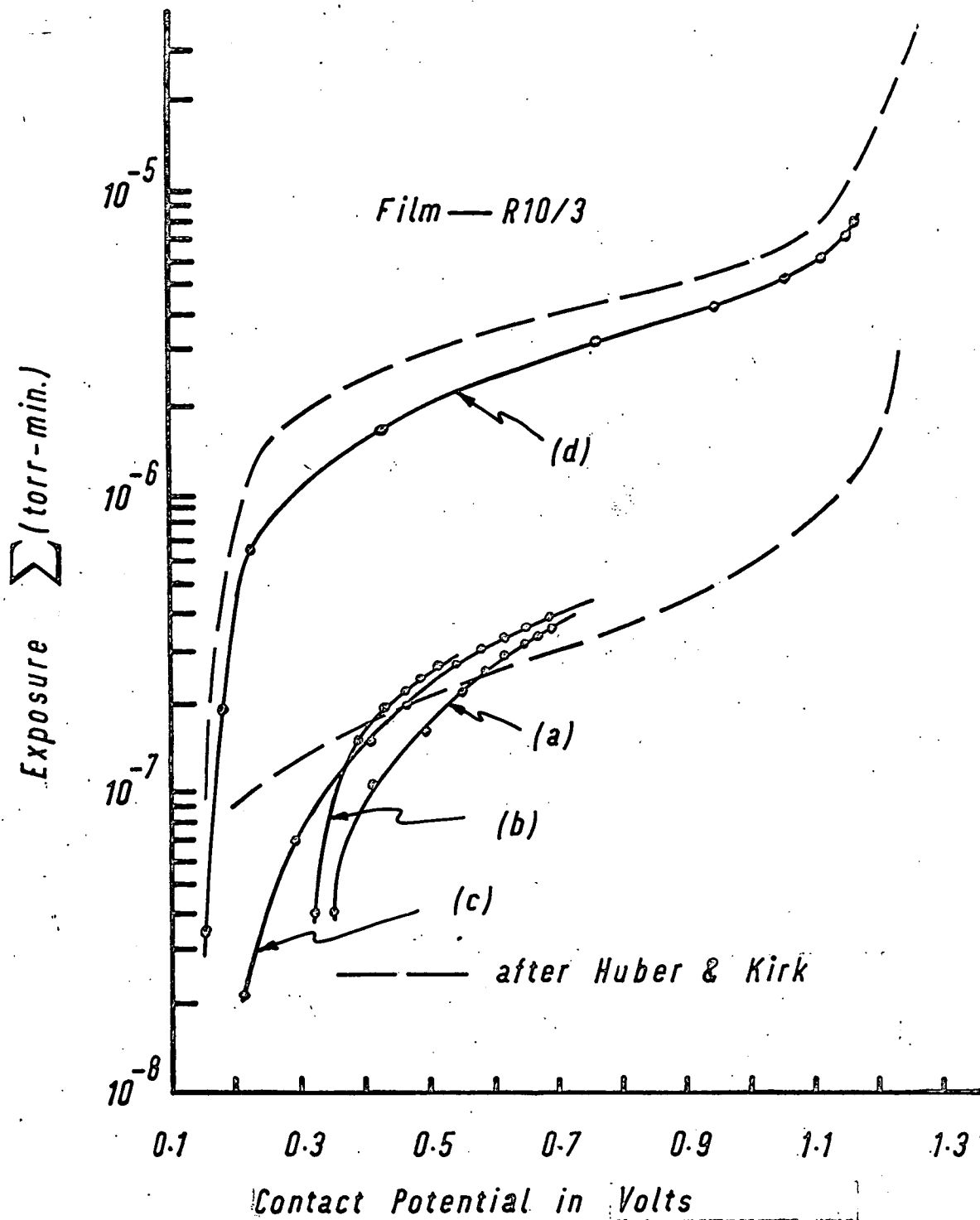
— Figure 5.5.2 —

— Resistance Change with Aluminium Overlayer —

The latter film was prepared by depositing a film of gold with a mean thickness of about $12\overset{\circ}{\text{Å}}$ onto a relatively thick ($\sim 100\overset{\circ}{\text{Å}}$) film of silver. By preparing the film in this way the areas of silver still exposed to the aluminium evaporation stream are thicker than the depth of alloying which is expected to take place between the silver and aluminium. From figure 5.4.2. in section 5.4.1. it is seen that depositing silver on gold to a coverage of say 50%, would result in a very thin silver film having a mean thickness of less than one atomic layer. The zero on the contact potential scale in figure 5.5.1. was made equal to the effective work function of gold films prepared in the vacuum chamber during the evacuations corresponding to the deposition of films R8/4 and R10/3 respectively. By doing this the contact potential scale zero for both films is the same, thus eliminating any change in the effective work function of the reference electrode which may have occurred. The possible range of error in each point plotted on figure 5.5.1. is then approximately twice the normal range. The frequency scale on figures 5.5.1. and 5.5.2. correspond to

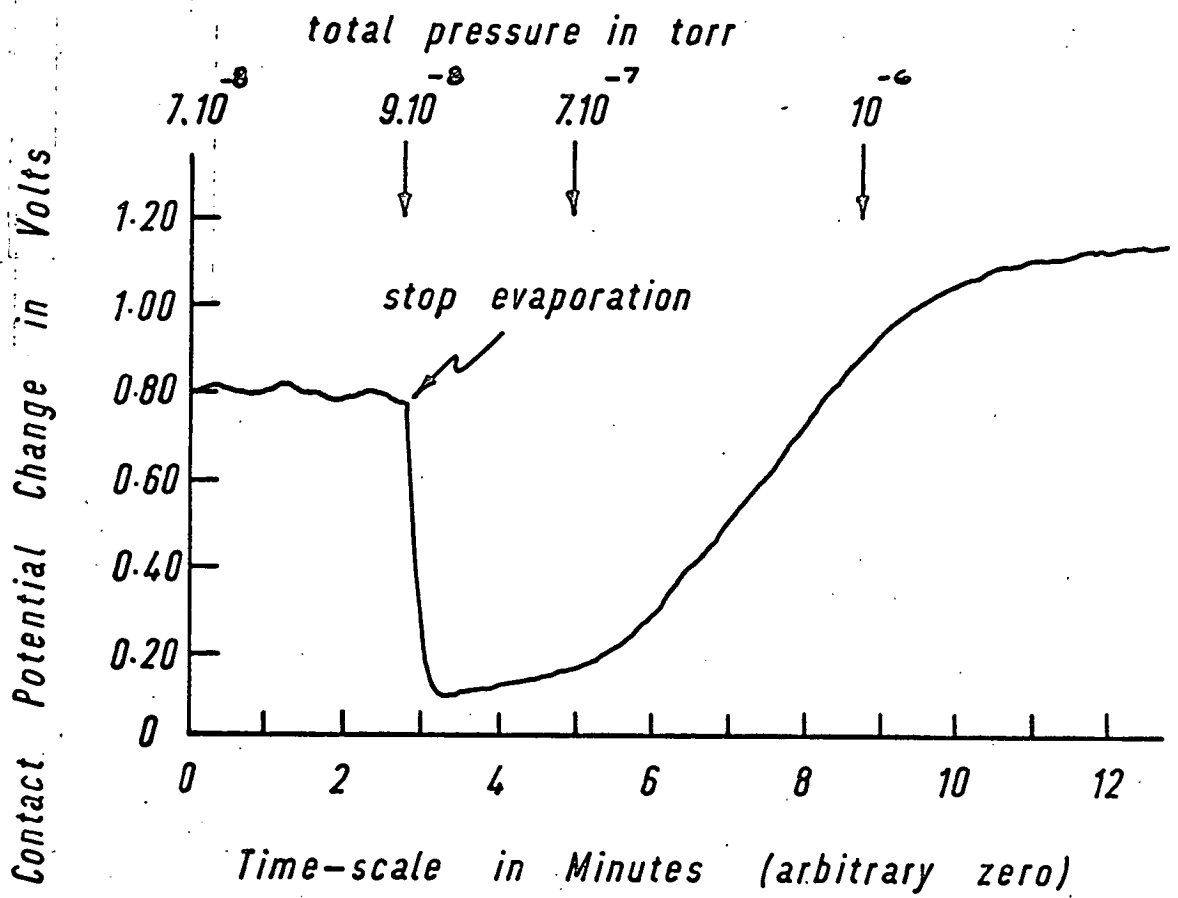
$$4.5 \text{ khz} \equiv 100\overset{\circ}{\text{Å}} \pm 20\%$$

Figure 5.5.2. shows the resistance changes which took place during the formation of the aluminium overlayers. The general shape of the variations for both films can be seen to be quite similar. Both films have two resistance maxima, at about $5\overset{\circ}{\text{Å}}$ and $12\overset{\circ}{\text{Å}}$ mean overlayer thickness, and the maximum increase in



— Figure 5.5.3 —

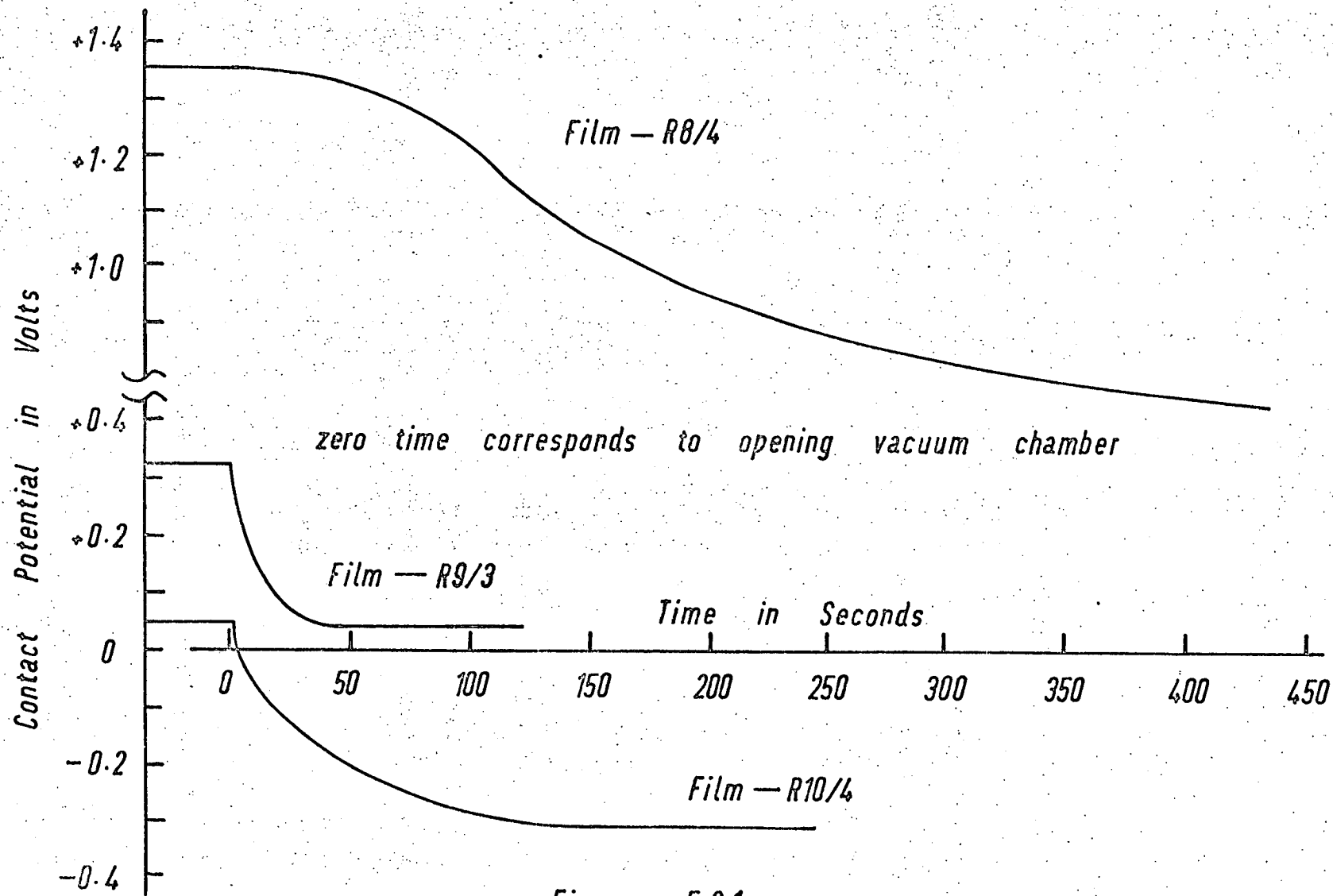
— Contact Potential Changes with Exposure for Aluminium Films —



— Figure 5.5.4 —

— Contact Potential During and After Al Evaporation —

resistance is in the range of 5% to 7%. The resistance curve for film R8/4 is continuous, and for film R10/3 a point by point plot was made because different techniques were used to measure the resistance of the two films. The substrates were nominally at room temperature, and the rate of deposition of the aluminium was about $20\text{\AA}/\text{minute}$. During the depositions the pressure in the chamber was approximately 10^{-8} torr. The time between successive evaporations for film R10/3 was short (approximately two minutes) up to an overlayer thickness corresponding to 0.3 khz, but after 0.3khz sufficient time lapsed to allow the monitoring of the contact potential variations on figure 5.5.3. The lower sets of points on curves (a), (b) and (c) are for mean thicknesses of approximately 8\AA , 12\AA , and 17\AA respectively. The top set of points on curve (d) are for an overlayer thickness of approximately 30\AA . The two curves drawn dotted on figure 5.5.3. are from the results of Huber and Kirk (29) with the contact potential axis shifted by 0.90 volts, i.e. Huber and Kirk have a contact potential value of about 1.1 volts and not 0.2 volts at an exposure of 10^{-7} torr x minutes. A typical recorder trace from which the upper set of points on figure 5.5.3. was obtained is shown in figure 5.5.4. During the evaporation the contact potential value is about 0.8 volts, but decreases immediately the evaporation is stopped to a value of 0.1 volts, and then slowly rises again to a value in excess of 1.1 volts with sufficient exposure. It is the minimum value of contact potential which is reached immediately after cessation of the



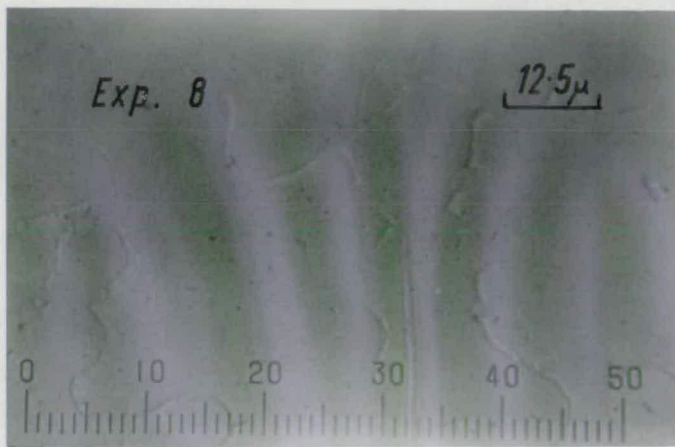
— Figure 5.6.1 —

— Contact Potential Changes when Vacuum Chamber is Opened —

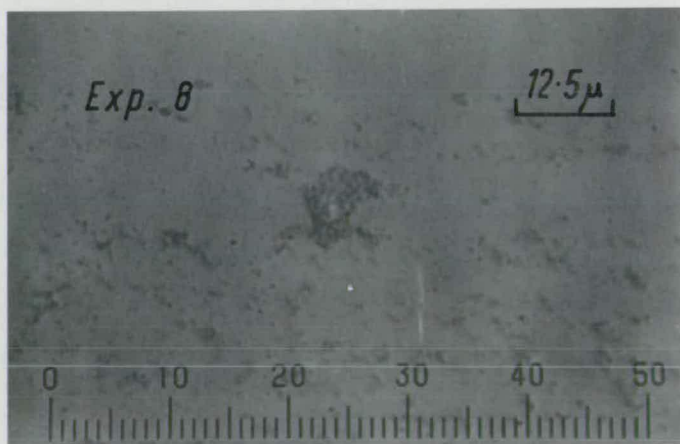
evaporation that is plotted on figure 5.5.1.. The pressure after stopping the evaporation is increased by bleeding oxygen into the vacuum chamber through the leak valve from a gas line which was flushed with oxygen to a pressure of 0.05 torr several times before it was opened to the chamber. Figure 5.2.1. shows the vacuum system used for flushing the line.

5.6. Examination of the Films after Venting the Vacuum Chamber to Atmospheric Pressure.

5.6.1. Contact Potential Changes on Venting Chamber. Figure 5.6.1. shows the contact potential changes as a function of time for films R8/4, R9/3 and R10/4 on opening the chamber to the atmosphere. The zero of the contact potential scale for each film is taken to be the effective work function of gold films deposited during the corresponding evacuation of the chamber. Film R8/4 has an overlayer of about 120\AA of aluminium deposited in steps of 8\AA , 9\AA , 11\AA , and $90\text{\AA} \pm 20\%$ onto a gold and silver film on a glass substrate. The substrate was nominally at room temperature, the pressure during deposition was about 10^{-8} torr, and the rate of deposition was approximately $20\text{\AA}/\text{minute}$. On opening the chamber the contact potential decreases by 0.20 volts in 100 seconds followed by an exponential decrease to a value of 0.66 volts within ten minutes. The time constant for the decrease is approximately three minutes. Film R9/3 has an overlayer of gold to approximately 50% coverage with a mean thickness of $\sim 6\text{\AA}$, as shown on figure 5.4.5.. The gold was deposited onto a silver film



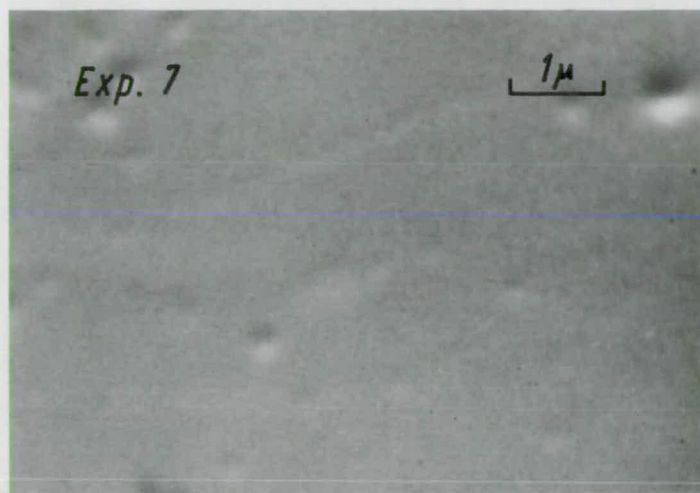
—— Typical Areas at Opposite ends of
Resistance - monitor Film ——



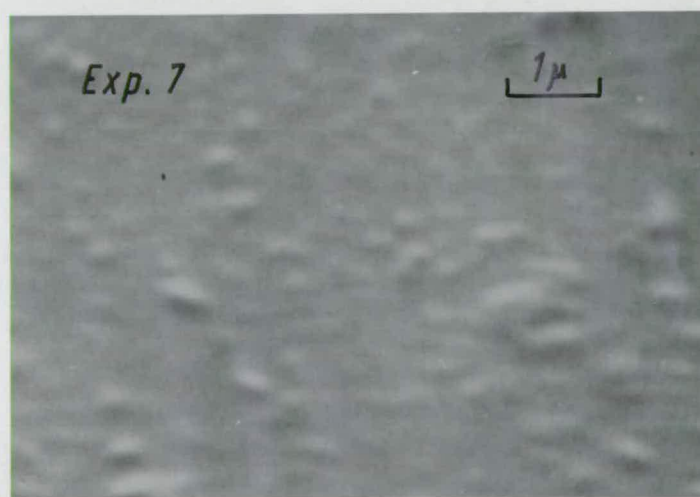
—— Figure 5.6.2 ——

on a glass substrate nominally at room temperature in a vacuum of 10^{-8} torr, or better, at a rate of about $20\text{\AA}/\text{minute}$. The contact potential initially has a value of 0.32 volts and drops exponentially by 0.27 volts on opening the chamber with a time constant of 15 seconds. Film R10/4 has an overlayer of about 85\AA of silver deposited onto a 55\AA thick aluminium film on a glass substrate nominally at room temperature in a vacuum of 10^{-8} torr at a rate of approximately $200\text{\AA}/\text{minute}$. The contact potential is initially at 0.05 volts, and on venting the chamber it decreases exponentially to ~ 0.31 volts with a time constant of approximately 40 seconds. Thus the net change in contact potential is a decrease of 360 millivolts.

5.6.2. Optical Microscope. With only one exception, all of the 36 films made during the series of experiments carried out had no features of interest which could be seen with the optical microscope. A few smears, scratches and large lumps on the surface, which were presumed to be contamination after removal from the vacuum chamber, were present on all of the films examined. Figure 5.6.2. shows photographs taken at either end of the film used to monitor resistance changes for experiment 8. The scale shown demonstrates that the photographs were taken at the resolution limit for an optical microscope. By defocussing the microscope slightly the pattern on the upper photograph was identified as hollows in the film, and similarly the almost spherical spots on the lower photograph were identified as lumps



— Area Baffled from Main Evaporation Stream —



— Area Exposed to Main Evaporation Stream —

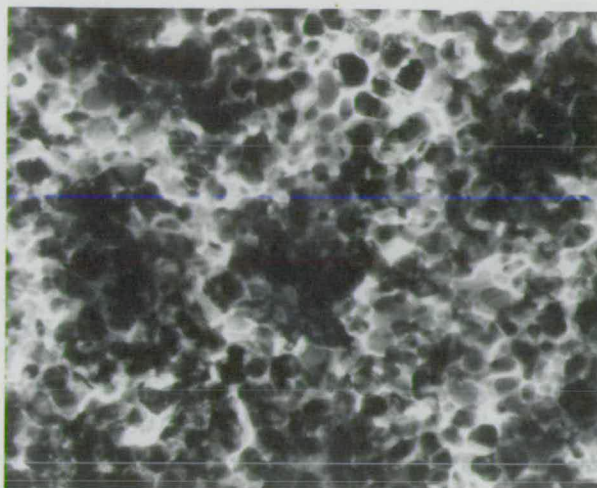
— Figure 5.6.3 —

— Areas of Film with and without Aluminium Overlayer —

of material. When the film has a resistance R greater than $1 \text{ M}\Omega$ the current passing through it is given approximately by $12/R$ amps. For experiments 9 and 10 an electrometer was used for measuring resistance and no hollows and clusters, as shown in figure 5.6.2. were seen.

5.6.3. Scanning Electron Microscope. Representative areas of the films for each experiment were mounted on the microscope mounting stubs by breaking off a part of the substrate approximately 0.5 cm. square, and fixing it to the stub with Areldite. A conductive path was then made to the film on the uppermost surface of the substrate by painting the edges of it with colloidal graphite. Patterns similar to those in figure 5.6.2. were observed for experiment 8. For experiments 9 and 10 the scanning electron microscope did not have quite enough resolution to be really useful. It was just possible to discern a grain structure at the best possible magnification, when a resolution of $\sim 400\text{\AA}$ was obtained. However, there was not sufficient contrast with these structures to make photographs worthwhile. In experiment 7 an overlayer of about 140\AA of aluminium was deposited on to a 170\AA polycrystalline gold film on a glass substrate. The aluminium was deposited at a pressure of 10^{-6} to $3 \cdot 10^{-5}$ torr at a rate of approximately $100\text{\AA}/\text{minute}$, and the evaporation stream was baffled to allow deposition on only about three quarters of the resistance monitor substrate positioned just above the wheel. Figure 5.6.3. shows in the upper picture

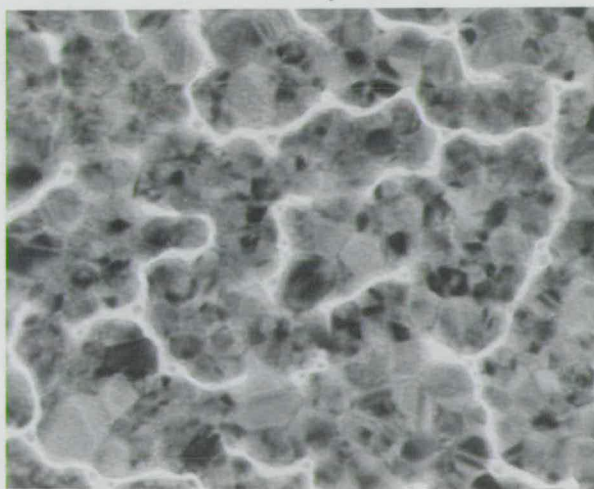
Exp. 7



10^3 \AA

— Film from Wheel-mounted Substrate —

Exp. 10



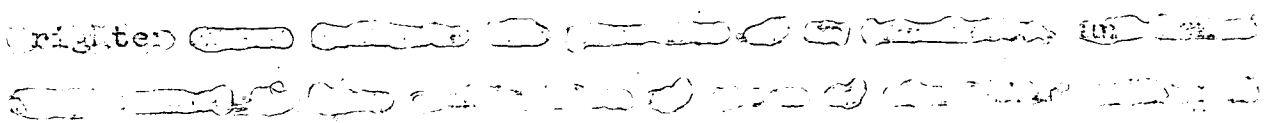
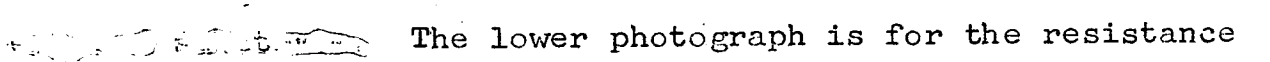
500 \AA

— Resistance-monitor Film —

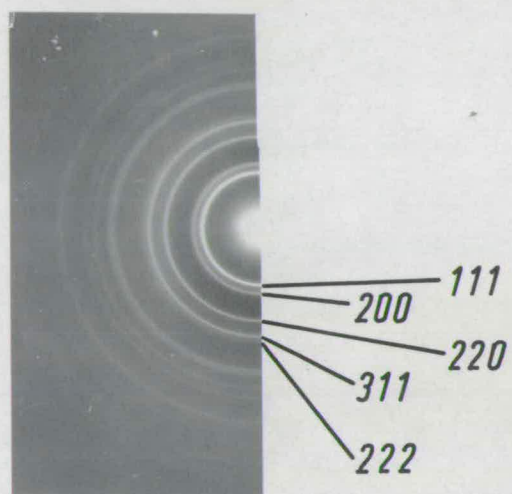
— Figure 5.6.4 —

— Transmission Electron Microscope Photographs —

a photograph taken of the film in the scanning electron microscope at a part of the resistance monitor substrate where only gold had been deposited, and the lower picture is of an area where the gold and aluminium had been deposited. It is apparent that the lower picture has a more granular structure, with a typical 'lump' diameter of 1200\AA to 3500\AA .

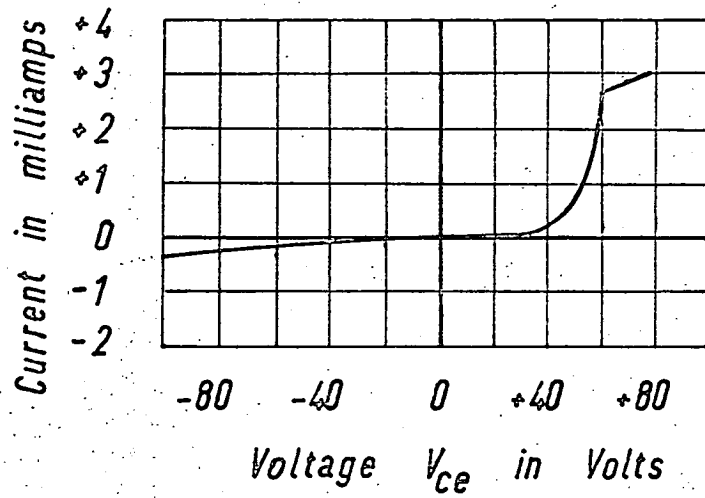
5.6.4. Transmission Electron Microscope. Samples of the films deposited were stripped from the substrates with Sellotape and then floated off the tape in a dish of chloroform. Small pieces of the films were then mounted on copper grids and examined in an A.E.I. EM6 electron microscope. Many of the films made were too thick to be examined in the microscope, however figure 5.6.4 shows photographs taken of two of the thinner films. The upper photograph is for one of the wheel mounted films of experiment 7, and is approximately 170\AA of gold with a 140\AA overlayer of aluminium. It is seen that it has a distinct grain structure, with the grain size 80\AA to 350\AA , having many 60° corners.  (right)  The lower photograph is for the resistance monitor substrate of experiment 10, and is a layer structure of gold, silver and aluminium having a total thickness of approximately 280\AA . A distinct grain structure exists, with a typical grain size of 100\AA to 200\AA , having many 60° corners. The fissures present also exhibit the 60° corners. An electron diffraction picture taken of the same area of film as the lower photograph

Resistance monitor film of experiment 10



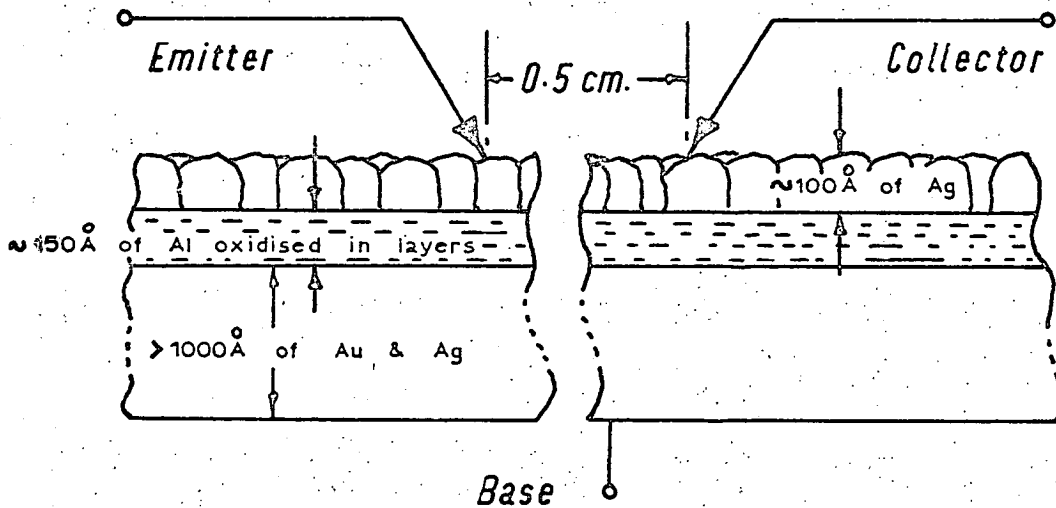
— Figure 5.6.5 —

— Electron Diffraction Picture —



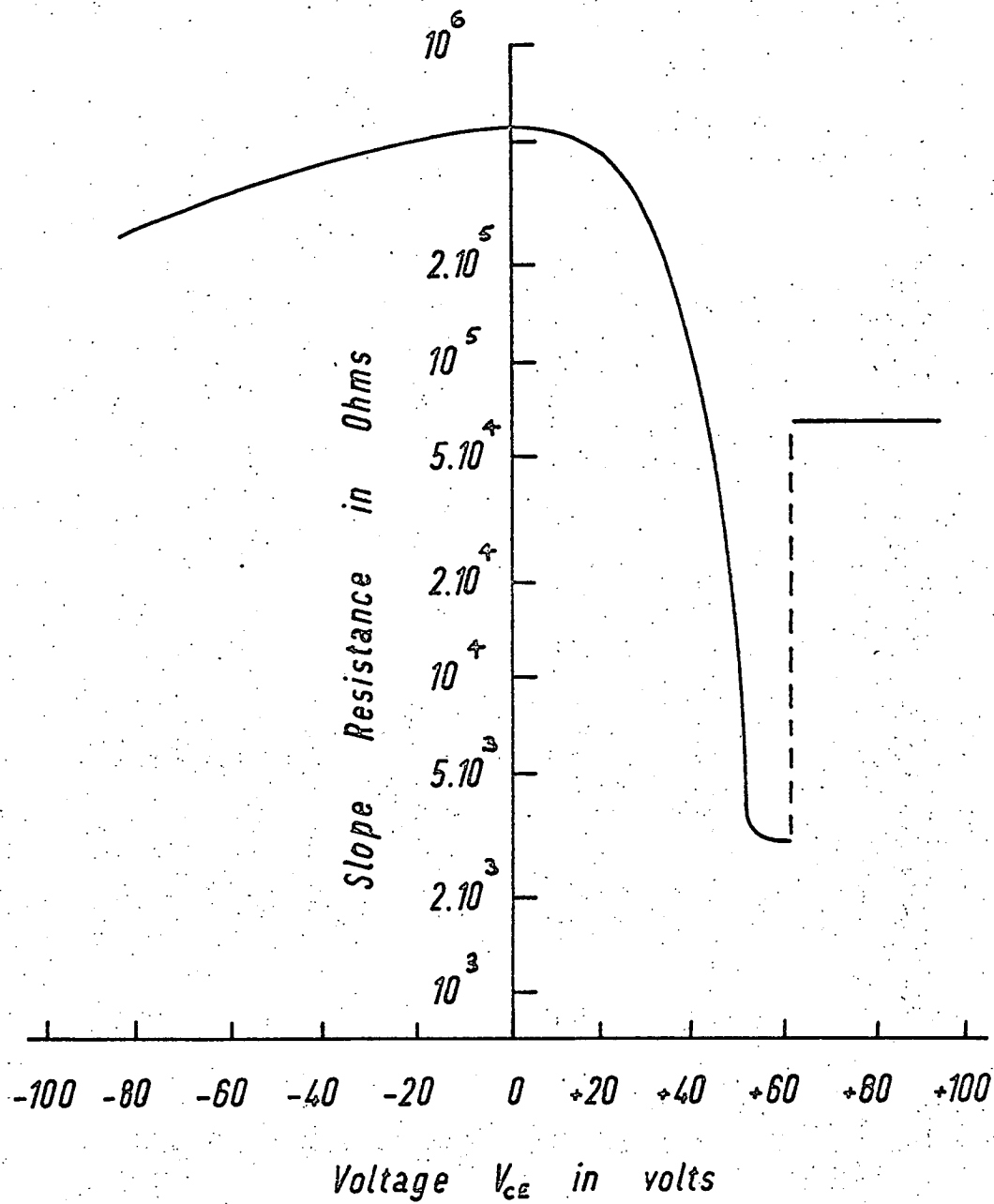
— Figure 5.6.6 —

— I-V Characteristic of the Thin Film 'Device' Shown Below —



— Figure 5.6.7 —

— Structure of Thin Film 'Device' —



— Figure 5.6.8 —

— Variation of "Device" Resistance with Voltage —

is shown in figure 5.6.5.

5.6.5. Other Examinations. All of the multi-layer films had their thicknesses, as deduced from the frequency shift of the quartz crystal monitor, checked with the Talysurf on their removal from the vacuum chamber. Repeated measurements on the same area of film agreed to within $\pm 25^{\circ}\text{\AA}$ of the arithmetic mean, and all of the measurements agreed to within $\pm 20\%$ of the values deduced from the frequency shift of the quartz crystal monitor.

After the films were removed from the chamber, gold plated probes were used to check their final resistance values in order to show up any bad electrical contacts in the measuring system. When one of the wheel mounted substrates of experiment 10 was probed it was discovered that a rectifying effect was obtained. Figure 5.6.6. shows a sketch of a typical current-voltage trace obtained on a Tektronix curve tracer, type 575, with a current drain setting of 0.001 milliamps for the base connection made to the ($\sim 1000\text{\AA}$) underlayer film. The structure of the thin film is shown in figure 5.6.7. Thus the thick gold film was made the base, and the two surface probes, separated by about 0.5 cm, the emitter and collector of a three-terminal device. The reverse direction impedance is $> 100\text{ k}\Omega$ and the forward impedance, before the abrupt change in slope resistance is reached, is approximately $3\text{ k}\Omega$. The slope resistance as a function of collector to emitter voltage, V_{ce} , is shown on figure 5.6.8. It is seen in figure 5.6.8. that the curve drawn has a discontinuity at $V_{ce} \simeq 60$ volts,

when the slope resistance changes abruptly from 3 k Ω to 60 k Ω . The structure and characteristics of these films are similar to those described by Szupillo (175) in a U.S. Patent application. After remaining in the laboratory for several months the characteristics shown on figure 5.6.6. could no longer be obtained for any of the eight wheel-mounted substrates of experiment 10.

CHAPTER 6.DISCUSSION AND CONCLUSIONSIntroduction.

The first four sections in this chapter are devoted to discussing the results reported in chapter 5. Conclusions reached as a result of this work are then listed, followed by several suggestions where future work on the conductivity on thin films, particularly employing the measurement of contact potential, may prove useful and which could follow on naturally from this work.

6.1. Thin Gold Films.

6.1.1. Film Conductivity During Initial Growth Period. Metallic films with a bulk conductivity σ_0 have a resistance / square of

$$R = \frac{1}{\sigma_0 \cdot F} \Omega \quad (6.1.1)$$

For gold $\sigma_0 = 4.96 \times 10^9$ / cm, and if the film thickness, F , is taken to be equal to 60 \AA , then equation (6.1.1), which assumes completely specular electron scattering at the film surfaces (i.e. P and $Q = 1$), yields upon substitution for F and σ_0

$$R = 4.03 \Omega / \text{square}$$

If however, the electron scattering at the film surfaces is assumed to be completely diffuse (i.e. P and $Q = 0$), and a value of 0.2 is taken as the ratio of film thickness to mean free path, then the value of resistance is

$$R = 12.5 \Omega / \text{square}$$

The actual measured resistance of film R9/1, which is about 60\AA thick, is two to three orders of magnitude larger than these above values, indicating that thin films such as R9/1 are not continuous sheets of metal. Assuming that the logarithmic relationship deduced in section 5.3. between electrical resistance and mean thickness continues to be valid until the film conductivity is near to the bulk value, then this should occur at a thickness $F\text{\AA}$, which for film R9/1 is the solution to the equations

$$\log_{10} R = 11.5 - 0.14 \cdot F \quad (6.1.2)$$

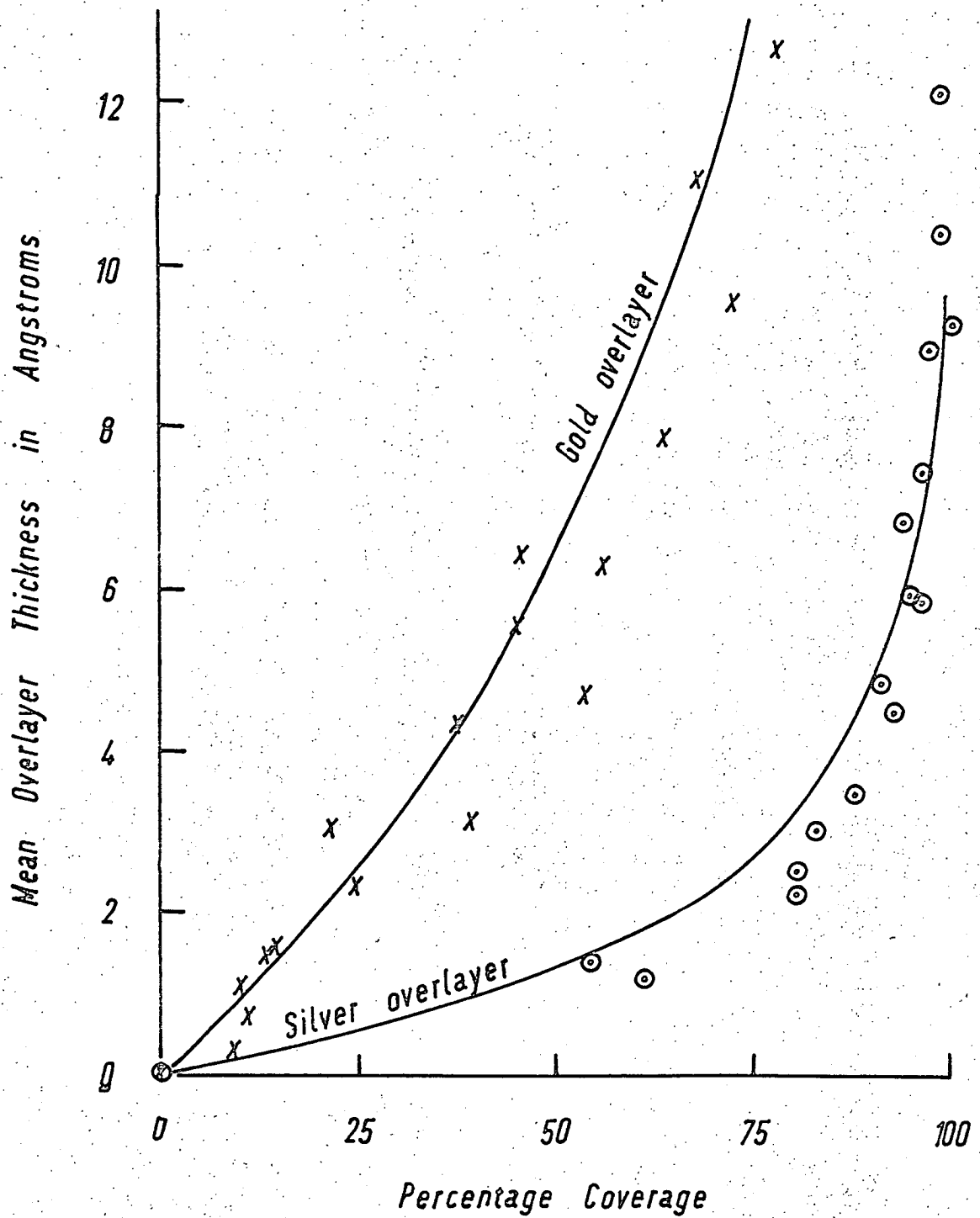
$$\text{and} \quad R = \frac{24.2}{F} \quad (6.1.3)$$

The solution to equations (6.1.2) and (6.1.3) is at $F \approx 90\text{\AA}$, and by solving a similar pair of equations for film R10/I the solution is at $F \approx 150\text{\AA}$. Thus bulk conductivity is not expected to be approximated for gold films deposited on to cold glass

substrates at a thickness of much less than 100\AA , and probably only at considerably greater thickness. The points plotted on figure 5.3.1. joined by the dotted line are for silver deposited onto a glass substrate nominally at room temperature (174), and correspond very well to the curve for film R9/1. The points are plotted to the same mean thickness scale as that for film R9/1 assuming that for gold $32\text{ khz} \equiv 100\text{\AA}$. The silver film only became completely continuous at a thickness of $\approx 250\text{\AA}$, and hence a value of the same order would be expected for the gold film R9/1. The electrical resistance over the range plotted on figure 5.3.1. is principally the result of the activated conduction process discussed earlier. The temperature coefficient of resistance changes from negative to positive at a resistance of about $10^6 \Omega$ / square. This is in agreement with Witzencamp and Bashara (176) who found a positive temperature coefficient for a gold film with a conductivity value six orders of magnitude less than that of the bulk. It is not, however, conclusive that the sharp changes in the lower curve on figure 5.3.1. at points A and B are consequences of the temperature coefficient variations. It is possible that the effect of self-annealing of the film could change the resistance in the same way. Lucas (19) reported sudden changes in the resistance of gold films when evaporation was stopped, which was attributed to self-annealing. The rate of deposition of gold films R9/1 and R10/1 was approximately $50\text{\AA}/\text{minute}$, and each of the wheel-mounted substrates was in the evaporation stream for one sixteenth of a revolution of the wheel.

Hence the temperature increase of the films prepared in this work is unlikely to be very large since the rate of deposition is a factor of twelve lower than that used by Belous and Wayman (130), whose work was referred to earlier in section 2.2.8., and in view of the fact that the substrate is only exposed to the source for one sixteenth of the total evaporation time. The results of Namba (177), in which temperature increases of up to 20°C, are reported, are probably more of the order experienced by the films prepared in the Varian vacuum system. Since only a small temperature increase appears to take place however, the quartz lamp used as a light source for the photo-diode may cause a small, but significant, increase in the temperature.

6.1.2. Effective Work Function of Gold. The contact potential measurements made with respect to the reference electrode showed that there is a difference of 0.400 volts \pm 10 mv. between the effective work function values of thin polycrystalline gold films prepared in a vacuum system with oil diffusion and rotary pumps, and the Varian system which has all-dry pumps. It was discussed in section 2.2.4. that it is only recently that the accepted work function value of gold was changed from about 4.8 eV to about 5.2 eV. The contact potential measurements made here are thus complementary to these of Huber (85), who showed that in a vacuum system with mercury diffusion pumps the effective work function value for gold is about 4.7 eV. If the effective work function value for gold is taken to be 5.22 eV then this implies a value of 4.82 volts \pm 10 mv. for the effective



— Figure 6.2.1 —

— Variation of Mean Thickness with Coverage —

work function value of a gold film prepared in a vacuum system with oil diffusion and rotary pumps. A contributory cause to the value of about 5.2 eV only recently being generally accepted as the value for an uncontaminated gold sample was probably that the value obtained in such vacuum systems is approximately 4.82 eV. Undoubtably some foreign species was present in or on the gold films prepared in the vacuum system with the diffusion pump which caused a Volta potential to exist in the films. This is indicated since the deposition of further layers of gold in the Varian system failed to increase the effective work function by more than 150 millivolts. A similar effect which occurred with aluminium films when silver was deposited onto them is discussed in section 6.3.

6.2. Conductivity Changes with Gold and Silver Overlayers.

6.2.1. Silver Overlayers on Gold. Before considering the conductivity (or resistance) changes with silver overlayers, it is preferable that the contact potential measurements are firstly examined in order to establish in what manner the silver overlayers were formed. The experimental points for the variations of mean overlayer thickness with coverage, deduced from contact potential measurements, are shown in figure 6.2.1. It is assumed in figure 6.2.1. that the fractional change in contact potential, $\frac{\Delta\phi}{\phi_2 - \phi_1}$, is equal to the fractional coverage of deposit, θ . A curve having the equation

$$100.\theta = \left(1 - e^{-(t/2)}\right) \quad (6.2.1)$$

is drawn through the experimental points for silver on figure 6.2.1. It is evident that equation (6.2.1) is a good fit to the mean of the experimental points plotted. Equation (6.2.1) has the form of one of the three types of variation of contact potential with coverage put forward in section 2.2. Referring to figure 2.2.3., the theory of Levine and Gyftopoulos (71) requires that the contact potential should have changed more rapidly with mean overlayer thickness than was the case. Also the latter theory is for a regular crystal surface and the transmission microscope pictures in figures 5.6.4. and 5.6.5. show that the films deposited were very polycrystalline. Hence these films do not satisfy the surface requirements for the application of the theory. Furthermore, the general form of the variations required to fit the theory of Jones (115) was not obtained. The third curve on figure 2.2.3. however, for the case where it is assumed that

$$\frac{\Delta\phi}{\phi_2 - \phi_1} = \theta \quad (6.2.2)$$

agrees with the experimental results on figure 6.2.1., and thus makes the relationships in equations (6.2.1) and (6.2.2) reasonable approximations.

The slight increase in effective work function which occurs, see figure 5.4.1., as the mean thickness of the overlayer increases is consistent with a decrease in the proportion of the less

stable crystal faces at the film surface as a result of self-annealing. It is well established that the less polycrystalline a surface becomes, the greater is its value of effective work function. For silver deposited onto annealed polycrystalline silver Clarke and Farnsworth (83) found that, provided the substrate temperature was less than 65°C ., the photoelectric work function was decreased, but could be increased to the original value by annealing the film for a short time at a temperature of only $80^{\circ} - 200^{\circ}\text{C}$. At a temperature within, say, 20°C . of room temperature the annealing process will be slower and the resulting increase in work function will be of the order shown in figure 5.4.1. It was shown previously that as the mean thickness of the overlayer tends to zero, then the actual thickness of deposit tends to the exponential 'time constant' in equation (6.2.1), i.e. The critical nucleus size is of the order of $2\overset{\circ}{\text{A}}$. If the nuclei can be considered to be hemispherical, then it follows that the critical nucleus radius is $\sim 3\overset{\circ}{\text{A}}$. Even if it is felt that the nuclei cannot be considered to be hemispherical, but only that the width is of the same order as the depth, it still follows that the critical nucleus has dimensions of a few angstroms. Hence it is deduced that the silver condenses onto the polycrystalline gold surface and nucleates, on average, either as individual atoms or in clusters consisting of only a few atoms. This demonstrates that thermodynamically, for the materials and environmental conditions employed in the experiments carried out, the silver prefers an extremely small

critical nucleus. Silver having large surface coverage for a thickness of only one atomic layer is in agreement with the L.E.E.D. measurements of Farnsworth (178).

The resistance changes during the growth of the overlayers are now considered. Assuming that the fractional change in the effective work function is equal to the coverage, then the relationship obtained between fractional resistance change, $\frac{\Delta R}{R_0}$, and coverage, θ , is

$$\theta = \left(1 - e^{-\left(\frac{\Delta R/R_0}{0.25}\right)} \right) \quad (6.2.3)$$

where R_0 is about 1000Ω / square

Equating equations (6.2.1) and (6.2.3) yields

$$\frac{\Delta R/R_0}{0.25} = \frac{t}{2}$$

$$\text{or } \Delta R/R_0 = 0.125 \cdot t \quad (6.2.4)$$

which is valid for $t \leq (1/0.125) \text{ \AA}$

In equation (6.2.4) the constant of proportionality between $\frac{\Delta R}{R_0}$ and t has a value between the values of 0.14 and 0.08 which were obtained for the proportionality constant in relationships similar to equation (6.2.4) applicable during the initial growth period of gold films R10/1 and R9/1 respectively. Thus, even at a resistance of a few hundred ~~atoms~~^{ohms} per square the fractional changes in resistance for small increases in thickness are similar

to the changes for very high resistivity discontinuous films. Furthermore, it follows from the resistance measurements that the growth of the silver overlayers on the polycrystalline gold surfaces is similar to that of gold deposited onto these surfaces, which agrees with the silver nucleation and growth discussed above.

The contact potential difference between a gold film prepared entirely in the Varian vacuum chamber and a silver film 50\AA thick deposited onto a gold underlayer on a glass substrate is 0.900 volts ± 25 mv. Assuming as before a value of 5.22 eV for the effective work function of gold, then the deduced effective work function of a thin polycrystalline silver film at room temperature is 4.32 volts ± 25 mv. in agreement with other authors (77).

The contact potential difference between the reference electrode and polycrystalline silver films decreased by 0.365 volts ± 8 mv. on exposing the films to atmospheric pressure, indicating that the silver had adsorbed gas molecules. The gas is most probably chemisorbed oxygen which is expected to cause an increase in the effective work function of a metal surface, and agrees with the fact that silver is known to react with oxygen.

The resistance of the resistance monitor film for experiment 9 increased by approximately 4% within 60 seconds of opening the chamber, which is further evidence that oxygen has been adsorbed on the surface. The oxygen would prevent many electrons at or near the silver surface from taking part in electrical conduction, and hence result in an increase in the electrical resistance. What is

unexpected however, is that when these silver films are reinstalled in the vacuum chamber, after being exposed to the atmosphere for approximately one day, and the chamber evacuated to $< 10^{-6}$, the contact potential returns to its previous value. This suggests that the adsorbed gas is pumped off the silver surface when a low pressure is reached. Oxygen incorporation into the bulk to form an oxide is expected to cause a change in the surface potential of the film as a result of a Volta potential across the oxide. Hence, in view of the contact potential returning to exactly its original value, within the experimental error, it is unlikely that the change can be explained by an adsorbed layer of oxygen being incorporated into the bulk to form a thin layer of oxide. Only if the silver oxide was very thin and a perfect dielectric with no foreign atoms or molecules bonded on its surface which would give a surface potential, would it explain the contact potential change. Evidence that silver only adsorbs oxygen for a high exposure is that several minutes at pressures as high as 10^{-5} torr produced no change in the contact potential with respect to the reference electrode. This agrees with Clarke and Farnsworth (83) who found that the photoelectric work function was independent of the pressure during the deposition of silver over the range 10^{-8} to 10^{-6} torr.

6.2.2. Gold Overlayers on Silver. The upper curve drawn on figure 6.2.1. has the equation

$$100.\theta = \left(1 - e^{-\left(t/9.5\right)} \right) \quad (6.2.5)$$

It is evident that equation (6.2.5) is a good fit to the experimental points plotted for gold on figure 6.2.1. Just as for the case of the silver overlayers in the previous section, the form of the variation of coverage, θ , with mean overlayer thickness, t , follows from the model for overlayer growth presented in section 2.1.

$$\text{i.e.} \quad \theta = 1 - e^{-t/\tau} \quad (6.2.6)$$

Assuming that coverage being equal to the fractional change in contact potential is a reasonable approximation, then equations (6.2.5) and (6.2.6) can be compared to yield $\tau = 95\text{\AA}$. This value for τ is much larger than the value obtained for silver on gold, which indicates that gold films have a greater mean thickness than the silver films for the same coverage. Furthermore, if a hemispherically shaped critical nucleus is assumed, then a value of about 14\AA is calculated as its radius. Hence, it is deduced that the gold critical nuclei each consist of on average a few tens of atoms. For simplification, in order to make the mathematics involved more manageable, a square island model was presented in section 2.1. for overlayer growth. Using this model and the coverage to thickness relationship of equation (6.2.6), values were calculated, employing Atlas Autocode computer programmes, for the variations of resistance with overlayer thickness for gold deposited onto thin annealed gold films. Although no measurements were made in the experiments carried out

which could be compared directly with these calculations, the computer results obtained were shown in section 2.1. to be in good agreement with the experimental results of other research workers. The theory does not require that the scattering parameter at the uppermost film surface is a complicated empirically derived function of the overlayer thickness. Instead it is assumed that an overlayer island growth structure is present which has a highly spectral surface scattering mechanism at the areas of the surface where no islands are present, and a highly diffuse scattering mechanism at the areas covered with islands. In order to fit the experimental results of Lucas (19), and others (53) (61), τ values of 20 to 25⁰ are required for the growth of gold on thin annealed gold films which have been deposited onto a nucleating layer of bismuth oxide on glass substrates, which are nominally at room temperature during depositions. The process of nucleation and growth of relatively large islands is reasonable in view of the structural differences between annealed gold films on bismuth oxide and polycrystalline unannealed gold films.

The fractional resistance changes with mean overlayer thickness which took place in film R9/3 are very similar to the changes for the silver films discussed in the previous section. The final resistance of film R9/3 was about 20 Ω /square, and the equation relating fractional resistance change to mean overlayer thickness was found to be

$$\frac{\Delta R}{R_0} = 0.16.t \quad (6.2.7)$$

which is nearly identical to the relationship for a small increase in thickness for the gold film in experiment 9 prepared on a bare glass substrate, and which had a resistance of $> 10^3 \Omega/\text{square}$. For film R8/3 however, the form of the fractional resistance changes with increase of overlayer thickness follows from the bulk conductivity considerations of section 5.2.4. Film R8/3 had a resistance of about $200 \Omega/\text{square}$, which is two orders of magnitude greater than the resistance of a similar film with bulk conductivity. Thus, although the resistance is still high, it appears that the overlayer is forming only on areas already completely covered with metal, and is not serving to reduce the electrical resistance by filling in holes or fissures in the film. The reason why this happened in this film and not with any of the others deposited under similar conditions is thought to lie in the method of resistance measurement employed. The contact potential measurements were very similar to those for other gold films, as shown in figure 5.4.4., and did not suggest that the films deposited onto the wheel-mounted substrates were in any way different. It must be remembered however, that the film used for resistance monitoring was not mounted on the wheel, and did not have its contact potential changes monitored. Had it been possible to do so then more evidence may have been obtained

for suggesting that the method of resistance monitoring using a 'constant current source' was causing considerable changes in the film growth. These changes would be most pronounced not when the resistance was low, but during the early stages of growth of the first gold layer, about 50\AA thick, when it was possible that a very high current density was passed through the film because of its discontinuous structure. That this did happen is shown by the optical microscope photographs indicating that mass-transport of film material had occurred. If a current density which was sufficiently large to do this was passing through the film, then it is reasonable to assume that the structure of the film would be significantly different from the films on the wheel-mounted substrates. Also an electric field of 6 volts/cm. was across the film during the deposition as a result of the resistance measurement technique. It has been established that electric fields of this order applied during early growth can considerably influence the growth of thin metallic films (179) (173). For all experiments after 8 an electrometer was used to measure the resistance which obviated the problem since no further similar abnormalities were observed.

6.3. Conductivity Changes with Aluminium Overlayers.

The variations of electrical resistance with aluminium overlayer thickness shown earlier in section 5.5. on figure 5.5.2. will now be discussed. Referring to figure 5.5.2. the initial increase in resistance is attributed to alloying of the

aluminium with silver at the film surface. This alloy zone, or alternatively surface layer with aluminium atoms which have penetrated the surface (4), causes an increase in the electron scattering near the film surface resulting in an increase in the electrical resistance. As the deposition and alloying proceeds however, the resistance begins to decrease as a result of the increase in film thickness. The resistance maxima, corresponding to the point where the rate of resistance increase is equal to the rate of decrease, occurs at about $3.5\overset{\circ}{\text{Å}}$, which represents an alloy zone of between one and two atomic layers. At an overlayer mean thickness of about $8\overset{\circ}{\text{Å}}$ the resistance once again increases. The total time elapsed from starting the deposition to reaching the resistance minima was 16 minutes and three minutes, at a pressure of 10^{-8} torr and 10^{-7} torr for films R10/3 and R8/4 respectively. For film R10/3 six steps of evaporation were carried out, and for film R8/4 only one, for this first $8\overset{\circ}{\text{Å}}$ of overlayer. This second increase is explained on the basis that when aluminium atoms can no longer alloy with silver, since all of the top few atomic layers of silver have already done so, then further aluminium atoms will react with oxygen together with any weakly alloyed aluminium atoms. It has been demonstrated (101) that aluminium deposited on a foreign substrate can rapidly adsorb oxygen until an oxide several atomic layers thick is formed which then acts as a suitable surface onto which the bulk growth of aluminium can take place. The aluminium during the subsequent growth does not adsorb oxygen so rapidly. The position of the

second maxima indicates that the fast oxygen reaction takes place for only a very few atomic layers in agreement with Grigson and Dove (101). The subsequent fall in resistance of the films on figure 5.5.2. is considered to be the onset of the growth of the bulk aluminium on the oxide layer. The slight increase in resistance is the effect of the oxygen-aluminium reaction. Depositing the aluminium beyond the 1 kHz mark on figure 5.5.2., (which corresponds to a mean thickness of about 22^oÅ), did not appreciably decrease further the electrical resistance. This is a consequence of allowing the thicker aluminium overlayers to be exposed for a considerable time to the residual gases in the vacuum chamber, and by intentionally introducing an oxygen leak into the system in order to monitor the effect of increasing the gas exposure of the films.

The contact potential measurements made during the growth of the aluminium overlayers for films R8/4 and R10/3 will now be discussed in order to show how they are complementary to the explanation of the resistance changes presented above. There is an increase in contact potential during the initial alloying period, indicating a decrease in the effective work function. The effective work function then increases steadily (decrease in contact potential) as the aluminium overlayer increases in mean thickness, with the exception of a range of about 8^oÅ in film R10/3, see figure 5.5.1., when the contact potential remained approximately constant. The latter can be attributed to the rapid

formation of the extremely thin oxide layer, which provided it was a perfect dielectric with no net surface charge, could result in the contact potential not changing as the thickness increased. The value on figure 5.5.1. at which the contact potential levelled out at with increasing thickness indicates that a Volta potential of about 0.47 volts existed in the aluminium films. Further proof of this is, that when a silver film approximately 90\AA thick was deposited onto the aluminium film R10/3, the contact potential with respect to the reference electrode indicated that a series potential of about 0.47 volts existed in the composite film. This is the difference between the deduced effective work function of the resulting surface and polycrystalline silver.

When aluminium films were subjected to sufficient residual gas exposure and to an industrial grade oxygen leak, results similar to those of Huber and Kirk (29) were obtained. The results for contact potential changes during the exposure, reported in section 5.5., indicate that, for very thin aluminium films, oxygen is rapidly adsorbed followed by the adsorption of water vapour. For thicker films however, oxygen is not firstly adsorbed and water vapour is slowly adsorbed. The residual gas in the vacuum chamber before opening the leak valve was predominantly water vapour, and even after the valve was opened to raise the total pressure from about 10^{-8} torr to 10^{-6} torr the mass spectrometer readings indicated that water vapour was still

the principal residual gas constituent. This is the result of the industrial grade oxygen used having a high water vapour content, (0.1 to 1.0% parts/ volume), and that the aluminium being deposited onto the vacuum chamber baffles etc., and the ion pump, would both act to remove oxygen preferentially from the gas mixture being admitted through the leak valve. In order to make the results correspond to those of Huber and Kirk their contact potential axis was shifted by 0.90 volts. The shift was necessary because of, firstly the difference in the effective work function of the gold reference electrode used by Huber and Kirk and the gold films prepared during this work, and secondly the Volta potential in the aluminium films. The first accounts for 0.400 volts, and the second for 0.470 volts, making a total of 0.870 volts \pm 20 mv. which is in reasonable agreement with the required 0.90 volts shift of the potential axis. The remaining discrepancy of 0.03 volts can be credited to the difference in the effective work function value of the polycrystalline gold films, 130 to 200^oÅ thick, prepared in the Varian vacuum system and the, presumably, much thicker gold films of Huber and Kirk on a stainless steel substrate. The effective work function of the reference electrode used in this work, which was also made by depositing gold onto a stainless steel substrate, was not the same as for a similar thickness of gold deposited onto a glass substrate under the same conditions.

When an aluminium film is suddenly exposed to atmospheric pressure there is an increase in the effective work function, in

accordance with the results of Boggio and Plumb (37). The resistance also increases, which follows from a formation of a thicker oxide layer. Evidence that a very thin aluminium oxide layer can act as a good insulator is that the 'device' made accidentally shows that a partly oxidised aluminium layer about 50\AA thick, withstands a voltage of > 50 volts with a leakage current of ≤ 0.001 milliamps.

The upper electron microscope picture on figure 5.6.4. shows that the crystallite size for an aluminium film approximately 140\AA thick deposited onto a 170\AA polycrystalline gold film on a glass substrate is, on average, about 200\AA . The upper picture of figure 5.6.4., and figure 5.6.3. are both for the films of experiment 7. The top picture in figure 5.6.3. is an area of the resistance monitor substrate which was hidden from the main aluminium evaporation stream by a baffle. The lower picture is for an area which was exposed to the stream. It can be seen that 'lumps' with a mean diameter of approximately 1500\AA are very prevalent on the lower, but not the upper picture. These pictures were taken on a scanning electron microscope, and hence the brightness of the lumps indicates that they are accumulating charge. This is consistent with the explanation that these lumps are areas covered with oxidised aluminium. The upper transmission electron microscope picture in 5.6.4. has several darkened areas approximately 1500\AA in diameter. These areas are hence the same size as the lumps already described. Being darker indicates that it is more

difficult for electrons to penetrate these areas, which makes it reasonable to deduce that oxidation, and hence an increase in the thickness of these areas has taken place. Thus, although the average crystallite size in the film is about 200\AA , it appears that lumps of oxidised aluminium are present which are approximately 1500\AA in diameter.

6.4. Conclusions.

In this section the specific conclusions reached as a result of this work on thin films of gold, silver and aluminium prepared by vacuum deposition are listed. They are presented under the four separate headings of Initial Growth, Silver Overlayers, Gold Overlayers and Aluminium Overlayers.

Initial Growth.

- a) The electrical resistance, R , of a gold (or silver) film grown on a 7059 Corning glass substrate, nominally at room temperature, varies with the thickness of the film, F , according to

$$\log R = A - K.F \quad (6.4.1)$$

where A and K are constants.

- b) The effective work function, ϕ , of a thick (about 1000\AA) gold film prepared by vacuum deposition onto a glass substrate at room temperature in a vacuum system with oil diffusion pumps is $4.815 \text{ eV} \pm 10 \text{ meV}$, assuming a

value of 5.22 eV for a gold film approximately 150^oÅ thick grown in an all-dry pumped vacuum system.

- c) A gold film grown on a glass substrate at room temperature at a pressure of $\leq 10^{-8}$ torr is very polycrystalline with a typical crystallite size of 100^oÅ to 300^oÅ.

Silver Overlayers.

- a) Silver overlayers deposited onto polycrystalline gold films on glass substrates grow according to

$$\theta = \left(1 - e^{-t/2} \right) \quad (6.4.2)$$

and hence a high percentage coverage at one or two atomic layers of overlayer thickness.

- b) The resistance changes for very thin silver overlayers on gold follow the relationship

$$\theta = \left(1 - e^{-\left(\frac{\Delta R / R_0}{0.125} \right)} \right) \quad (6.4.3)$$

for films having resistance values as low as several hundred Ω / square.

- c) Measuring contact potential can yield information which helps determine the overlayer growth mechanism of the silver vacuum deposited onto gold on glass substrates.
- d) The effective work function of a polycrystalline film

of silver at room temperature, assuming a value of 5.22 eV for gold, is 4.295 eV \pm 15 meV.

- e) Beyond approximately $10\overset{\circ}{\text{Å}}$ mean overlayer thickness of silver on gold the effective work function increases by 20 meV in going to a thickness of about $50\overset{\circ}{\text{Å}}$.
- f) On exposing a thin polycrystalline silver film to atmospheric pressure there is a decrease of 365 meV in its effective work function and an increase in its electrical resistance, but the work function change is reversed when the film is returned to a low pressure.

Gold Overlayers.

- a) Gold overlayers deposited onto silver films on glass substrates grow according to

$$\theta = \left(1 - e^{-\left(\tau/4.5\right)}\right) \quad (6.4.4)$$

which means a greater thickness for the same coverage ~~as~~ ^{than} for silver deposited onto gold.

- b) Using a square island model and the growth law in (a) the resistance changes for gold deposited onto annealed gold films, which were grown on bismuth oxide on glass substrates, can be explained quantitatively.
- c) For gold films grown on polycrystalline silver films on glass substrates at room temperature the resistance changes for small increases in overlayer thickness can

be described by

$$\theta = \left(1 - e^{-\left(\frac{\Delta R}{R_0}\right)} \right) \quad (6.4.5)$$

when the resistance is as low as several hundred Ω / square.

- d) A high current density through metal films on glass substrates onto which an overlayer of gold is subsequently deposited can result in an overlayer growth mechanism which causes the resistance to change according to bulk considerations, even when the film has a conductivity value 2 orders of magnitude lower than bulk material.

Aluminium Overlayers.

- a) Aluminium alloys with silver and causes an increase in the resistance of thin polycrystalline silver films.
- b) A Volta potential of 0.47 volts can exist in thin aluminium oxide films.
- c) Aluminium rapidly adsorbs oxygen for very thin layers of aluminium deposited on a foreign metal film.
- d) Water vapour is readily adsorbed onto the surface of a thin aluminium film causing a large (about 1.2 eV) decrease in the effective work function, but no noticeable change in the electrical resistance of the film.

- e) The effective work function of an aluminium film deposited in high vacuum increases substantially upon exposing the film to the atmosphere, with a corresponding increase in its electrical resistance.
- f) A 50\AA thick aluminium film oxidised in layers can be a good insulator.
- g) Rectifying device characteristics can be obtained using only the metals gold, silver and aluminium. A switch with an ON impedance of about $3\text{k}\Omega$ and an OFF impedance of about $0.5\text{M}\Omega$ which has a discontinuous slope resistance can be made.

6.5. Further Work.

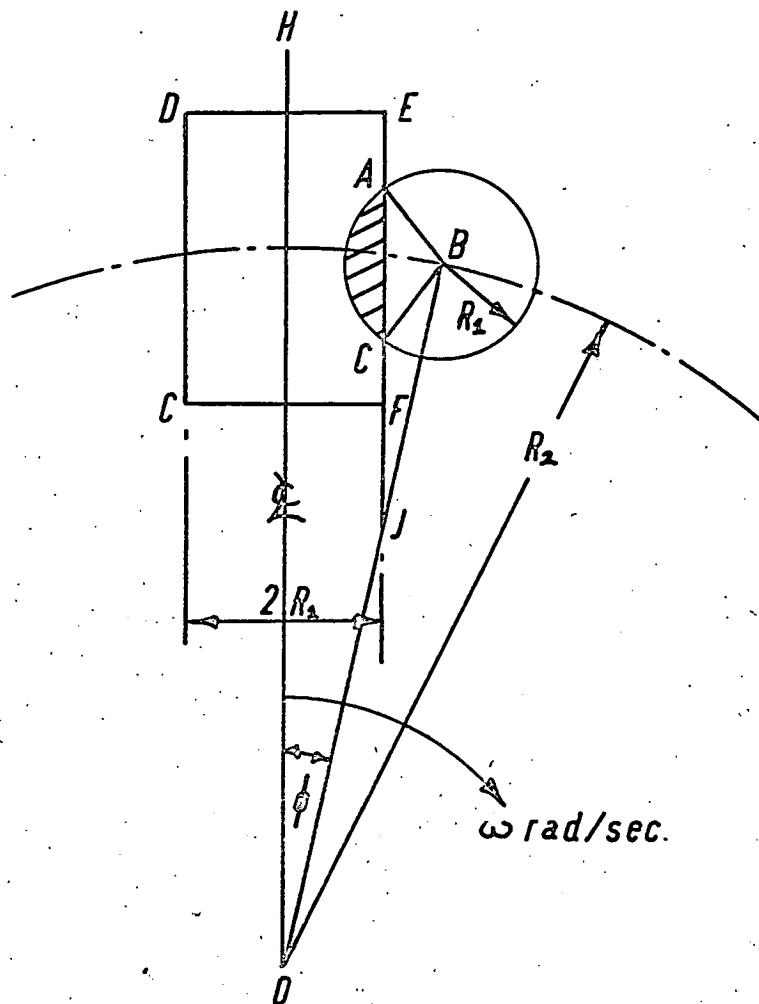
In order to deposit thin metal films which have values of conductivity close to that of the bulk material it is usually necessary to make the films thicker than most of the films made during this study. If thin metallic films deposited on glass substrates are annealed, then bulk conductivity is approached at a thickness of a few hundred angstroms. This is of course assuming that no nucleating layer such as bismuth oxide is used, when very thin high conductivity films can be obtained upon being annealed. It would have been difficult in this work to have made films with a thickness of, say, $>200\text{\AA}$ since each substrate was only in the evaporation stream for one sixteenth of the total evaporation time. Also, in order to obtain a uniform film over the entire substrate surfaces the source-to-substrate distance

was approximately 12". One way in which the apparatus could be modified to allow thicker films to be prepared, or films of the same thickness in a shorter time, is to interchange the roles of the reference electrode and the wheel-mounted substrates. By making thick gold films on the wheel-mounted substrates the reference surfaces, then the surface under investigation becomes what is now the reference electrode. Suitable electrical connections would be made to a glass substrate positioned on the top of the dynamic capacitor gap push rod. This substrate could then be heated if required in order to anneal the film on it, and no problems, as experienced in this work, would be encountered in measuring the film resistance since it would be stationary with permanent electrical connections. With the same geometry of the wheel films eight times as thick could be prepared if required.

Various useful experimental investigations could then be carried out. The most interesting of these would probably be to investigate the changes in the effective work function and conductivity of a thin metallic film during annealing, with particular emphasis on the case of thin polycrystalline gold films. The work function and conductivity could be monitored throughout the process of depositing an overlayer onto the annealed film. By doing this, some more insight should be gained in the role that contact potential plays in the changes in conductivity which take place when thin overlayers are deposited onto thin metallic films having conductivity values close to the bulk material.

On the theoretical aspects of effective work function and conductivity changes, there is still much to be done in the field of multilayer metallic films. The theory of square islands developed in this work is obviously a gross simplification of the true picture, but gave results which agree with experimental work well enough to suggest that these ideas are worth pursuing further.

The instrument designed and built for this study has many applications in the fields of catalysis, charge accumulation, adsorption kinetics, etc., etc., and most important of all; in the field of thin film fabrication using vacuum deposition. Further work is to be carried out in order to develop the technique into a commercially viable instrument.



— Figure A1 —

— Rotating Dynamic Capacitor Electrodes —

APPENDIX 1

Figure A.1 shows a circle with centre 'B' and radius R, and a rectangle DEFG with GF = 2.R₁. These shapes represent two of the electrodes of a rotating dynamic capacitor.

The rectangle has its centre line on a radius of a circle with centre 'O', and is rotating about 'O' at a rate of ω radians/second. The centre 'B' of the circular electrode is at a distance R₂ from 'O'. The circle and rectangle meet at points 'A' and 'C', and let A₀ be the area of overlap, as shown shaded in figure A.1.

L₀ is the spacing between the electrodes, and ϕ is the angle between the line OB and the radius OH bisecting GF. The angle ϕ is related to line t, in seconds, by

$$\phi = \phi_0 + \omega_0 t \quad (\text{A.1}).$$

where ϕ_0 is the value of ϕ at $t = 0$.

By way of construction produce EACF to meet OB at J.

Then from figure A.1 it can be seen that

$$OJ = \frac{R_1}{\sin \phi} \quad (\text{A.2}).$$

$$\therefore BJ = R_2 - \frac{R_1}{\sin \phi} \quad (\text{A.3}).$$

and hence

$$\frac{R_1}{\sin \phi} = \frac{\left(R_2 - \frac{R_1}{\sin \phi}\right)}{\sin \angle BCJ} \quad (\text{A.4}).$$

or rearranging equation (A.4)

$$\sin \angle BCJ = \left(\frac{R_2}{R_1} \sin \phi - \right) \quad (\text{A.5}).$$

Also

$$\angle ABC = 2 \cdot \angle BCJ - \pi \quad (\text{A.6}).$$

and hence substituting for BCJ from equation (A.5) in equation (A.5) in equation (A.6) yields

$$\angle ABC = 2 \left[\sin^{-1} \left(\frac{R_2}{R_1} \sin \phi - 1 \right) \right] - \pi \quad (\text{A.7}).$$

The area of overlap, A_0 , is given by

$$A_0 = \frac{1}{2} \angle ABC \cdot R_1^2 - \frac{1}{2} \sin \angle ABC \cdot R_1^2 \quad (\text{A.8}).$$

substituting for ABC from equation (A.7) in equation (A.8) yields

$$A_0 = R_1^2 \left[\sin^{-1} \left(\frac{R_2}{R_1} \sin \phi - 1 \right) - \frac{\pi}{2} - \frac{1}{2} \sin \left(2 \cdot \sin^{-1} \left\{ \frac{R_2}{R_1} \sin \phi - 1 \right\} - \pi \right) \right] \quad (\text{A.9}).$$

Simplifying equation (A.9) gives

$$A = R_1^2 \left[\cos^{-1} z - z \sqrt{1 - z^2} \right] \quad (\text{A.10}).$$

where

$$z = \left(\frac{R_2}{R_1} \sin \phi - 1 \right)$$

The rate of change of capacitance, c , with respect to time, t , assuming no fringe effects is

$$\frac{dc}{dt} = \frac{\epsilon_0 \epsilon_r}{L_0} \cdot \frac{dA_0}{dt} \quad (\text{A.11}).$$

where ϵ_0 and ϵ_r are the absolute and relative permittivity respectively of the medium between the electrodes.

Substituting for A_0 from equation (A.10) in equation (A.11) yields

$$\frac{dc}{dt} = \frac{\epsilon_0 \epsilon_r}{L_0} \cdot \frac{d}{dz} \left(R_1 \left[\cos^{-1} z - z \sqrt{1 - z^2} \right] \right) \cdot \frac{dz}{d\phi} \cdot \frac{d\phi}{dt} \quad (\text{A.12})$$

Carrying out the differentiation and expressing the result as a function of ϕ gives

$$\frac{dc}{dt} = \frac{\epsilon_0 \epsilon_r}{L_0} \cdot (\omega \pi R_1^2) \left[\frac{2}{\pi} \left(\frac{R_2}{R_1} \right)^2 \left\{ \frac{2 R_1}{R_2} \sin \phi - \sin^2 \phi \right\}^{1/2} \right] \cos \phi \quad (\text{A.15}).$$

The capacitance C is related to the current, i , generated by a dynamic capacitor through the relationship

$$i = V \cdot \frac{dc}{dt} \quad (\text{A.14}).$$

where V is the time-independent voltage across the electrodes.

Substituting for $\frac{dc}{dt}$ from equation (A.13) in equation (A.14) yields the following expression for the current as a function of ϕ

$$i = V \cdot \frac{\epsilon_0 \epsilon_r}{L_0} (\omega \pi R_1^2) \left[\frac{2}{\pi} \left(\frac{R_2}{R_1} \right)^2 \left\{ \frac{2R_1}{R_2} \sin \phi - \sin^2 \phi \right\}^{1/2} \right] \cos \phi \quad (\text{A.15}).$$

which is valid for $\sin^{-1} \frac{R_1}{R_2} \leq \phi \leq \sin^{-1} \frac{2R_1}{R_2}$

and similarly for

$$\sin^{-1} \frac{R_1}{R_2} \leq \phi \leq 0 \quad (\text{A.16}).$$

$$i_{\phi} = i(\pi - \phi)$$

for

$$0 \leq \phi \leq -\sin^{-1} \frac{R_1}{R_2}$$

(A.17).

$$i_{\phi} = -i(\phi - \pi)$$

for

$$-\sin^{-1} \frac{R_1}{R_2} \leq \phi \leq -\sin^{-1} \frac{2R_1}{R_2}$$

(A.18).

$$i_{\phi} = -i(2\pi - \phi)$$

However for a vibrating capacitor system with equilibrium spacing of L_0 between the plates and the same geometry as described above then the instantaneous value of current generated is, from equation (3.4.3)

$$i = V \cdot \frac{\epsilon_0 \epsilon_r}{L_0} (\omega \pi R_1^2) \left[\frac{L_1/L_0}{(1 + L_1/L_0 \cos \omega t)^2} \right] \sin \omega t \quad (\text{A. 9}).$$

where L_1 is the amplitude of vibration.

Thus the quantities to be compared for the rotating and vibrating systems are, from equations (A.15) and (A.19) respectively

$$\frac{2}{\pi} \left(\frac{R_2}{R_1} \right)^2 \left\{ \frac{2R_1}{R_2} \sin \phi - \sin^2 \phi \right\}^{1/2} \cos \omega t \quad (\text{A.20}).$$

and

$$\frac{L_1/L_0}{(1 + L_1/L_0 \cos \omega t)^2} \cdot \sin \omega t \quad (\text{A.21}).$$

With $\frac{R_1}{R_2} = 0.95/5.1$, figure 3.4.1 compares the fundamental components of the sinusoidal variations of equation (A.20) to that of (A.21), with an arbitrary amplitude scale, for various values of L_1/L_0 . An Atlas Autocode computer program was written to calculate the fundamental component amplitudes.

REFERENCES.

1. DRUDE (P.) Ann. Phys. Lpz. 1 (4) 1960, 566
2. THOMSON (J.J.) Proc. Camb. Phil. Soc. 11, 1901, 120
3. SWANN (W.F.G.) Phil. Mag. 28, 1914, 467
4. PASHLEY (D.W.) Advances in Physics, 14, 1965, 327
5. SWANSON (J.G.) The electrical properties of thin metal films. Ph. D. thesis, Imperial College, London, 1967.
6. MOSTOVETCH (N.) & VODAR (B.) IN Henisch (H.K.) Semiconducting materials, 1951. pp. 260-281.
7. NIFONTOFF (N.) C.R. Acad. Sci. Paris, 237, 1953, 24
8. HARTMAN (T.E.) J. Appl. Phys., 34 (4 part 1) 1963, 943
9. HILL (R.M.) Proc. Roy. Soc. A, 309, 1969, 377
10. WEI (L.Y.) J. Chem. Phys., 39, 1963, 2709.
11. WEALE (R.A.) Proc. Phys. Soc. Lond., A, 62, 1949, 135
12. APPLEYARD (E.T.S.) & LOVELL (A.C.B.) Proc. Roy. Soc. A, 158, 1937, 718
13. FUCHS (K.) Proc. Camb. Phil. Soc., 34, 1938, 100
14. SONDEHEIMER (E.H.) Advances in Physics, 1, 1952, 1
15. JURETSCHKE (H.J.J.) J. Appl. Phys., 37, 1966, 435
16. ENNOS (A.E.) Brit. J. Appl. Phys., 8, 1957, 113
17. GILLHAM (E.J.) et.al. Phil. Mag., 46, 1955, 1051
18. LUCAS (M.S.P.) J. Appl. Phys., 36 (5) 1965, 1632
19. LUCAS (M.S.P.) Thin Solid Films, 2, 1968, 337
20. PARROT (J.E.) Proc. Phys. Soc., 85, 1965, 1143
21. JURETSCHKE (H.J.J.) Surface Science, 5, 1966, 111
22. PATERSON (C.H.) Unpublished work.

23. LUCAS (M.S.P.) The effects of surface characteristics on the conductivity of gold films. Ph. D. thesis, Duke University (U.S.A.), 1964.
24. CAMPBELL (D.S.) The theory and application of electrical conduction processes in thin films. Thesis, Diploma Imperial College, London, May 1967.
25. PLESSEY Co. Ltd. (Allen Clark Research Centre, Caswell). Research on thin metallic films, Report No. 1, June 1966.
26. CHOPRA (K.L.) & RANDLETT (M.R.) J. Appl. Phys., 38, 1967, 3144
27. JURETSCHKE (H.J.J.) Surface Science, 2, 1964, 40
28. PLESSEY Co. Ltd. (Allen Clark Research Centre, Caswell). Research on thin metallic films, Report No. 3, June 1967.
29. HUBER (E.E.) & KIRK (C.T.) Surface Science, 5, 1966, 447
30. SUHRMANN (R.) Advances in Catalysis, 7, 1955, 303
31. WOOD (R.W.) Phil. Mag., 3, 1902, 396
32. LANGMUIR (I.) Proc. Nat. Acad. Sci. Wash., 3, 1917, 141
33. FRENKEL (J.) Zeit. fur Phys., 26, 1924, 117
34. DYUBUA (B. Ch.) et.al. Radio Engineering and Electronic Physics, 9, 1964, 1716
35. HOPKINS (B.J.) & PENDER (K.R.) Brit. J. Appl. Phys., 17, 1966, 281
36. RIVIÈRE (J.C.) Proc. Phys. Soc., 70, 1957, 676
37. BOGGIO (J.E.) & PLUMB (R.C.) J. Chem. Phys., 44 (3)1966, 1081
38. CULVER (R.V.) & TOMPKINS (F.C.) Advances in Catalysis, 11, 1959, 67
39. ELEY (D.D.) & WILKINSON (P.R.) Proc. Roy. Soc. A, 254, 1960, 327
40. MENZEL (E.) Reports on Progress in Physics, 26, 1963, 47

41. PEASE (R.F.W.) & NIXON (W.C.) J. Sci. Instr., 42, 1965, 81
42. MULLER (E.W.) Advances in Electronics and Electron Physics, 13, 1960, 83
43. SWANSON (J.G.) & CAMPBELL (D.S.) Thin Solid Films, 1, 1967, 183
44. SCHWARTZ (N.) & BERRY (R.W.) Physics of Thin Films, 2, 1964, 363
45. WEIMER (P.K.) Proc. Inst. Radio Enginrs., 50, 1962, 1462
46. MEAD (C.A.) Proc. Inst. Radio Enginrs., 48, 1960, 359
47. RASMANIS (E.) NEREM Record, 4, 1962, 160. (Paper presented at the IRE Northeast Electronics and Engineering Meeting, Nov., 1962.)
48. BLOCH (F.) Zeit. fur Phys., 52, 1928, 555
49. SOMMERFELD (A.) Zeit. fur Phys., 47, 1928, 1
50. LORENTZ (H.A.) Proc. Acad. Sci. Amst., 7, 1904-5, 438, 585, 684
51. MATHEISSEN (A.) Rep. Brit. Ass., 32, 1862, 144
52. SONDHEIMER (E.H.) Proc. Roy. Soc. A, 203, 1950, 75
53. MEYER (D.T.) Thin Solid Films, 2, 1968, 27
54. PLESSEY Co. Ltd. (Allen Clark Research Centre, Caswell). Research on thin metallic films, Report No. 2, December, 1966.
55. CHOPRA (K.L.) et.al. J. Appl. Phys., 34 (6), 1963, 1699
56. FELDMAN (C.) J. Appl. Phys., 34 (6), 1963, 1710
57. NEUMAN (M.R.) & KO (W.H.) J. Appl. Phys., 37 (8), 1966, 3327
58. MEYER (D.T.) A demonstration of the existence of a surface phase of gold. Ph.D. thesis, Duke University, (U.S.A.), 1966.
59. YING (C.Fu) & FARNSWORTH (H.E.) Phys. Rev., 85 (3), 1952, 485

60. MIHAMA (K.) & YASUDA (Y.) J. Phys. Soc. Japan, 21 (6) 1966, 1166
61. PLESSEY Co. Ltd. (Allen Clark Research Centre, Caswell).
Research on thin metallic films, Report No. 1,
June 1966.
62. NEWMAN (R.C.) & PASHLEY (D.W.) Phil. Mag., 46, 1955, 917
63. SHIRAI (S.) et.al. J. Phys. Soc. Japan, 16 (10) 1961, 1989
64. NEUGEBAUER (C.A.) & WEBB (M.B.) J. Appl. Phys., 33 (1) 1962, 74
65. HILL (R.M.) Nature, London, 204, 1964, 35
66. HERMAN (D.S.) & RHODIN (T.N.) J. Appl. Phys., 37, 1966, 1594
67. HILL (R.M.) Proc. Roy. Soc. A, 309, 1969, 397
68. LESTER (H.H.) Phil. Mag., 31, 1916, 197
69. HERRING (C.) & NICHOLS (M.H.) Rev. Mod. Phys., 21, 1949, 185
70. ZADMUKIN (Z.N.) & YEGIYEV (V.G.) Fiz. Metal. Metalloved., 22 (1) 1966, 121
71. GYFTOPOULOS (E.P.) & LEVINE (J.D.) J. Appl. Phys., 33 (1) 1962, 67
72. ALLEN (F.G.) & GOBELI (G.W.) Phys. Rev., 127 (1) 1962, 150
73. HENSLEY (E.B.) J. Appl. Phys., 32 (2) 1961, 30
74. DOBRETSON (L.N.) & MATSKEVICH (T.L.) Soviet Physics - Tech. Phys., 11 (8) 1967, 1081
75. SAMSONOV (G.V.) et.al. Soviet Physics - Tech. Phys., 11 (8) 1967, 1070
76. RIVIERE (J.C.) U.K.A.E.A. Report. AERE - 125526, 1967.
77. HOPKINS (B.J.) & RIVIERE (J.C.) Brit. J. Appl. Phys., 15, 1964, 941
78. ITSKOVICH (F.I.) Soviet Physics - JETP, 24 (1) 1967, 202
79. LEWIS (T.J.) Proc. Phys. Soc. B, 67 (3) 1954, 187

80. TRACY (J.C.) & BLAKELY (J.M.) Surface Science, 13, 1968, 313
81. HOPKINS (B.J.) & PENDER (K.R.) Brit. J. Appl. Phys., 17, 1966, 281
82. LEE (T.J.) et.al. Appl. Phys. Letters, 11 (11) 1967, 361
83. CLARKE (E.N.) & FARNSWORTH (H.E.) Phys. Rev., 85 (3) 1952, 484
84. HOLSCHER (A.A.) Surface Science, 4, 1966, 89
85. HUBER (E.E.) Appl. Phys. Letters, 8, 1966, 169
86. SACHTLER (W.M.H.) et.al. Surface Science, 5, 1966, 221
87. YING (C. Fu) & FARNSWORTH (H.E.) Phys. Rev., 85 (3), 1952, 485
88. BLACKMER (L.L.) & FARNSWORTH (H.E.) Phys. Rev., 77, 1950, 826
89. KOBAYASHI (H.) & KATO (S.) Surface Science, 12, 1968, 398
90. DOWDEN (D.A.) J. Chem. Soc., Part 1, 1950, 242
91. HOPKINS (B.J.) et.al. Brit. J. Appl. Phys., 15, 1964, 865
92. GONZALEZ (O.D.) & PARAVANO (G.) J. Amer. Chem. Soc., 78, 1965, 4533
93. SAZONOVA (I.S.) & KEIER (N.P.) Kinetika I Kataliz (Kinetics and Catalysis USSR) 6, 1965, 448
94. CLARK (D.) et.al. Trans. Faraday Soc., 55, 1959, 1937
95. HONDROS (E.D.) & GLADMAN (D.) Surface Science, 9, 1968, 471
96. DILLON (J.A.) & FARNSWORTH (H.E.) J. Appl. Phys., 28 (2) 1957, 174
97. RIVIERE (J.C.) Brit. J. Appl. Phys., 15, 1964, 1341
98. OGAWA (I.) et.al. J. Appl. Phys. Japan, 21, 1952, 223
99. BENTON (A.F.) & ELGIN (J.C.) J. Amer. Chem. Soc., 51 (1) 1929, 7

100. HOPKINS (B.J.) & ROSS (K.J.) Brit. J. Appl. Phys., 15, 1964, 89
101. GRIGSON (C.W.B.) & DOVE (D.B.) J. Vac. Sci. Technol., 3 (3) 1966, 120
102. HACKERMAN (N.) & LEE (E.H.) J. Phys. Chem., 59, 1955, 900
103. KLEMPERER (D.F.) J. Appl. Phys., 37, 1966, 452
104. ROBERTS (M.W.) & WELLS (B.R.) Surface Science, 8, 1967, 453
105. HUBER (E.E.) & KIRK (C.T.) Surface Science, 8, 1967, 458
106. JONA (F.) Bull. Amer. Phys. Soc., 12, 1967, 137
107. HUBER (E.E.) & KIRK (C.T.) Surface Science, 9, 1968, 217
108. RAMSEY (J.A.) Surface Science, 8, 1967, 313
109. WALTON (D.) et.al. J. Chem. Phys., 38, 1963, 2698
110. LOTHE (J.) & POUND (G.M.) J. Chem. Phys., 36, 1963, 2080
111. GRETZ (R.D.) Surface Science, 5, 1966, 239
112. ANDERSON (J.C.) ed. The use of thin films in physical investigations. Academic Press, London and New York, 1966.
113. MACDONALD (J.R.) & BARLOW (C.A.) J. Chem. Phys., 39, 1963, 412
114. SANDEJAS (J.S.) & HUDSON (J.B.) Surface Science, 11, 1968, 175
115. JONES (J.J.) Proc. Roy. Soc. A, 284, 1965, 469
116. GRETZ (R.D.) & POUND (G.M.) Appl. Phys. Letters, 11 (2) 1967, 67
117. LANGMUIR (I.) & TAYLOR (J.) Phys. Rev., 44, 1933, 423
118. MOORE (G.E.) & ALLISON (H.W.) J. Chem. Phys., 23, 1955, 1609

119. LEA (C.) & MEE (C.H.B.) Surface Science, 8, 1967, 417
120. AMERICAN INSTITUTE OF PHYSICS. Handbook. McGraw-Hill Book Co., New York, 1957.
121. MIGNOLET (J.C.P.) Bull. Soc. Chim. Belg., 65, 1956, 837
122. GORDY (W.) & THOMAS (W.J.O.) J. Chem. Phys., 24, 1956, 439
123. PASHLEY (D.W.) & STOWELL (M.J.) J. Vac. Sci. Technol., 3, 1966, 156
124. CABRERA (N.) & MOTT (N.F.) Reports on Progress in Physics, 12, 1949, 163
125. LANYON (M.A.H.) & TRAPNELL (B.M.W.) Proc. Roy. Soc. A, 227, 1955, 387
126. HART (R.K.) Proc. Roy. Soc. A, 236, 1956, 68
127. MENTALECHETA (Y.) et.al. C.R. Acad. Sci. Paris, B, 262, 1966, 892
128. QUINN (C.M.) & ROBERTS (M.W.) Trans. Faraday Soc., 60, 1964, 899
129. ABEY (A.E.) J. Appl. Phys., 39 (1) 1968, 120
130. BELOUS (M.V.) & WAYMAN (C.M.) J. Appl. Phys., 38 (13) 1967, 5119
131. POTTER (J.) Phys. Rev., 58, 1940, 623
132. SHELTON (H.) Phys. Rev., 107, 1957, 1553
133. FINE (J.) et.al. Surface Science, 3, 1965, 227
134. FRY (R.K.) & CARDWELL (A.B.) Phys. Rev., 125, 1962, 471
135. LEA (C.) & MEE (C.H.B.) Surface Science, 8, 1967, 417
136. MELMED (A.M.) & Surface Science, 6, 1967, 481
137. VLADIMIROV (V.I.) Soviet Physics - Solid State, 7 (6) 1965, 1536
138. ROLLINS (T.L.) & WELCHMAN (F.L.) Phys. Stat. Solidi, 15, 1966, 233

139. BARDEEN (J.) Phys. Rev., 71, 1947, 717
140. BRYLA (S.M.) & FELDMAN (C.) J. Appl. Phys., 33, (1) 1962, 774
141. WAGENER (S.) The oxide-coated cathode. Vol. 2. Chapman and Hall, London, 1951.
142. KAMINSKY (M.) Atomic and ionic impact phenomena on metal surfaces. Springer-Verlag, Berlin, 1965.
143. THOMSON (W.) Later Lord Kelvin. Phil. Mag., 46, 1898, 82
144. ZISMAN (W.A.) Rev. Sci. Instruments, 3, 1932, 367
145. SIMON (R.E.) Phys. Rev., 116, 1959, 613
146. PETIT-CLERK (Y.) & CARETTE (J.D.) Rev. Sci. Instruments, 39, 1968, 933
147. MITCHINSON (J.C.) et.al. To be published.
148. KOLM (H.H.) Rev. Sci. Instruments, 27, 1956, 1046
149. DELCHAR (T.) et.al. J. Sci. Instruments, 40, 1963, 105
150. SIMMONS (J.G.) Phys. Rev. Letters, 10, 1963, 10
151. NOTTINGHAM (W.B.) Phys. Rev., 49, 1936, 78
152. PRITCHARD (J.) & TOMPKINS (F.C.) Trans. Faraday Soc., 56 1960, 540
153. OATLEY (C.W.) Proc. Roy. Soc. A, 155, 1936, 218
154. ANDERSON (P.A.) Phys. Rev., 47, 1935, 958
155. HAAS (G.A.) & THOMAS (R.E.) Surface Science, 4, 1966, 64
156. GREEN (M.) et.al. Surface Science, 12, 1968, 405
157. FOWLER (R.H.) Phys. Rev., 38, 1931, 45
158. JUENKER (D.W.) J. Appl. Phys., 28, 1957, 1398
159. SUHRMANN (R.) & Von EICHBORN (J.L.) Zeit. fur Phys., 107, 1937, 523
160. SUHRMANN (R.) & WEDLER (G.) Zeit. Angew. Phys., 14, 1962, 70

161. FOWLER (R.H.) & NORDHEIM (L.W.) Proc. Roy. Soc. A, 119, 1928, 173.
162. NORDHEIM (L.W.) Proc. Roy. Soc. A, 121, 1928, 626
163. YELINSON (M.I.) et.al. Radio Engineering and Electronic Physics, 6, 1961, 1191
164. HOLSCHER (A.A.) Surface Science, 4, 1966, 89
165. DELCHAR (T.A.) & EHRLICH (G.) J. Chem. Phys., 42 (8) 1965, 2686
166. MITCHINSON (J.C.) Honours Degree Report. Ref. H.S.P./40. Dept. Elect. Engin., University of Edin., 1966.
167. REID (M.A.) A study of the thin film triode. Ph.D. thesis, University of Edinburgh, 1968.
168. PISTOULET (B.) & LASSABATERE (L.) Le Vide, 21, 1966, 467
169. HARRIS (P.C.) & BLOORE (E.W.) Surface Science, 14, 1969, 270
170. JAEGER (H.) et.al. Surface Science, 6, 1967, 309
171. FEINLEIB (M.) Paper presented at the Conference on Physical Electronics, M.I.T., March 31st 1961. "New approaches to sorption pumping".
172. CHOPRA (K.L.) & RANDLETT (M.R.) Rev. Sci. Instruments, 37, 1966, 1421
173. CHOPRA (K.L.) J. Appl. Phys., 37, (6) 1966, 2249
174. REALE (C.) Electronic Components, 1969, p. 826
175. SZUPILLO (E.) U.S. Patent No. 3474305, 1969. "Discontinuous thin film multistable state resistors".
176. WEITZENKAMP (L.A.) & BASHARA (N.M.) Trans. Metall. Soc. AIME, 236, 1966, 351
177. NAMBA (Y.) Japan. J. Appl. Phys., 7, 1968, 783
178. FARNSWORTH (H.E.) Phys. Rev., 49, 1936, 605
179. ALSFORD (R.W.) et.al. Electronics Letters (G.B.), 2, 1966, 327

180. LUCAS (M.S.P.)

Applied Physics Letters, 4 (4) 1964, 73

181. ANDERSON (P.A.)

Phys. Rev., 88, 1952, 665